Author:
Fisher, Adam A J

Title:
Uncertainty in composite manufacturing and consequences for thermoplastic-thermoset co-curing

Uncertainty in Composite Manufacturing and Consequences for Thermoplastic-Thermoset Co-curing

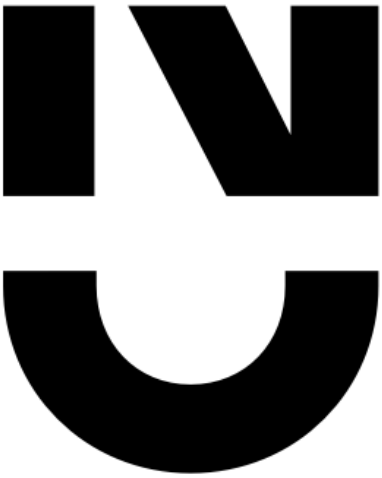

Adam Fisher

A dissertation submitted to the University of Bristol and Nantes Université in accordance with the requirements for award of the degree of Doctor of Philosophy in the Bristol Faculty of Engineering and Laboratoire de Thermique et Energie de Nantes.

September 2023

Word count: 35449

Abstract

This work had four primary objectives:

1. Identify the influential parameters during epoxy curing.
2. Quantify the effect of measured process variability on curing.
3. Propose manufacturing concepts for cure gradients desirable for co-curing.
4. Demonstrate the influence of initial degree of cure on thermoplastic-thermoset co-curing.

The most influential sources of variability in composite processing were determined by sensitivity analyses using coupled heat transfer and cure kinetics models. The analyses showed, that in the standard aerospace case considered, cure temperature has the most influence and diffusion limiting cure kinetic effects become highly influential post vitrification.

To demonstrate the effect a source of process variability can have, calorimeter measurements from industrial scale ovens and autoclaves were used as inputs to a numerical model. It was shown that with the higher heat transfer coefficients in the autoclaves, spatial variability in thermal conditions was less influential. However, this effect was counteracted by the greater variability in the autoclaves, resulting in comparable repeatability between the two vessel types.

Combinations of tool material, tool thickness and heat transfer coefficient were explored for maximising part stiffness while retaining bonding surface reactivity for co-curing. A thick, thermally diffusive tool for the bonding surface and a thin, low diffusivity tool elsewhere, in an out-of-autoclave environment was proposed.

The effect of initial degree of cure on thermoplastic-thermoset co-curing was investigated at the laminate level. A diffusion model was derived from in-situ measurements of interdiffusion between polyetherimide and a model epoxy system. The model predicted that any increase in initial degree of cure decreased the interaction across the interface. This was supported by mechanical test results and interphase thickness measurements. The results indicated that unlike conventional co-curing, the manufacturing efficiency benefits from increasing the initial degree of cure cannot justify the significant decrease in bond strength.

Résumé en Français

Le but de ce travail était de contribuer à une approche plus efficace pour le collage de composites à matrice polymère. Cette approche, connue sous le nom de co-cuisson, a été envisagée pour l'assemblage de composites à matrice thermodurcissable ou de l'assemblage hybride entre des composites à matrice thermodurcissable et à matrice thermoplastique de grade aérospatial. La variabilité durant la mise en œuvre des stratifiés composites thermodurcissables sera également discutée. Les contributions ciblées à propos de ces deux sujets sont énoncées dans les objectifs, comme suit :

1. Identifier les paramètres influents lors de la polymérisation ou la cuisson de l'époxy.
2. Quantifier l'effet de la variabilité du processus mesurée sur la polymérisation.
3. Proposer des concepts de fabrication pour les gradients de polymérisation souhaitables pour la co-cuisson.
4. Démontrer l'influence du degré initial de polymérisation sur la co-cuisson thermodurcissable-thermoplastique.

Le plein potentiel des matériaux composites n'est pas toujours réalisé en raison de l'utilisation de techniques de fabrication développées pour les métaux. Un domaine clé est l'assemblage de pièces composites thermodurcissables polymérisés ou cuits, où les approches héritées sont laborieuses et compromettent les performances structurelles. Les fixations mécaniques et les adhésifs sont souvent les approches utilisées.

La co-cuisson est une solution potentielle. Classiquement, cela implique un collage via la réticulation qui se produit entre les substrats en polymère thermodurcissable lorsqu'ils sont cuits en contact à partir d'un état cru ou non polymérisé. Lorsque des substrats en polymère thermoplastique sont inclus, le collage se produit également, mais par interdiffusion.

La combinaison efficace de composites thermoplastiques et thermodurcissables présente plusieurs avantages possibles. Les nombreuses propriétés contrastées des matériaux offriraient une plus grande liberté de conception pour optimiser les performances. La possibilité de mise en forme par fusion des thermoplastiques permet un collage efficace entre les substrats thermodurcissables cuits. Le soudage devient possible via la co-cuisson thermoplastique sur les surfaces extérieures des substrats.

Le grand nombre de paramètres impliqués dans la mise en œuvre des matériaux composites fait que les procédés de fabrication sont sujet à une forte variabilité. Les principales sources de variabilité sont l'environnement de fabrication, les paramètres matériaux et la séquence

d’empilement des pré-imprégnés ou plis. La co-cuisson nécessite un contrôle précis du procédé pour obtenir un collage fiable. Par conséquent, afin d'obtenir systématiquement un collage souhaitable, il est crucial de comprendre et de réduire cette variabilité.

Ce travail était composé de quatre lots de travail principaux, chacun ciblant l'un des objectifs énoncés précédemment. Ce qui suit est un résumé de chaque lot de travail.

L'influence des paramètres procédé clés sur la cuisson des stratifiés thermodurcissables

Le virage de l'industrie aérospatiale vers les composites à matrice époxy haute performance a entraîné une augmentation de la demande en matériaux composites. Cependant, les variations dans les propriétés des matériaux et les conditions de mise en œuvre peuvent entraîner une augmentation des rebuts, une réduction de l'efficacité des procédés et des coûts plus élevés pendant la fabrication. Pour remédier à cela, une méthodologie est proposée pour identifier et hiérarchiser les paramètres influents qui impactent la robustesse de la mise en œuvre des stratifiés thermodurcissables.

La méthodologie utilisée dans ce lot de travail consistait à combiner une analyse de sensibilité et une simulation numérique pour évaluer l'influence des paramètres. Une métrique représentative de la sensibilité a été développée, prenant en compte le taux de variation du temps de cuisson, divers paramètres liés au procédé, à la géométrie et au matériau. Pour tenir compte de l'incertitude liée aux expériences expérimentales, la métrique prend également en compte les écarts types des valeurs de paramètres mesurées expérimentalement. Cette métrique combinée indiquait dans quelle mesure chaque paramètre affectait la variabilité du temps de cuisson.

Des simulations par éléments finis ont été menées sur COMSOL Multiphysics pour résoudre les équations de transfert de chaleur transitoire à une dimension et de cinétique de polymérisation. Le modèle représentait un ensemble de polymérisation avec des matériaux composites aérospatiaux mis en œuvre dans une étuve industrielle.

La méthodologie a permis de classer l'influence des paramètres en calculant les valeurs absolues de la métrique d'influence associées à un degré de polymérisation spécifique. Par exemple, la température de palier est devenue plus influente à mesure que la polymérisation progressait. La vitesse de chauffage et le coefficient de transfert de chaleur (HTC) ont eu un impact plus important avant d'atteindre la température de palier en raison de leur interaction. L'importance des paramètres de la cinétique de polymérisation avait tendance à augmenter vers la fin du processus de polymérisation. En revanche, les paramètres liés au procédé et à la

géométrie avaient des influences variables à différentes étapes de la polymérisation. Comprendre la source de la variabilité permet d'optimiser la caractérisation des matériaux, l'équipement de fabrication ou les tolérances des outils.

L'objectif 1 a été satisfait en présentant une méthodologie offrant un cadre pour évaluer et hiérarchiser les paramètres affectant la variabilité de la cuisson des composites thermodurcissables. Selon le degré de polymérisation ciblé, le classement des paramètres influents varie. Les résultats peuvent guider les décisions pour optimiser les procédés de fabrication, l'outillage et la conception, conduisant à une meilleure cohérence et à une réduction des rebuts. Par exemple, dans le cas considéré, un outillage avec une homogénéité et une répétabilité de la température serait un meilleur investissement.

Effets des variations du coefficient de transfert de chaleur sur la cuisson des composites

En réponse à l'objectif 2, ce lot de travail a étudié la variabilité spatiale du coefficient de transfert thermique (HTC) à l'intérieur des cuves industrielles et comment cette variabilité influence la mise en œuvre des composites thermodurcissables. Les HTC provenant de divers étuves et autoclaves industrielles ont été collectés à l'aide d'un ensemble de calorimètres mis en place pendant une montée en température. Une nouveauté de ce travail était la prise en compte des étuves, car en raison de leur héritage, les autoclaves ont été au centre des travaux précédents.

L'effet de la variabilité mesurée du HTC a été prédit à l'aide d'un modèle numérique. Les équations couplées de cinétique de polymérisation et de transfert de chaleur en transitoire ont été résolues en une dimension pour capturer le processus de polymérisation à travers l'épaisseur d'un stratifié thermodurcissable renforcé de fibres de carbone. La configuration géométrique était un stratifié composite en contact avec un outil en invar, imitant des scénarios de fabrication réels. Les propriétés matériau étaient représentatives de HexPly M21, un stratifié époxy renforcé de fibres de carbone de grade aérospatiale. Les HTC mesurés ont été appliqués par le biais de conditions limites de convection de chaque côté de la géométrie.

Pour quantifier l'effet de la variabilité mesurée, cinq métriques ont été définies. Deux d'entre elles ont porté sur la distribution transversale de la température, et trois sur le processus de polymérisation. Pour la distribution de la température, l'homogénéité et le gap entre les conditions imposées et celles dans le stratifié ont été pris en compte. Le processus de polymérisation a été examiné à travers le temps de cuisson, le dépassement de température et le temps de gélification.

L'analyse statistique des mesures a révélé que l'amplitude ainsi que la variabilité du HTC sont plus importantes dans les autoclaves, comme illustré dans la Figure 1. Les valeurs plus élevées sont connues pour être liées à la pression appliquée. La plus grande variabilité a été attribuée à la grande différence de vitesse de l'air entre l'avant et l'arrière des autoclaves ; ce qui est également observé dans d'autres travaux. L'absence d'importants flux d'air dans les étuves entraîne une faible variabilité.

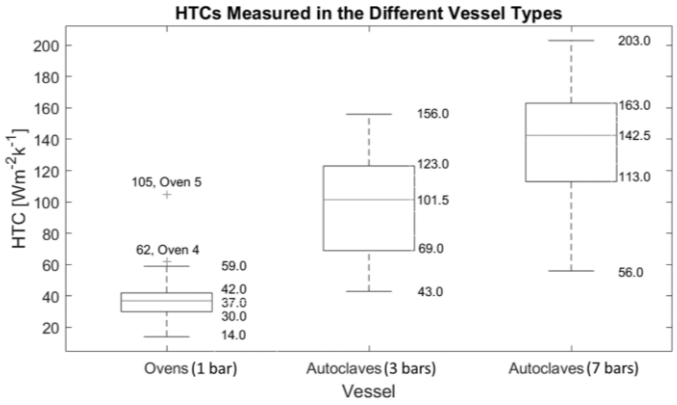

Figure 1. Valeurs HTC mesurées dans les étuves à 1 bar et les autoclaves à 3 et 7 bars.

L'effet de ces observations a été capturé par les métriques définies plus tôt. Un HTC plus élevé a permis un chauffage convectif efficace et la dissipation de la chaleur exothermique ; ce qui signifie que l'historique de température a été imposé plus efficacement. Le résultat a été que le gap entre les températures imposées et les températures des pièces est réduit et l'homogénéité de la température est accrue. La relation étroite entre les températures imposées et les températures des pièces facilite la conception du procédé.

Il a été montré que la sensibilité des indicateurs de cinétique de polymérisation au HTC diminue avec l'augmentation du HTC. En utilisant le graphique du temps de gélification dans la Figure 2 comme exemple, la sensibilité était très élevée aux niveau des HTCs représentatifs de l'étuve avant de rapidement se stabiliser en approchant des valeurs d'autoclaves, tendant vers une valeur asymptotique. Ce résultat signifie qu'en dépit de la plus grande variabilité spatiale mesurée dans les autoclaves, les intervalles de confiance prédits à 95 % des métriques avaient des plages similaires dans les deux types de cuves. Ce résultat suggère une répétabilité similaire du procédé entre les étuves et les autoclaves.

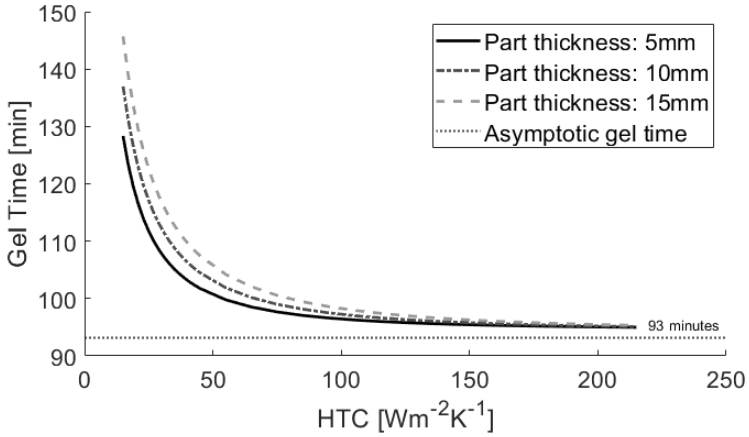

Figure 2. Temps de gel approximatif pour la géométrie sur la plage des HTCs observés pour des épaisseurs de pièces de 5, 10 et 15 mm. Le temps de gel si la matière a suivi le cycle est de 93 minutes.

Environnements de mise en œuvre pour contrôler les gradients de polymérisation des composites thermodurcissables

Ce lot de travail était axé sur l'optimisation des gradients de polymérisation dans les structures composites thermodurcissables en vue de leur assemblage par co-cuisson. La co-cuisson repose sur la réactivité à l'interface des substrats pour que le mécanisme de réticulation ou d'interdiffusion favorise le développement de l'adhésion. Cependant, la manipulation de pièces peu rigides, collantes et non polymérisées nécessite des outils complexes et réduit l'efficacité de la production. L'étude visait à obtenir des gradients de polymérisation permettant d'obtenir des pièces semi-polymérisées rigides avec une réactivité suffisante à l'interface.

La recherche a utilisé une approche éléments finis bidimensionnels pour résoudre les équations couplées de cinétique de polymérisation et de transfert thermique. Le composite HexPly M21 a été utilisé. Il a été mis en œuvre selon le cycle de polymérisation recommandé par le fabricant. La géométrie d'un raidisseur oméga a été utilisée comme cas d'étude. Diverses conditions de fabrication ont été simulées, en l'occurrence différents matériaux, géométries et épaisseurs d'outillage, coefficients de transfert thermique (HTC) et tapis chauffants.

Les principales conclusions pour chaque paramètre étaient les suivantes :

Géométrie : L'orientation de la pièce par rapport à l'outillage a un impact significatif sur le gradient de polymérisation. Le chauffage par convection est la principale source de chauffage dans la plupart des cuves de cuisson. Par conséquent, la chaleur appliquée à la surface

d’adhésion par convection était généralement plus efficace que le chauffage par conduction depuis l'outil. Ainsi, les orientations où la surface de liaison était en contact avec l'outil ont généralement produit un gradient de polymérisation plus favorable. Il s'agissait d'un outilllage convexe pour le raidisseur oméga, comme illustré dans la Figure 3. Cependant, isolément, l'amélioration globale était minime.

Matériau de l'outillage : Différents matériaux d'outillage influencent la redistribution de la chaleur exothermique. La combinaison de matériaux avec des diffusivités thermiques distinctes a montré des opportunités pour obtenir de meilleurs gradients de polymérisation. Dans l'exemple, un outillage avec une base en aluminium et un corps en composite pour la partie centrale s'est avéré optimal. La base en aluminium agissait comme un dissipateur thermique ; le corps en composite limitait la dissipation de la chaleur exothermique.

Coefficient de transfert thermique (HTC) : Les résultats montrent que des valeurs de HTC globales plus faibles améliorent les gradients de polymérisation, qu'ils soient favorables ou défavorables. L'effet augmentait avec l’amplitude du gradient. À condition que le gradient de polymérisation soit favorable, ce résultat indiquait la pertinence des environnements hors autoclave tels que les étuves.

Épaisseur de l'outillage : La variation de l'épaisseur de l'outil affecte le gradient de polymérisation. Différentes épaisseurs pour la base et les parties centrales des outillages, en particulier en utilisant la combinaison optimale de matériaux, ont joué un rôle important dans l'obtention de gradients de polymérisation souhaitables. L'augmentation de l'épaisseur de la base de l'outillage permettait une plus grande dissipation de la chaleur exothermique, un outillage avec une zone centrale plus mince avait l'effet inverse. Combinée aux résultats obtenus jusqu'à présent, l'ajustement de l'épaisseur de l'outillage de cette manière a donné le premier gradient de polymérisation satisfaisant.

Géométrie de l'outillage : Elle affecte la distribution de la masse thermique. Dans le cas d'un raidisseur oméga, un outillage de faible épaisseur à simple face sur la partie centrale s'est avéré plus efficace pour améliorer le gradient de polymérisation. La division de l'outil des deux côtés de la base (où se trouvait la surface d’adhésion) a été moins efficace pour utiliser la masse thermique pour dissiper la chaleur par rapport à un outil à simple face en contact direct avec la surface d’adhésion.

Tapis chauffants : L'application de tapis chauffants directement sur la partie centrale, en dehors d'une étuve, a créé d'importants gradients de polymérisation. Dans l'exemple, en

utilisant des nattes chauffantes sur la partie centrale, lorsque le matériau avait commencé à polymériser, le degré de polymérisation à la surface d'adhésion était minimal. En augmentant exclusivement la température de la partie centrale, l'ajout d'isolant sur cette partie a considérablement amélioré l'efficacité tout en maintenant le gradient de polymérisation. L'augmentation significative du degré de polymérisation de la partie centrale causée par l'isolant et l'importance de limiter cela à la partie centrale pour minimiser le degré de polymérisation de la bride sont illustrées dans la Figure 3.

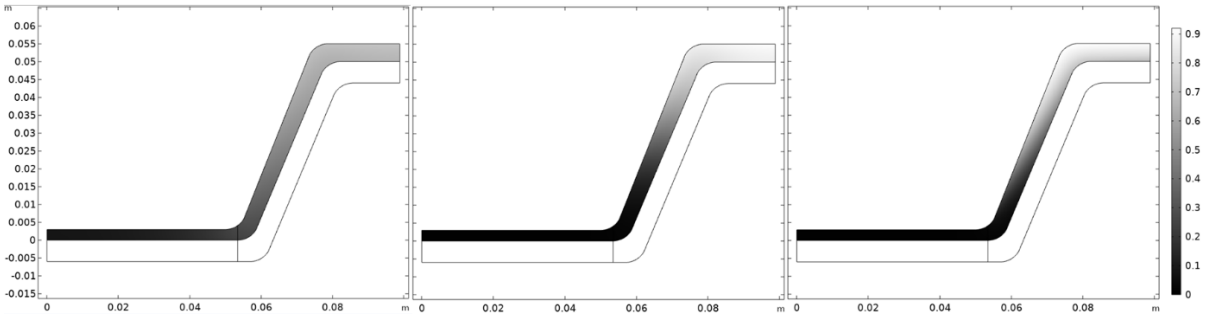

Figure 3. Répartition de la polymérisation avec des tapis chauffants au début de la gélification dans la bande avec une isolation complète (A), une isolation de la bande (B) et aucune isolation (C).

En conclusion, l'article a démontré qu'une combinaison de facteurs, tels que le matériau de l'outillage, l'épaisseur et le coefficient de transfert thermique, peut être manipulée pour obtenir des gradients de polymérisation significatifs pour un assemblage efficace, par des moyens passifs. Des gradients de polymérisation extrêmes ont été prédits en utilisant des tapis chauffants avec une isolation adéquate. L'objectif 3 a été satisfait à travers ces approches proposées.

Effet d'une pré-polymérisation sur les interfaces thermoplastiques-thermodurcissables

Pour répondre à l'objectif 4, le focus de ce lot de travail était l'effet du degré initial de polymérisation sur l'épaisseur de la couche de gel et la ténacité à la rupture dans les stratifiés thermodurcissables-thermoplastiques co-cuits. L'étude impliquait la caractérisation de stratifiés avec différents degrés initiaux de polymérisation et le développement d'un modèle de diffusion à partir de mesures de diffusion in-situ.

Les matériaux considérés étaient un stratifié thermoplastique composé de PolyEthereImide (PEI grade Ultem 1000) renforcé de tissu en fibres de carbone de type sergé 5 fils. Le second substrat était un stratifié thermodurcissable fabriqué à partir de résine époxy (Solvay EP2410)

renforcée de tissu en fibres de carbone de type sergé 5 fils. En raison du vieillissement de la résine, le degré de polymérisation avait progressé jusqu'à 0.2.

Deux des panneaux thermodurcissables ont été fabriqués par infusion de résine à chaud sous vide, suivie d'une polymérisation partielle. Après l'infusion, les panneaux ont subi une polymérisation partielle selon des profils de température spécifiques pour atteindre le degré de polymérisation ciblé. Le choix du degré de polymérisation était stratégique, avec 0.7 légèrement en dessous du point de gélification et 0.85 au-dessus.

Par la suite, les panneaux thermodurcissables partiellement polymérisés ou mi-cuits ont été assemblés avec des plaques de PEI et soumis à un processus de co-cuisson. Un film de TEFLON a servi à créer une fissure contrôlée à l'interface. Cet assemblage a ensuite été cuit selon un cycle de température dans une étuve sous bâche à vide.

Un troisième panneau a été fabriqué en une seule étape pour minimiser le degré initial de polymérisation. L'infusion a été réalisée à 120 °C pendant que le tissu en fibres de carbone était en contact avec une plaque de PEI. Après l'infusion, la température a été augmentée à 180°C puis maintenue jusqu'à la polymérisation de la résine thermodurcissable.

Pour évaluer la ténacité, des éprouvettes de Double Cantilever Beam (DCB) ont été découpées dans les panneaux co-cuits et testées. Le panneau fabriqué à partir du panneau thermodurcissable partiellement polymérisé à 0.85 a cédé avant que les éprouvettes ne puissent être fabriquées, indiquant une interaction limitée à l'interface. Les résultats avec les autres panneaux ont montré une réduction significative de l'adhésion due à l'augmentation du degré initial de polymérisation, comme indiqué dans la Figure 4.

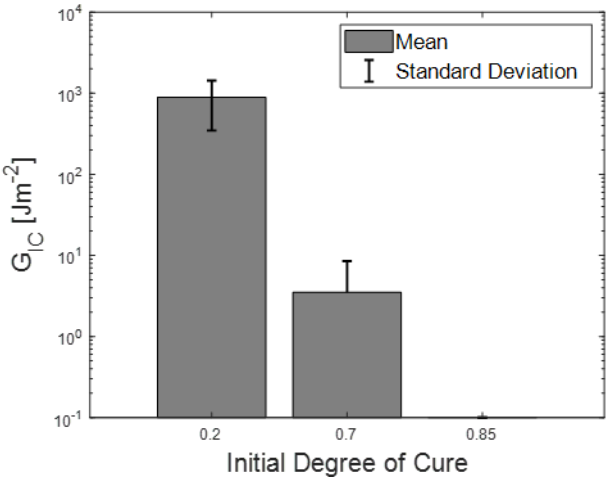

Figure 4. Résistance à la rupture interlaminaire mode 1 des échantillons IC20 et IC70.

Des échantillons de microscopie ont été préparés, impliquant le polissage. Les mesures de l'épaisseur de la couche de gel ont révélé une réduction de moitié de cette dernière avec des spécimens ayant un degré initial de polymérisation plus élevé. Les micrographies ont indiqué une morphologie plus souhaitable avec un degré initial de polymérisation plus faible et une plus grande porosité à l'interface avec un degré initial de polymérisation plus élevé. La plus grande porosité a été attribuée à la supériorité de l'infusion directe pour obtenir un contact de surface intime et à la viscosité plus élevée de la résine plus polymérisée.

Un modèle de diffusion a été créé pour prédire une tendance plus générale entre la formation de la couche de gel et le degré initial de polymérisation. Les mesures de l'épaisseur de la couche de gel issues d'expériences de microscopie en étape chaude utilisant un système époxy modèle ont servi de base pour le modèle. Le modèle de diffusion a été couplé à un modèle de cinétique de polymérisation et résolu numériquement. Une fonction en escalier a été ajoutée pour prendre en compte la fin supposée de la diffusion à la gélification.

Comme illustré dans la Figure 5 et guidé par les observations expérimentales, le modèle a suggéré qu'à la différence de la co-cuisson thermodurcissable-thermodurcissable, l'adhésion est influencée par toute augmentation du degré initial de polymérisation dans la co-cuisson thermodurcissable-thermoplastique. Sur la base de ce résultat, une semi-polymérisation du substrat thermodurcissable ne semblait pas viable. Étant donné la chute significative de l'adhésion entre les deux degrés de polymérisation initiaux et l'importance des performances mécaniques spécifiques dans les structures aérospatiales, les gains d'efficacité de production ne peuvent justifier la baisse de performance.

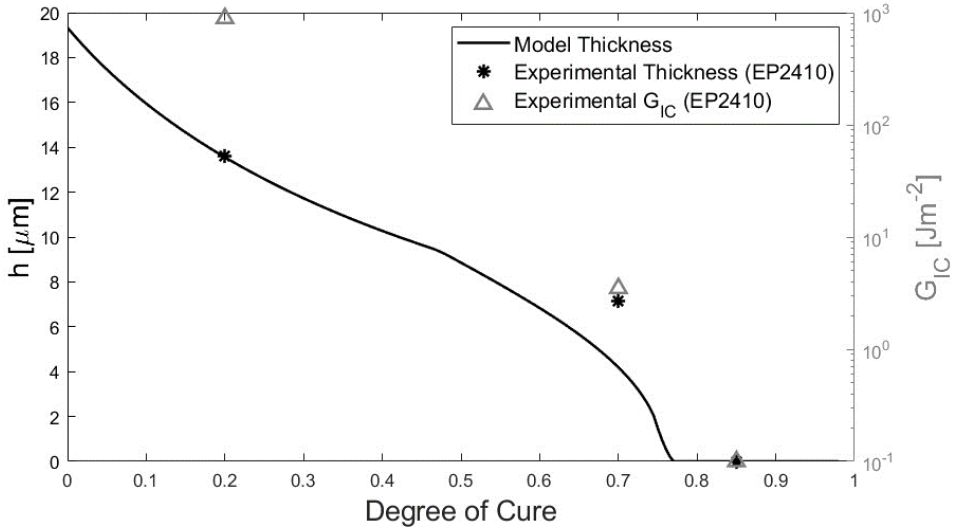

Figure 5. Épaisseur de la couche de gel avec degrés initiaux de durcissement à 180°C, prévus et mesurés.

Conclusion

Le travail discuté dans cette thèse satisfait l'objectif d'étendre la compréhension de la co-cuisson thermoplastique-thermodurcissable au niveau du stratifié.

L'influence prédominante de l'environnement thermique était une découverte clé lors de la hiérarchisation de l'influence des paramètres procédé sur la cuisson des thermodurcissables. Dans ce contexte, l'analyse de la variabilité dans une gamme de cuves industrielles a été une contribution utile pour comprendre l'incertitude dans le degré de polymérisation/semi-polymérisation. Ces conclusions préliminaires ont été appliquées à la co-cuisson thermoplastique-thermodurcissable en caractérisant l'influence du degré initial de polymérisation sur la formation de l'interface.

À partir de la variabilité mesurée dans l'environnement de polymérisation, le résultat selon lequel n'importe quel niveau de semi-polymérisation affecte négativement la formation de l'interface était important. Ce constat indiquait que la semi-polymérisation des substrats thermodurcissables avant la co-cuisson avec les thermoplastiques, pour l'efficacité de l'assemblage, n'est pas approprié étant donné l'importance des propriétés mécaniques spécifiques dans les structures aérospatiales. Ce résultat ne découle pas de la co-cuisson classique et a été le premier à prendre en compte le degré initial de polymérisation dans la co-cuisson de stratifiés thermoplastique-thermodurcissable.

Pour atténuer l'effet de la semi-polymérisation avant la co-cuisson, des concepts d'outillage et de chauffage pour des pièces semi-polymérisées avec des gradients de polymérisation favorables à la co-cuisson ont été démontrés à l'aide de simulations.

List of Publications

Journal Articles:

Chapters 3 and 4 present the following published work respectively.

1. Fisher, A., A. Levy, and J. Kratz, Effects of heat transfer coefficient variations on composite curing. Journal of Composite Materials, 2022.
2. Fisher, A., et al., The influence of key processing parameters on thermoset laminate curing. Composites Communications, 2023.

Conference Papers:

1. Fisher, A., J. Kratz, and A. Levy, Ranking the influence of key uncertainties in the curing of thermoset laminates, in 20th European Conference on Composite Materials, ECCM20. 2022: Lausanne, Switzerland.

Conferences:

1. 20th European Conference on Composite Materials, Lausanne, Switzerland, 2022
2. International Conference on Manufacturing of Advanced Composites, Online, 2021

Acknowledgements

I would like to thank my supervisors, James Kratz and Arthur Levy for the opportunity to do this project. It goes without saying this project would not have been possible without them. Their continued guidance, support, and tuition kept the project moving forward. I feel I have come a long way under their guidance, I apologise for the sheer amount of proof reading and feedback it has taken to get to this point.

The support of Arjun Radhakrishnan was invaluable, particularly his support during the experimental campaign. The latter stages of the project were made a lot easier thanks to his guidance and expertise, I only wish we had crossed paths sooner.

I am incredibly grateful to Julie Teuwen at TU Delft for the generous provision of the diffusion data that was central to the final stages of the project. In addition, her insights and willingness to answer any related questions was an enormous help.

I would like to thank my reviewer Paul Weaver for giving his time to make sure everything was going ok. Paul's advice, outside perspective and anecdotes were always immensely valuable. Without the moments of reflection offered by these annual review meetings, it would have been easy to get lost.

The BCI lab team and workshop staff were fantastic throughout the project. Their hard work in supporting all aspects of practical work is greatly appreciated.

Merci beaucoup to everybody I had the pleasure of meeting at Nantes Université. I will always treasure my time in France. Everybody was very accommodating throughout my stay, despite my pitiful efforts at learning the language.

Author’s Declaration

I declare that the work in this dissertation was carried out in accordance with the requirements of the University's *Regulations and Code of Practice for Research Degree Programmes* and that it has not been submitted for any other academic award. Except where indicated by specific reference in the text, the work is the candidate's own work. Work done in collaboration with, or with the assistance of, others, is indicated as such. Any views expressed in the dissertation are those of the author.

SIGNED: Adam Fisher DATE: 07/09/2023

Table of Contents

List of Tables

List of Figures

1 Introduction

1.1 Background and Motivation

1.1.1 Polymer Matrix Composites

Generally, polymer matrix composite materials have two main components, the matrix, and the reinforcements. Reinforcements are available in a range of forms and materials. This work considered materials for primary aerospace structures, where laminates consisting of a polymer matrix reinforced by continuous carbon fibres are common [1].

The primary function of the matrix is to distribute applied loads across the fibres to mitigate localised failure [2]. In addition, the matrix makes the material more robust by providing impact and environmental protection, geometry preservation and support to the often-brittle reinforcements. Polymer matrices can be divided into two main groups, thermosets and thermoplastics.

Thermoset polymers are initially in an unreacted state [1] and must be processed to acquire the desired properties for a composite matrix. Classically this has been done in an autoclave under applied pressure to aid consolidation [3]. More recently, the need to reduce energy consumption and accommodate larger parts has motivated the use of Out-Of-Autoclave (OOA) approaches such as vacuum bag only oven consolidation [4].

Functionality, the number of reactive groups per molecule [5], controls the crosslink density and hence stiffness, thermal stability and toughness [6]. For a given thermoset, additives and the nature of the curing reaction drive the properties of the finished product, providing numerous levers to control them [2]. The resulting versatility has contributed to the popularity of thermoset matrices.

The properties of thermoplastics are significantly influenced by crystallinity, the extent to which the polymer chains are aligned into regular, low energy configurations [1]. High performance is typically associated with crystallinity [7], with higher degrees yielding superior chemical resistance, high temperature mechanical performance and fatigue resistance.

Thermoplastics can be divided into two main groups: semi-crystalline, those in which crystallinity forms; and amorphous, those in which it does not. The term semi-crystalline is used because interference from the long molecular chains limits the achievable degree of

crystallinity [1]. Some key, often contrasting properties of thermosets and thermoplastics are presented in Table 1.1.

Table 1.1. Advantageous properties of thermoset and thermoplastic polymers [1, 7-9].

Thermosets	**Thermoplastics**
High stiffness	Excellent toughness
Low temperature and pressure processable	Solvent and chemical resistance (semi-crystalline)
Additive compatibility	Melt processable
Tacky when uncured	Fatigue resistance
Low viscosity possible	Unlimited shelf-life
Solvent resistance	Vibration dampening
Good fibre wetting	Impact resistance
Good drapability	Damage tolerance
High creep resistance	Hot/wet performance
	No cure required
	Short processing times
	Low moisture absorption
	High strain to failure
	Delamination resistance

Despite the advantages of thermoplastics, adoption has been hindered. Engineering grade thermoplastic polymers are typically more expensive than the epoxies they would replace. Furthermore, the high processing temperatures and pressures required to address the high viscosity are very energy intensive, and a lack of tack is not conducive to many established manufacturing methods, such as hand lay-up [1]. More recently there has been some niche applications such as Polyphenylene Sulfide (PPS) composite in the leading edge of the Airbus A380 and rudder and elevator of the Gulfstream 650 [10], and Polyetherimide (PEI) for 3D printed parts in the Airbus A350 XWB [11].

The processing of thermoplastics and thermosets is fundamentally different. Thermoset processing generally takes longer as the material must be cured, usually following a tailored temperature/pressure cycle. Thermoplastic processing is typically much faster, but the high viscosity demands greater temperatures and pressure.

A typical aerospace epoxy is cured at 180 °C. To be workable, amorphous thermoplastics must be heated above glass transition temperature (217 °C for PEI) and semi-crystalline materials must be melted to remove crystallinity (343 °C for Polyether ether ketone), resulting in 300-400 °C processing temperatures for aerospace grade thermoplastics [1].

1.1.2 The Need for Efficient Composite Bonding

The adoption of polymer matrix composite materials in place of metal alloys has accelerated in recent decades. Particularly those with thermoset matrices. However, the full potential of these materials is not always realised due to the use of manufacturing techniques developed for metals [12]. One area is the joining of cured thermoset composite parts, where legacy approaches slow production and compromise structural performance. Overcoming this issue is necessary to achieve the metal comparable production rates required to accommodate the booming demand.

Co-curing and co-bonding are techniques that involve the formation of bonds among thermoset polymer adherends when all and at least one is uncured respectively [13]. These provide efficient ways of bonding thermoset matrix composites during processing; however, no analogous approach exists for when all parts are fully cured.

Metal components can be joined in various ways, notably through the efficient process of welding. Thermoset matrix composites are not melt-processable, so welding is not possible. Joining is performed using, other, less optimal metal joining techniques. These methods rely on additional materials such as mechanical fasteners and adhesives for joining. Such methods have several undesirable characteristics such as labour intensiveness, additional weight, the introduction of defects and discontinuities.

A thermoplastic matrix would allow welding; however, thermoplastics are not currently used for primary aerospace structures. Thermosets are generally preferred due to superior processability, adaptability and lower material costs.

Bonding cured thermoset matrix composites through a combination with thermoplastics would bring more than efficiency benefits. A thermoplastic-thermoset hybrid composite with suitable joining could exhibit advantageous properties from both materials, opening up new applications.

If configured correctly, a hybrid thermoset-thermoplastic matrix composite could enable welding in primary aerospace structure manufacture and repair. There is potential to use a modified co-curing method to manufacture these materials. This concept has been validated, cured thermoset composite adherends have been successfully welded via thermoplastic films co-cured to the surface [14].

1.1.3 Example Applications

1.1.3.1 Offshore Wind Turbine Leading Edge Protection

The described hybrid thermoset-thermoplastic composite structures have a range of potential applications. For wind turbine fan blades, the high tip velocities from increasing blade sizes have introduced issues with leading edge erosion [15]. This occurs when the epoxy-glass composite leading edges collide with water droplets and particulates at high speed during operation. Figure 1.1 shows the stages of degradation, the main mechanism being crack propagation, facilitated by the low toughness of epoxy [16]. This erosion reduces the aerodynamic efficiency of the blades and reduces service life. Addressing this issue would have significant consequences for the levelized cost of electricity from offshore wind turbines [17], while reducing the environmental impact associated with frequent replacement [18].

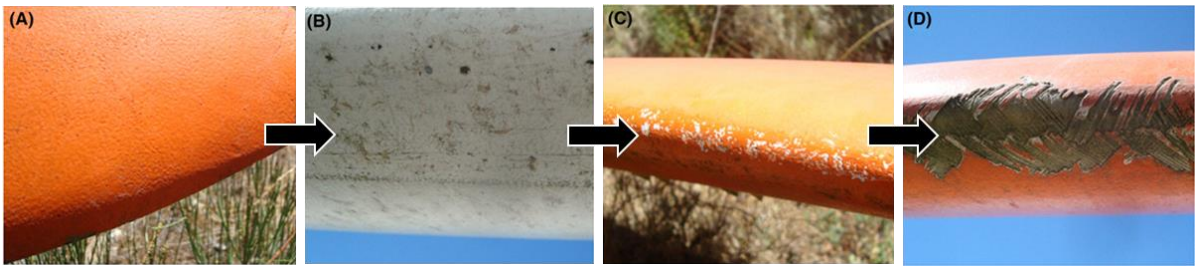

Figure 1.1. Stages of wind turbine blade leading-edge rain erosion: (A) pitting, (B) cracking, (C) cratering, (D) delamination. Adapter from [16].

Current solutions include protecting the leading edge with in-mould applied gelcoats and post-mould applied coatings, tapes and erosion shields [19]. Gelcoats are often a similar thermoset material to the blade matrix, so have poor erosion resistance [15]. Post-mould solutions are often more resistant to erosion but are more labour intensive to apply, add processing steps, are susceptible to debonding and interfere with aerodynamic performance, reducing power output [19].

Co-curing a tough thermoplastic layer to the leading edge in-mould could increase erosion resistance without compromising aerodynamics or adding processing steps [20]. The melt-processability of thermoplastics would allow the possibility of welding patches of fresh thermoplastic to eroded areas, as was successfully demonstrated for aircraft structures by the German HyPatchRepair consortium [21]. This mode of repair would likely be a significant improvement over the current use of tape, which can reduce blade performance further [22].

1.1.3.2 Attaching End Fitting to Pultruded Parts

The concept of thermoplastic-thermoset joining is used by Epsilon Composite as an efficient means of attaching end fittings to thermoset pultruded parts as shown in Figure 1.2 [23]. The

process involves over moulding, where a thermoplastic is injected at high temperature over the top of the thermoset composite tube. Efficiency comes from the few steps involved in the process, while producing a high-performance assembly. The process has benefits of lower cost, weight saving and impact tolerance over adhesive bonding, chemical fasteners and filament winding of the end feature. The absence of solvents and adhesives from the process make it more sustainable than some traditional methods. This technology has found applications in aerospace and agriculture.

Figure 1.2. Over-moulded end fittings on thermoset pultruded parts. Image by Epsilon Composites.

1.1.3.3 Aerospace Structure Joining

Mechanical fasteners, originally designed for metals, are currently used extensively for joining composites parts in aerospace manufacturing [24]. In addition to extensive heritage, mechanical fasteners provide easy assembly, tolerance to environmental damage and surface finish and help prevent delamination. However, due to the lower toughness of aerospace composites, the required holes have a more significant stress enhancing effect than with metals, compromising load carrying capacity.

The ability to join composites without fasteners is highly desirable in the aerospace industry, yielding benefits to performance and manufacturing efficiency. For context, each wing spar of the mostly composite Airbus A350XWB requires approximately 16000 holes to be drilled [24]. Given the requirement for proof that each adhesive joint will not separate at the critical design load, exclusive use of adhesive bonding has not been possible [12].

Welding has been seen as a promising alternative; this is currently limited to thermoplastic composites. Figure 1.3 shows a thermoplastic composite stringer being welded to the thermoplastic composite skin, part of the Airbus-led Multifunctional Fuselage demonstrator. However, the low penetration of thermoplastics within aerospace structures complicates widespread implementation. Given the heritage of thermosets, the welding of thermosets

through thermoplastic films co-cured to the surface (as described in Section 1.1.2) could massively increase the uptake of the joining method.

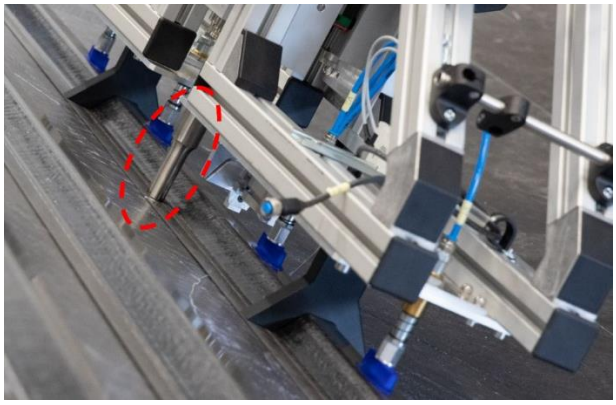

Figure 1.3. An omega stringer being conduction welded to the fuselage skin, both thermoplastic composites. Image by SAM|XL.

1.1.4 Variability in Composite Manufacturing

The interaction between adherends during thermoplastic-thermoset co-curing means the process is more sensitive to variability in the processing environment than when mechanical fasteners are used. Parameters of the processing environment such as ramp rate [25], and material parameters such as initial degree of cure [26] have been shown to have a significant influence on bond formation.

The manufacture of composite materials has complexity in both the material and the process [27]. The need to combine multiple materials together to produce a composite leads to inherently greater complexity compared to more traditional homogeneous materials, such as metals. Even in the simple case of a composite consisting of a thermoset polymer and fibres, there are many sources of variability coming from the material, layup and processing conditions, Table 1.2 present some examples listed by Potter [28].

Table 1.2. Examples of sources of variability in the material, layup and processing conditions [28].

Material parameters	Layup parameters	Processing parameters
Fibre volume fraction	Operator skill	Temperature history
Fibre wetting	Dimensional tolerance of the tooling	Temperature variation within the vessel
Voids in the resin	Tooling material	Heat transfer coefficient variation within the vessel
Matrix degree of cure	Vacuum level in bag	Pressure variation within the vessel
Matrix composition	Resin tack	
Fibre diameter	Layup thickness	
Fibre orientation	Coefficient of thermal expansion difference between part and tool	
Fibre length	Tool thickness	
Resin storage history		

These many parameters give the potential for large amounts of uncertainty and variability in the final product. To reliably produce composite parts within specified tolerances this variability must be understood and accounted for in design. However, given the large number of parameters, it is not practical to address them all, hence, to ensure resources are used most effectively, it is important to identify which have the greatest influence on the outcome.

The potential for large variability in composite manufacturing complicates the use of novel processing-based methods, particularly those which require precise process control, such the co-curing process discussed above. For example, variations in the curing conditions across the bonding interface due to non-uniform temperature, heat transfer coefficient and tool thickness, could lead to an unreliable bond.

1.2 Aim and Objectives

The aim of this work is to extend the level of understanding of co-curing between thermosets and thermoplastics from neat resins to fibre reinforced laminates. Consideration will be given to the key sources of variability when composites are processed in a vessel and how they influence the bonding process.

The process of achieving the aim can be decomposed into the following objectives:

1. Identify the most influential parameters on the curing of aerospace grade epoxy.
2. Quantify the effect of measured process variability on the curing of aerospace grade epoxy.
3. Propose manufacturing concepts to achieve the desired degree of semi-cure for co-curing.
4. Investigate the influence of degree of semi-cure on thermoplastic-thermoset interphase formation.

1.3 Novelty

1.3.1 Industrial Scale Oven Calorimeter Measurements

Industrial curing vessels are often large. This size gives significant scope for spatial variations in conditions. A non-uniform processing environment causes cure to proceed at different rates within a part, leading to defects such as residual stresses and geometric deformations. As a result, a number of studies have been performed to understand the processing environment, often using thermocouples to map the interior. Given the dominance of autoclaves for industrial curing applications, these studies have focused on autoclave environments.

The increasing demand for composites coupled with the drive for sustainability in many sectors, has put the energy demands of composite manufacturing under greater scrutiny. This movement has increased the interest in out of autoclave processing, such as the use of ovens, due to lower energy consumption [29]. Considering this, this work includes the analysis of thermocouple data from industrial ovens of a range of sizes, focusing on the level of heat transfer coefficient variability and how this compares to autoclaves.

1.3.2 Influence Hierarchy of Parameters in Aerospace-Grade Epoxy Curing

Sensitivity analysis within composite manufacturing typically focuses on a single element, such as cure kinetics [30]. This work solves for coupled heat transfer and cure kinetics through the thickness of a composite laminate, subject to an industrial cure cycle. To take a more holistic approach, parameters from the material, the part, tooling geometry, and the processing environment are considered. Furthermore, a more representative indication of parameter influence is achieved by incorporating empirical variability into the metric. Ranking the parameters according to this metric gives a more complete indicator of the most

influential variables in composite processing than is currently available. The benefit being an initial indicator as to the parameters to prioritise to most effectively optimise a process.

1.3.3 Co-Curing of Thermoplastic and Thermosets Laminates

The majority of the work on co-curing thermoplastics and thermosets has focused on the formation of the interphase. The formation process is more easily observed between neat resins, hence little research has considered the bonding between composite laminates of the two materials. Considerations of interphase formation rarely extend to the level of mechanical adhesion.

A hybrid material of thermoplastic and thermoset laminates has potential structural applications; thus, it is important that the bond between them is understood. To address this, this work focuses on the bond formation between aerospace grade thermoplastic and thermoset composite laminates, considering the level of adhesion at the interface through both microscopy of the interphase and mechanical testing.

1.3.4 Combining Semi-Curing and Thermoplastic-Thermoset "Co-Curing"

Considering laminates allows the extension of work that has been conducted, combining semi-cured thermoset laminates and co-curing. It has been found that semi-curing a thermoset adherend prior to co-curing can simplify manufacturing by increasing stiffness, without compromising the quality of the bond, providing the adherend does not undergo gelation. Extending this work to include a thermoplastic laminate adherend will show how the relationship between degree of cure and the level of adhesion compares. This will be explored through microscopic analysis and mechanical testing of the different interphases.

1.3.5 Tooling Concepts and Heating Technologies

The cure distribution of a semi-cured part optimised for co-curing is unique. For ease of assembly, it is desirable for the part to be stiff to increase handleability and minimise tool complexity. However, there must be sufficient reactivity at the bonding surface for co-curing. Therefore, unlike typical process design which targets cure uniformity [31], this work looks at tooling and heating concepts to maximise the cure gradient between the bonding surface and the rest of the part.

1.4 Thesis Structure

The research in this thesis is presented in seven Chapters. Chapters 3 and 4 are published journal articles, Chapter 5 is in a format suitable for publication and Chapter 6 is ready for submission. As depicted in Figure 1.4, each chapter addresses one of the stated objectives. The contribution of the student to the publications is stated in the preamble to the relevant chapter, following the Contributor Roles Taxonomy (CRediT). The thesis is structured as follows:

Chapter 1 – *Introduction*

Chapter 2 – *Literature Review:* Background and state of the art in topics related thermoplastic-thermoset bonding. Literature relevant to the modelling in the thesis also features.

Chapter 3 – *The Influence of Key Processing Parameters on Thermoset Laminate Curing*: A methodology is presented to identify the most influential parameters based on a metric concerning sensitivity and measured variability.

Chapter 4 - *Effects of Heat Transfer Coefficient Variations on Composite Curing*: Spatial variation in heat transfer coefficient measurements from industrial scale ovens and autoclaves are compared, and the implications on composite curing are predicted.

Chapter 5 – *Controlling the Cure Gradient Through Tool Design*: The tooling concepts and heating technologies needed to deliver a semi-cured thermoset part suitable for co-curing are considered.

Chapter 6 – *The Effect of Initial Degree of Cure on the Interphase between Thermoplastic and Thermoset laminates*: The interphase formed between thermoplastic and thermoset laminates co-cured at different degrees of cure is assessed through mechanical testing and microscopy.

Chapter 7 - *Conclusion*: The contributions are summarised and assessed in terms of the aims and objectives. Possible directions for future work to build on the presented results are suggested.

Chapter 8 - *References*

Chapter 9 – *Appendices*

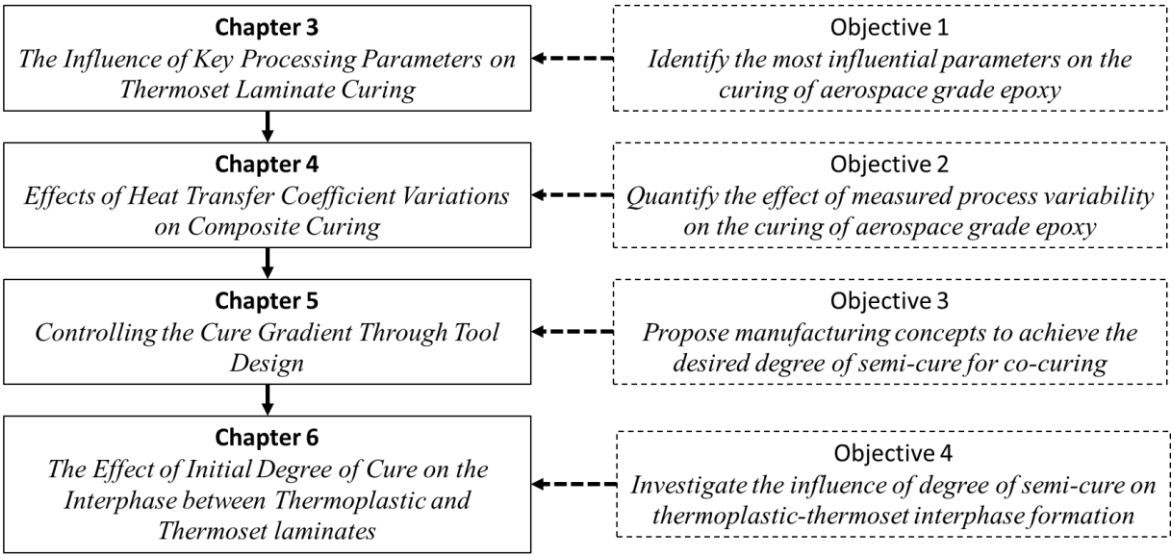

Figure 1.4. Thesis structure showing how the main content chapters relate to the objectives.

2 Literature Review

This chapter presents the literature and was solely written by the author. Firstly, thermoplastic-thermoset bonding is presented, including relevant background, details of the mechanism and resulting interphase, followed by a discussion of suitable materials. Secondly, applicable numerical modelling tools are presented. A summary identifies the gaps in existing work that need to be addressed to understand the bonding of thermoplastic and thermoset composites.

2.1 Thermoplastic-Thermoset Bonding

2.1.1 Background

2.1.1.1 Motivation and Challenges

The set of unfavourable properties that is generally characteristic of aerospace grade thermoset polymers is mostly disjoint to that of thermoplastics. This includes brittleness caused by high cross-linking density, long processing times, poor impact properties and susceptibility to high moisture absorption [5, 32]. The contrasting properties of the two types of polymers suggests that combing them could yield a composite material with an augmented set of properties compared to either of them individually. Where in a similar manner to fibre metal laminates [33], the favourable properties of one constituent off-set the undesirable properties of the other.

The central issue of this topic is the general incompatibility between thermoplastic and thermoset polymers. In the context of aerospace, this is both chemical and processing incompatibility. For example, the process temperature difference between a typical epoxy resin and PEEK is no less than 163 °C [2, 34]. At the lower end of this temperature range, the thermoplastic remains highly viscous, at the upper end, the thermoset will be thermally degraded. Hence to produce thermoplastic-thermoset hybrid matrix composite laminates a means of processing the two polymers without degrading the thermoset is crucial.

2.1.1.2 Thermoplastic-Thermoset Systems

A well-established example of combining thermoplastics and thermosets, is the use of thermoplastics as toughening agents in epoxy systems. The thermoplastic phase mitigates the significant brittleness that arises from the high degree of cross-linking needed to produce parts with high thermal stability and elastic modulus [2]. This is a significant improvement over the traditional use of rubbers, where detrimental effects such as increased water uptake and reductions in glass transition temperature (T_g), tensile strength and modulus [35, 36],

limit use in primary structures [37]. Furthermore, the toughening mechanism of thermoplastics are less dependent on matrix ductility, meaning they are still effective in high functional epoxies and other high-performance thermosets [6, 38-40]. Crucially, these systems can be cured following regular epoxy cure cycles. Although the inclusion of thermoplastics augments thermoset systems, with the thermoplastic only being around 20 %wt, thermoset properties remain dominant.

A thermoplastic-thermoset solution specific to composites is the use of interleaves, thick material interlayers between plies. Continuous thermoplastic films or particles are often used. Interleaves address the poor out of plane performance of many composite materials, with the aim to supress delamination damage caused by low energy impacts [41]. The severity of this damage was demonstrated by Byers [42], showing reductions in compression strength of 60%.

Due to the reduced proportion of prepreg, interleaving can result in lower global stiffness, strength and fibre volume fraction [41]. With a mass penalty, this can be addressed with additional plies [37]. By using discreate interleaves such as strips [43], rings [44], and grids [41] to contain rather than suppress delamination growth, post impact compressive strength can be improved with minimal reduction of global stiffness and fibre volume fraction [44]. However, discontinuous layers between plies cause fibre waviness, with the potential to degrade in-plane properties [41].

There is another possible approach. It has been shown the superior damage tolerance of thermoplastics is retained with fibre reinforcements [45]. It follows that a composite containing both thermoplastic and thermoset prepreg layers could allow more of the advantageous characteristics of both polymers to be exploited than with blends and without the dilution of favourable properties seen with interleaves. From a practical perspective, thermoplastics have been shown to display damage more clearly, making it more likely for issues to be detected during inspections [45].

2.1.1.3 Conventional Joining Techniques

Traditionally, the issue of incompatibility has been tackled by approaches that do not require chemical interaction between substates. Typically, this involved using mechanical fasteners or adhesive bonding. Both these methods are labour intensive and have a number of undesirable effects. Mechanical fasteners cause stress concentrations from broken fibres and drilled holes [46, 47], galvanic corrosion, thermally induced stress, inefficient load transfers [48] and add

mass [49]. Adhesive bonding avoids these issues; however, requires extensive surface preparation and time for adhesive curing [50]. Furthermore, the lack of a suitable failure criteria means that adhesive joints are often overdesigned and reinforced with mechanical fasteners [51]. To produce a hybrid material that leverages the favourable properties of the two materials it is necessary to identify a more suitable means of joining them.

2.1.1.4 Co-Curing

Co-curing refers to an approach to bonding thermoset substrates together. In contrast to the conventional techniques, the substrates start in an uncured state and are cured together while in contact [1]. Adhesion develops between the substrates via the chemical cross-linking mechanism taking place during cure [52], creating a fully integrated component. The key points of the process are illustrated in Figure 2.1.

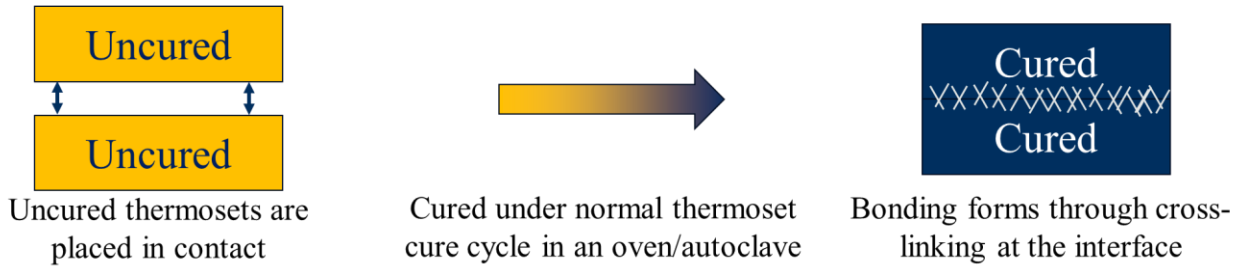

Figure 2.1. A diagram of the key stages of cure-curing.

Motsch-Eichmann et al [13] explored a modification to the co-curing process where the degree of cure of one of the thermoset adherends was increased prior to bonding. Figure 2.2 shows the stages of the modified process. The greater stiffness of this semi-cure adherend required less complex tooling. When degrees of cure between 0.6 and 0.8 were tested under Mode I loading, comparable performance to conventional co-curing was observed [53]. Short beam bending tests showed only minor decreases in apparent interlaminar shear strength until the semi-cure reaches gelation, when the value dropped sharply [13]. DCB tests suggested a similar trend for Mode I fracture toughness [13], however there was insufficient data to be confident.

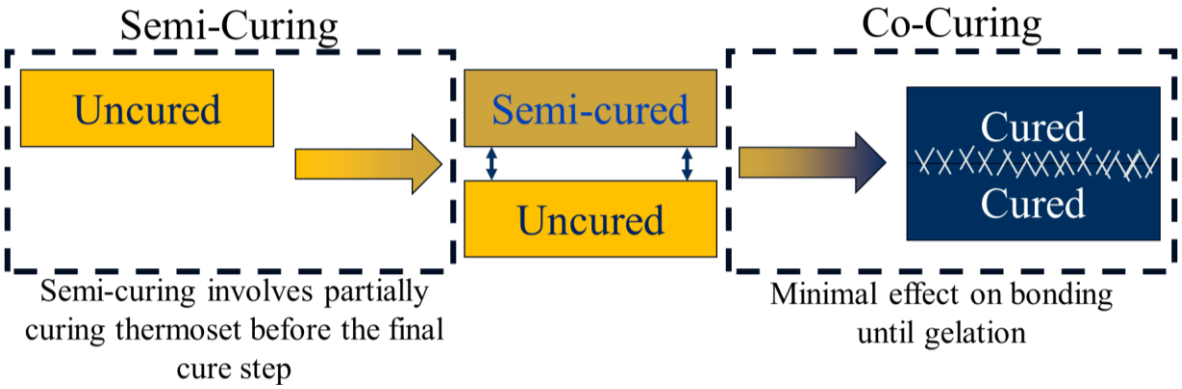

Figure 2.2. A diagram of the co-curing process with an initial semi-cure step.

2.1.1.5 Thermoplastic-Thermoset Co-Curing Analogy

The mechanism involved in thermoplastic-thermoset blends can be leveraged to adapt the co-curing process used to join uncured thermosets. Following the same procedure, including a thermoset cure cycle [54], with one of the uncured thermoset adherends replaced by a thermoplastic adherend, a bond is formed at the interface. The bonding process is analogous to the interdiffusion process in thermoplastic-thermoset blends, resulting in similar morphologies across the interphase (see Section 2.1.3.1). The key stages of thermoplastic-thermoset co-curing are presented in Figure 2.3.

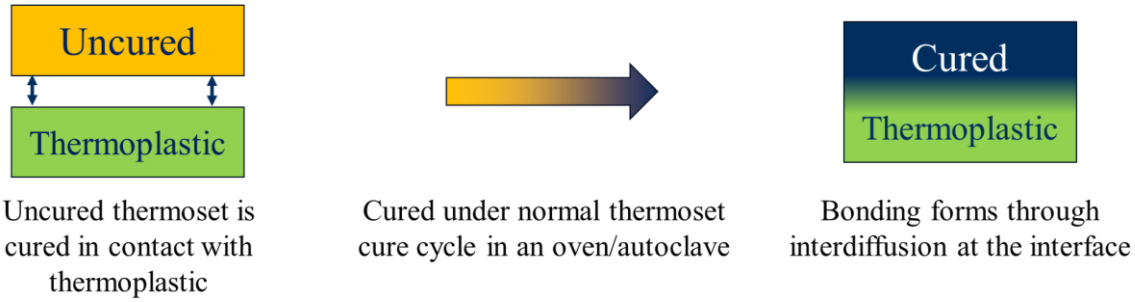

Figure 2.3. A diagram of the key stages of thermoplastic-thermoset co-curing.

The use of the modified co-curing process with a thermoplastic laminate adherend would avoid the issue of the low stiffness uncured laminate. The modified process diagram is shown in Figure 2.4. As the only low stiffness adherend, if the degree of cure of the thermoset is increased prior to co-curing, the need for complex tooling is entirely reduced. However, the trends from [13] do not necessarily apply, classical co-curing is based on cross-linking, whereas the analogy is based on inter-diffusion. In accordance with Gibbs law of mixing [55] (see Section 2.1.2), as the molecular mass of the thermoset increases with degree of cure, the miscibility that enables the thermoset-thermoplastic interaction is reduced. This was demonstrated by Lestriez et al [26] who showed a fundamental difference in the process when starting at 0.23 degree of cure compared to uncured. Villegas et al [56] cited the use of

a partially cured (B-stage) resin instead of an uncured (A-stage) resin as a reason for the large difference in interphase thickness [56] compared to Lestriez et al [26].

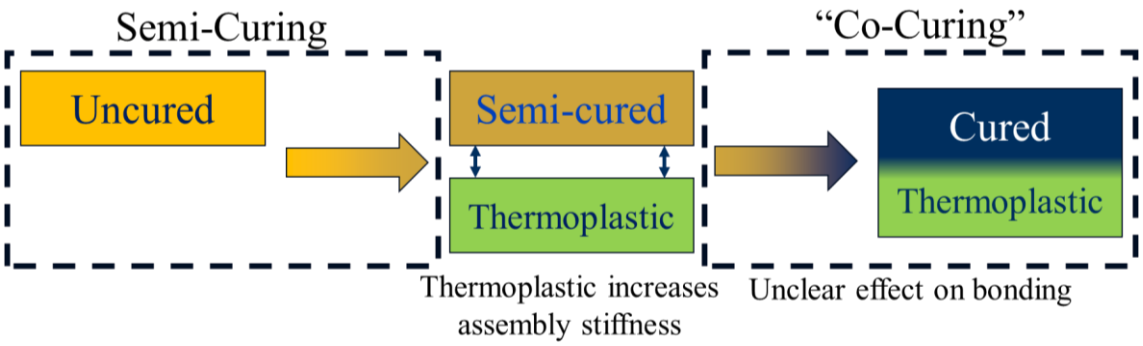

Figure 2.4. A diagram of thermoplastic-thermoset co-curing with an intial semi-cure step.

A popular application for the co-curing analogy in the literature is for attaching thermoplastic films to epoxy composite substrates. Fusion bonding between co-cured films enables welding between cured epoxy laminates, much more efficient than the traditional methods previously discussed [56-58]. Villegas et al [56] showed that thermoset adherends joined in this way have comparable lap shear strength to conventionally co-cured adherends. It was also reported that cohesive failure in the epoxy composite adherend was the dominant failure mode [56], indicating the structural merit of the thermoplastic-thermoset interface adhesion. Further studies demonstrated the level of adhesion using lap-shear and three-point bending tests, apparent shear strength and fracture toughness were shown to be comparable to high-performance aerospace structural adhesives [48, 59, 60].

This work extends the research of Lestriez et al [26] to the laminate level. Co-curing thermoset prepregs at different degrees of semi-cure with thermoplastic prepreg, to consider the feasibility of semi-curing the thermoset prepreg in thermoplastic-thermoset hybrid laminates.

2.1.2 Mechanism

The following is a description of the interdiffusion mechanism that underpins the bonding process. The description is based on the process between uncured epoxy in contact with a glassy PEI film [57]. This material combination is particularly well documented [6, 38, 58, 61-64]. The key stages of the process are summarised in Figure 2.5.

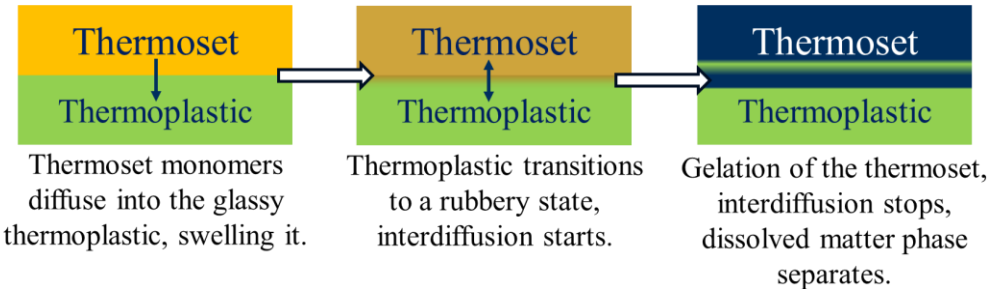

Figure 2.5. The three key stages of the thermoplastic-thermoset co-curing mechanism. The darkening of the thermoset illustrates the increasing degree of cure.

Before a penetration front is established, the local weight fraction of reactive thermoset monomers at the interface must reach a threshold level. The time for this to occur is known as the induction time. At this point the once glassy thermoplastic is sufficiently swollen for glass-to-rubber transition, followed by localised dissolution. The dissolved thermoplastic is then able to diffuse into the liquid thermoset resin. The swollen region, marked by the penetration front, advances at a constant rate into the glassy thermoplastic. The interdiffusion process continues until the thermoset reaches gelation. The gelation time dictates the time available for network formation in the polymers, a key determinant of the interphase morphology [65].

After gelation, the reduced miscibility between the now rubbery thermoset and thermoplastic causes phase separation to occur [26]. Phase separation produces a gradient morphology of the two materials across the interface, from pure thermoset on one side to pure thermoplastic on the other, this is commonly referred to as a gradient interphase [56, 57]. The final morphology of the interphase is driven by the competition between the phase separation and reaction rates [25, 61]. As with thermoplastic-thermoset blends, the morphology has a significant influence on the mechanical properties of the end product [66].

This work aims to contribute to the understanding of the interdiffusion process by testing co-cured joints involving thermoset prepreg semi-cured to points above and below gelation. Mechanical tests and microscopy shall look at the process terminating effects of gelation, including the abruptness of the onset.

2.1.2.1 Diffusion Across the Interface

The diffusion of the epoxy monomers into the glassy thermoplastic at the initiation of the bonding process can be thought of as that of a solvent into a glassy polymer [67]. The process is complicated by the need for the glassy polymer to undergo relaxation before the solvent is able to proceed [68], this takes the form of swelling in this context [63]. The rearrangement of the glassy polymer is a slow process to the extent that it inhibits diffusion,

making the process relaxation controlled [69]. This is in contrast to classical Fickian diffusion which assumes negligible relaxation times. Whereas Fick's first law states the rate of diffusion is proportional to the concentration gradient, with a constant coefficient of diffusion, the rate limiting effect of the relaxation process causes the diffusion front to proceed at a constant velocity. The observed process is therefore an example of non-Fickian diffusion (anomalous diffusion).

The observed diffusion process is often classed as Case II diffusion [68, 70]. This occurs when the composition change during interdiffusion is such that the ratio of relaxation time to the process timescale, referred to as Deborah number [71], decreases by several orders of magnitude [72]. Case II diffusion is a limiting case of anomalous diffusion that can occur during interdiffusion of polymers when one is initially glassy [73].

Case II diffusion exhibits a unique set of characteristics [68]. These characteristics are a result of the disparity between the rates of diffusion and the swelling process. The impediment of diffusion produces a sharp penetration front, behind which a region of constant solvent concentration has time to form, in front of which concentration is very low. The resulting concentration profile is described as 'step like' because of a region of low solvent concentration ahead of the sharp front, suggested by Peterlin [74] to result from Fickian diffusion across the front into the glassy polymer. The description suggests the size of this Fickian 'infiltration layer' was dependent on the velocity of the Case II front, becoming infinite in the limiting case of zero velocity i.e. diffusion is purely Fickian [74].

The contrast between Case II and Fickian diffusion is illustrated by the optical micrograph of an interphase between PEI and epoxy, produced by Zweifel et al [63], in Figure 2.6. The concentration of PEI on the left, which has followed Fickian diffusion, appears to decrease with distance away from the interface. The diffusion of epoxy on the right has the sharp penetration front characteristic of Case II diffusion.

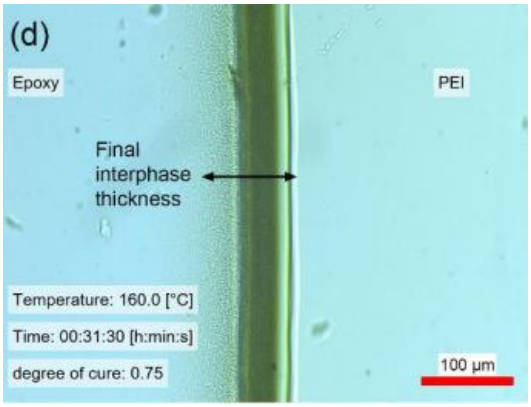

Figure 2.6. An optical micrograph of an interphase formed between epoxy and PEI during co-curing [63].

In-situ Raman spectroscopy measurements of epoxy/PEI interdiffusion, by Zweifel et al [63], shown in Figure 2.7 [63], display the increase in concentration of the diffusing species at a fixed location. The plots clearly illustrate the different diffusion characteristics between Fickian and Case II diffusion. Most notably, the rate of PEI concentration increase reduces gradually with time as the spatial concentration gradient decreases (Figure 2.7A), this is in contrast to the mostly linear progression of the sharp epoxy front observed with Case II diffusion (Figure 2.7B). With the PEI diffusion, concentration initially appeared to increase proportionally to the square root of time, characteristic of Fickian diffusion, but stopped abruptly as the epoxy cured. From a practical perspective, the less distinct penetration front makes the diffusion distance of the PEI harder to determine [63].

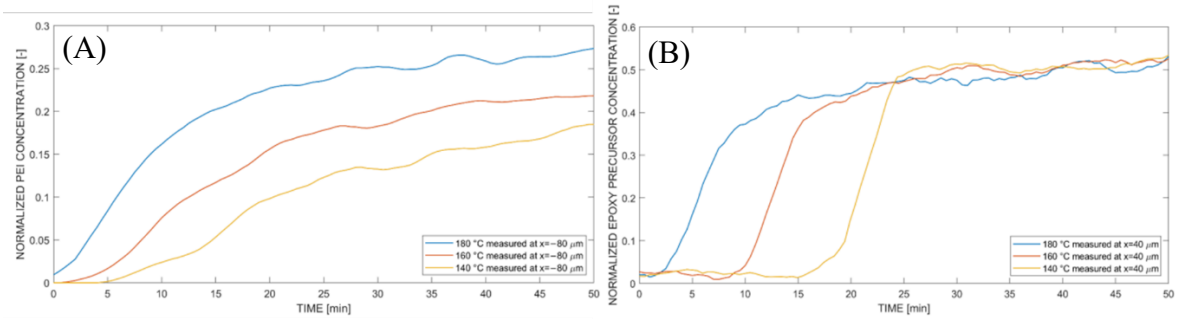

Figure 2.7. Raman Spectroscopy results showing the change in concentration with time at a fixed point with PEI diffusion into epoxy (A) and epoxy diffusion into PEI (B) [63].

The interpenetration of the phases across the interface has been identified as one of the mechanisms that improves the mechanical properties of the bonded product [54]. However, this process is complicated by the multi-component nature of epoxy systems. Epoxy systems typically consist of components with a range of molecular weights, leading to a fractionation effect [26] where the smaller molecules, aided by entropic forces [65], are able to diffuse further into the thermoplastic phase. The result being that the composition and hence the

properties of the epoxy system change across the interphase. For example, Oyama et al [54] observed that due to the lower molecular weight of Diaminodiphenyl sulfone (DDS) compared to Diglycidyl ether of bisphenol A (DGEBA), starting with a stoichiometric combination, the greater diffusivity of the DDS resulted in a range of compositions across the interphase. Consequences of lower than bulk concentrations of DDS across the interphase include increased interfacial thickness [61] due to slower rates of reaction, greater brittleness and a lower T_g, reducing the high temperature performance [54].Before consideration was given to this fractionation effect, it was assumed that for single dwell cycles the onset of phase separation indicated the termination of the diffusion process [61]. However, Voleppe et al [75] observed diffusion of the thermoset beyond phase separation for epoxy/PES, a lower critical solution temperature system. This observation was extended to upper critical solution temperature systems by Farooq et al [61] who observed it with epoxy/PEI. The continuation of epoxy diffusion after the onset of phase separation when subjected to a further, higher temperature dwell has been attributed to the fractionation effect, which results in different reaction rates across the interphase [61]. The reaction rate at the epoxy penetration front was believed to be less than the bulk value predicted by the cure kinetics model, hence epoxy in this region will have longer diffusion times [61]. The onset of phase separation has been shown to occur at higher degrees of cure as temperature increases [62], attributed to greater solubility.

As they typically consist of a single component, increasing the amount of diffusion of the thermoplastic phase involves fewer complications. It has been shown that decreasing the molecular weight of the thermoplastic increases the size of the interphase [54], however this also has the effect of reducing the T_g of the thermoplastic, lowering high temperature performance. Naturally, the reduced viscosity that results at higher temperatures results in faster diffusion [61].

By comparing co-cured joints with thermoset prepreg semi-cured to points up to and after gelation, this work illustrates the consequences of fractionations effect for bonding. This builds on current research on fractionation to consider laminates and non-zero initial degrees of cure.

2.1.2.2 Underlying Thermodynamics

2.1.2.2.1 Gibbs free energy of mixing

The underlying thermodynamics of the inter-diffusion process provide insight into the mechanisms discussed at the start of Section 1.2. Miscibility, the ability of the thermoplastic and thermoset to form a homogenous mixture, has a significant influence on the process. The basic thermodynamic relationship governing this central aspect was defined by Gibbs [55] as,

$$\Delta G_m = \Delta H_m - T\Delta S_m \tag{2.1}$$

Where ΔG_m is the Gibbs free energy of mixing, ΔH_m is enthalpic contribution, ΔS_m is the entropic contribution and T is the absolute temperature. The miscibility of a mixture is subject to two criteria:

- ΔG_m must be negative.
- $\frac{\delta^2 \Delta G}{\delta {\varphi_i}^2}$ must be positive [76], where φ_i is the volume fraction of the i^{th} component.

The terms on the right-hand side of Equation 2.1 represent the two predominant driving forces involved in reaction induced phase separation. The dominant contribution comes from the decrease in the absolute value of the entropic contribution, which decreases during cure as the molecular weight of the thermoset prepolymer species increases [2, 77]. The enthalpic contribution is less influential and can act either to advance or delay phase separation depending on the nature of the system [77].

The general relationship outlined by Gibbs was expanded upon in the Flory-Huggins equation (Equation (2.2)) [78]. On the right-hand side, the first term is the enthalpic contribution and the second is the entropic contribution [79].

$$\Delta G_m = kTV\left(\frac{\varphi_1 \varphi_2 \chi_{12}}{\upsilon_r} + \left[\frac{\varphi_1}{V_1}\ln \varphi_1 + \frac{\varphi_2}{V_2}\ln \varphi_2\right]\right) \tag{2.2}$$

Where k is the Boltzmann constant, V_i is the molecular volume of component i, V is the total volume, χ_{12} is the interaction parameter and υ_r is the interaction segment volume (reference volume e.g., that of a repeat unit).

The interaction parameter should be considered to be a function of temperature, composition and the average degree of polymerisation of the modifier [2], but unlike the entropic component the effect of molecular mass is relatively small [77]. The interaction parameter controls the enthalpic contribution, the secondary driving force of phase separation, an

increase acts to advance and a decrease acts to delay phase separation [77]. The value of the interaction parameters changes with degree of cure, in the cases of DGEBA -Methylene bis(2,6-diethyl-3-chloroaniline) (MCDEA) and DEGBA-DDS with PEI, it decreased in value [77], aiding miscibility. Additives to the epoxy system can be used to influence the interaction parameter, for example Bonnaud et al [64] found that adding the trifunctional epoxy triglycidyl para-amino phenol (TGPAP) to DGEBA/PEI and DGEBA/PES blends reduced the interaction parameter, hence improving miscibility.

2.1.2.2.2 Phase separation

The significance of viscoelastic effects during phase separation of epoxy/thermoplastic blends is such that classical descriptions of phase separation are inadequate. The viscoelastic phase separation model which assumes the final morphology to be dependent on a balance between viscoelastic and thermodynamic forces has been shown to be more suitable [65]. The different T_g and molecular weight of epoxies and thermoplastics causes dynamic asymmetry, this is where the growth of the low viscosity epoxy phase is impeded by the high viscosity thermoplastic phase, this strongly influences the final morphology [80-82].

Phase separation can occur through two different mechanisms, ‘nucleation and growth’ and ‘spinodal decomposition’. The mechanism depends on the nature of the thermoset/thermoplastic mixture and the curing conditions [39, 65, 81], both influence the final interphase morphology in a characteristic manner. Despite epoxy/thermoplastic blends being the most widely documented and hence the basis for this section, similar observation have been observed with blends containing other thermosets such as cyanate ester [39, 81] and Bismaleimide [83].

In nucleation and growth groups of isolated particles form nuclei which acquire additional volume over time through diffusion [25]. Nucleation occurs with apparent spontaneity, subsequent growth results in an irregular distribution of thermoplastic spheres in an epoxy matrix [25], referred to as a 'sea-island' morphology [35]. This is typically the phase separation mechanism that occurs in areas of low thermoplastic concentration (<10 wt%) [26, 35].

The final morphology is influenced by processing conditions and local composition. Particle size and number, and the volume fraction of the phase separated domain increase with thermoplastic concentration, while higher cure temperatures cause a reduction in particle size

but an increase in particle number [35]. The former simply being a consequence of there being more thermoplastic present in the system, in the latter the enlargement and coalescence of particles is limited by the increased polymerisation rate of the epoxy [35].

The characteristic sea-island morphology is poor at enhancing toughness, the resulting crack branching around the highly dispersed thermoplastic phase does little to impede crack propagation [60] and produces little shear banding, indicating minimal yielding [6]. Toughness still largely comes from yielding in the resin matrix [84], similar to mechanism with rubber toughening, hence this morphology becomes less effective with increasing cross-link density [85].

In spinodal decomposition, a liquid-liquid phase transition caused by composition fluctuations [76], spinodal decomposition generally occurs in regions of higher thermoplastic concentration (>15 wt%) [35, 76]. It is characterised by a phase inverted morphology, that is concentrated spherical epoxy particles periodically dispersed in a thermoplastic matrix. Before the phase inverted morphology is achieved, there is a highly interconnected morphology referred to as being co-continuous [2]. These two characteristic morphologies are highly desirable for maximising toughness [66, 86].

A phase inverted morphology is excellent for toughening, the continuous thermoplastic phase being capable of significant deformation [84]. However, it can result in a local decrease of other properties, such as stiffness, as the highly cross-linked epoxy resin in no longer the continuous phase [87]. Furthermore, the co-continuous morphology has been shown to exhibit the lowest compressive strength, hardness, and re-hardening capacity of all the interphase morphologies.

As depicted in Figure 2.8 [25], there are generally two routes to the final morphology of interconnected globules, either they grow directly from the initial interconnected morphology or there is an intermediate stage where the droplets are able to spread out before re-joining via growth, the latter is only possible providing the viscosity is sufficiently low [25]. Phase separation is controlled by system viscosity [36, 39], with higher cure temperatures leading to fewer, larger particles due to the enhancement of coalescence, conversely, with higher viscosity and thermoplastic concentration the size of the epoxy spheres is reduced [35].

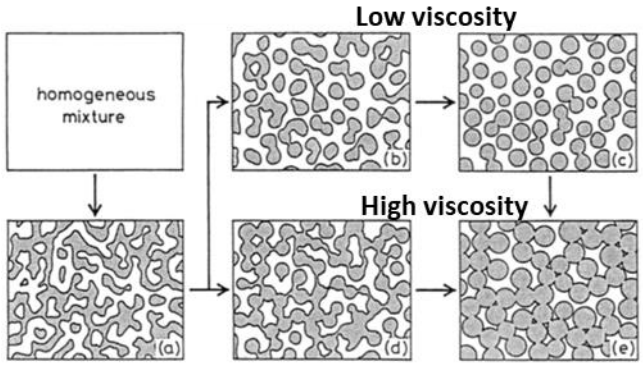

Figure 2.8. Viscosity dependant paths to interconnect morphology via spinodal decomposition [25].

2.1.2.2.3 Phase diagrams

Phase diagrams provide a tool for visualising the phase separation process. From left to right the two diagram topologies shown in Figure 2.9 are associated with Lower Critical Solution Temperature (LCST) and Upper Critical Solution Temperature (UCST) systems. The miscibility of partially soluble polymer blends with UCSTs increases with temperature, while the miscibility of those with LCSTs is higher at low temperatures. It is worth noting that the widely used epoxy/PEI mixtures have UCST characteristics [2, 64], hence they are blended at elevated temperatures. Epoxy/PES – common among thermoplastic toughened epoxy systems [47] – is a highly documented example of a mixture with LCST characteristics [25, 64, 88].

The position of the unstable region in the phase diagram is subject to change during cure, for example in UCST mixtures as cure proceeds and the molecular weight of the epoxy increases (decreasing absolute entropic contribution value), the unstable region moves into higher temperature regions of the diagram as shown in Figure. 2.10[25], therefore, under iso-thermal conditions an initially miscible system will undergo phase separation given sufficient epoxy conversion.

The initial miscibility comes from the strong favourable effects of combinatorial mixing entropy on the miscibility of small molecules, this effect is inversely proportional to molar mass, hence the reduction in miscibility as cure proceeds [65]. This decrease in the miscibility of the system as the epoxy conversion progresses means that the initial degree of cure of the epoxy system will dictate the size of the unstable region and hence the miscibility of the epoxy with the thermoplastic before curing.

When using B-stage epoxy systems, the effect of lower initial miscibility is compounded by the slowed rate of interdiffusion caused by the high initial viscosity of the thermoset, and the

reduced time to gelation, which combine to significantly reduce the extent of the interphase region. Furthermore, the dissolution process is dependent on there being low weight epoxy monomers to diffuse into and swell the thermoplastic [26], thus the maximum degree of cure is limited to where these monomers are no longer present in sufficient number. These factors provide a trade-off to stiffness for selecting the degree of cure when preforming this process with semi-cured epoxy laminates.

Phase diagrams can be used to visualise when the above-mentioned phase separation mechanisms will occur. As shown in Figure 2.9 phase diagrams contain three regions: the single-phase region, containing all the combinations of temperature and composition where the system exists as a single phase; the meta-stable region, where conditions are suited for phase separation through nucleation and growth and the unstable region, where phase separation occurs through spinodal decomposition. It is noted that the unstable region is significantly larger than the metastable region, this illustrates the fact that spinodal decomposition is generally the most likely mechanism of phase separation in thermoplastic modified thermosets [2]. Although a system usually passes through the meta-stable region in-order to get to the unstable region, the time spent there can be brief and phase separation through nucleation and growth is a slow process and is therefore often skipped [2, 25].

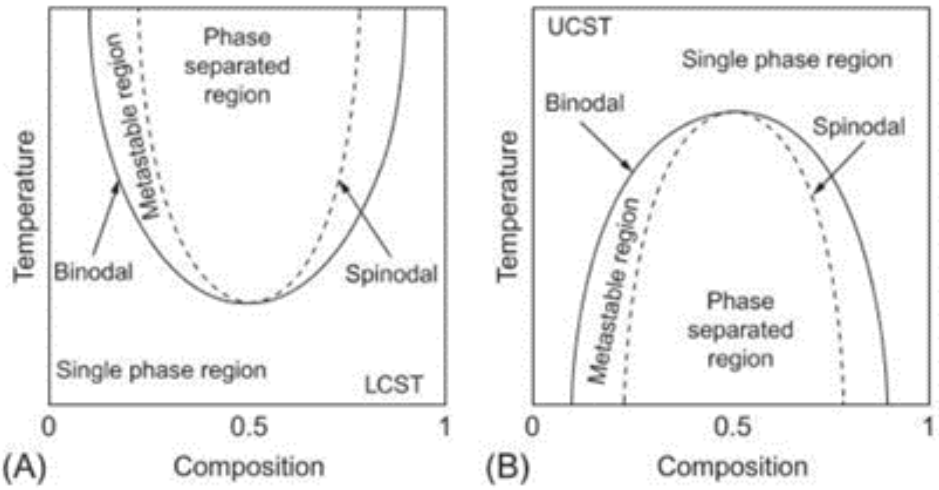

Figure 2.9. Examples of phase diagrams of partially soluble polymer blends with LCST (Left) and UCST (Right) [2].

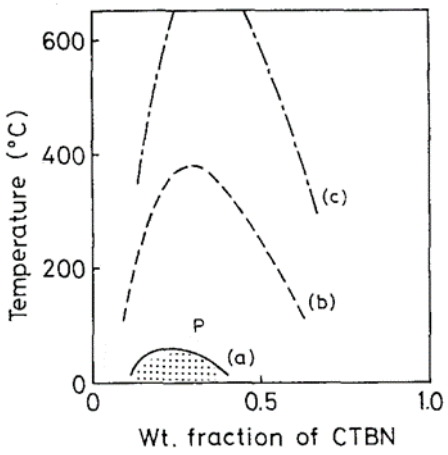

Figure 2.10. The effect of increasing epoxy molecular weight (from (a) to (b)) on the spinodal on the spinodal curve in a UCST phase diagram [25].

2.1.3 The Interphase

2.1.3.1 Morphology

Research into the nature of the interphase formed during thermoplastic-thermoset interdiffusion identified three distinct layers [89], shown in Figure 2.11. Assuming a sufficiently low initial degree of cure [26], starting from the thermoset side there is the liquid layer, gel layer and the infiltration layer. The liquid layer consists of dissolved thermoplastic that diffused into the thermoset by Fickian diffusion [63]. The gel layer contains swollen thermoplastic in a rubberlike state due to the diffusion of thermoplastic precursors. The infiltration layer is the region of farthest propagation into the thermoplastic, formed ahead of the sharp front by Fickian diffusion [74].

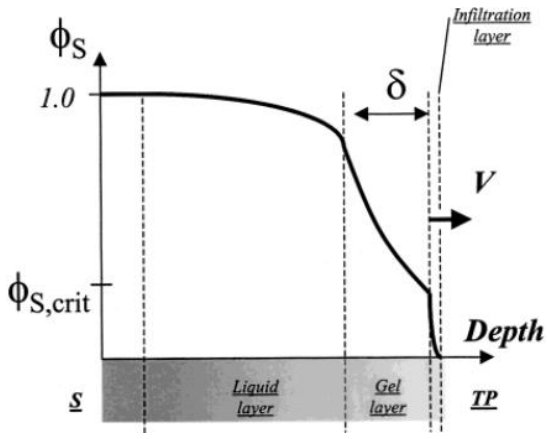

Figure 2.11. The layers that form during diffusion across a thermoplastic-thermoset interface with the corresponding normalised thermoplastic concentration [26].

A large proportion of the work on phase separation has been done in the context of thermoplastic-thermoset blends where the composition is easy to control and make spatially uniform. Although this gives insight into the morphology to expect for a given thermoplastic

concentration, joining thermoplastics and thermosets at an interface has the added complication of a concentration gradient. Given the dependence of phase separation on concentration, producing the same level of uniformity of morphology is not realisable to the same extent. The result being a range of morphologies across the interphase which is heavily influenced by the local composition [26]. The form of the final morphologies has many other dependencies that further complicate efforts to predict it, including [61]:

- Molecular structure of the thermoplastic and thermoset
- Molecular weight of the thermoplastic and thermoset
- Dwell temperature and time
- Solubility parameters of the components
- Stoichiometric ratio of curing agent to epoxies
- Curing agent chemistry and functionality
- Presence and type of accelerator

The interphases formed during interdiffusion of compatible materials are typically in the microscale [90], therefore techniques such as Scanning Electron Microscopy (SEM) and Transmission Electron Microscopy (TEM) are effective for observing the morphology [26, 56, 57].

The range of morphologies that can be present across an interphase was demonstrated by Lestriez et al [26], who bonded a PEI film with an epoxy-amine mixture. Figure 2.12 shows a TEM image of the interphase produced [26]. At the top where the PEI concentration is greatest there is a phase inverted morphology with epoxy particles (lighter phase) in a continuous PEI phase, the particles increase in size as the epoxy concentration increases. As the PEI concentration decreases the epoxy particles become entangled and the morphology becomes co-continuous [25]. Regions (a) and (b) correspond to the gel layer. At the other extreme, near the pure epoxy there is the sea island morphology that is characteristic of nucleation and growth, this is the liquid layer.

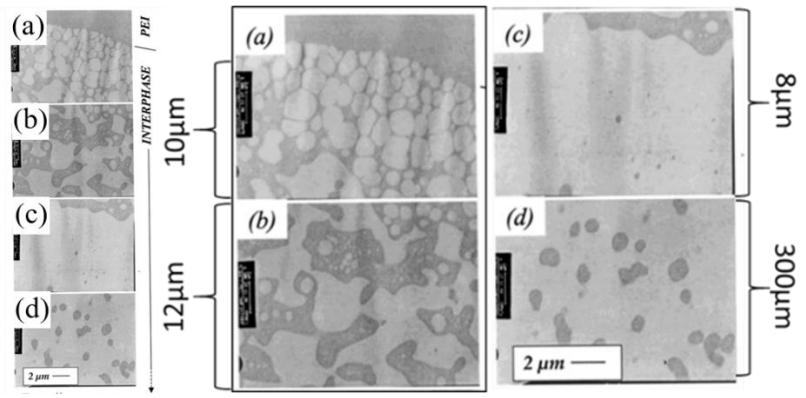

Figure 2.12. The morphology of an interphase formed by interdiffusion between an epoxy amine and PEI, in order (left) and magnified (right). Adapted from [26].

The tendency to produce a diversity of morphologies makes controlling the properties of a gradient interphase much more challenging than it is with a conventional blend. For example, in Figure 2.12 despite the effectiveness of the morphologies in (a) and (b) at impeding crack propagation, a crack would still be able to pass through the interphase largely unchecked due to the uninterrupted regions of brittle epoxy in (c) and (d). Voleppe et al [60] observed that once in the thermoplastic rich zone (a)-(b) the crack is trapped by the tougher pure thermoplastic on one side and the higher strength epoxy zone (c) on the other. This is a useful result providing the crack is initiated or migrated into the toughness part of the interphase (a)-(b).

The amount of diversity in the morphologies across an interphase can be controlled to some extent by adding the thermoplastic into the epoxy system. Villegas et al [56] bonded HexPly M18-1 epoxy prepreg, quoted as having 20 wt% PEI content with a PEI film. This raises the minimum PEI concentration above that typical for a sea island morphology. The micrograph in Figure 2.13 shows the resulting interphase has only phase inverted and co-continuous morphologies. By removing the liquid layer, this approach is effective for increasing toughness. It should be noted that of all morphologies, the co-continuous morphology was shown to produce the lowest yield strength [60].

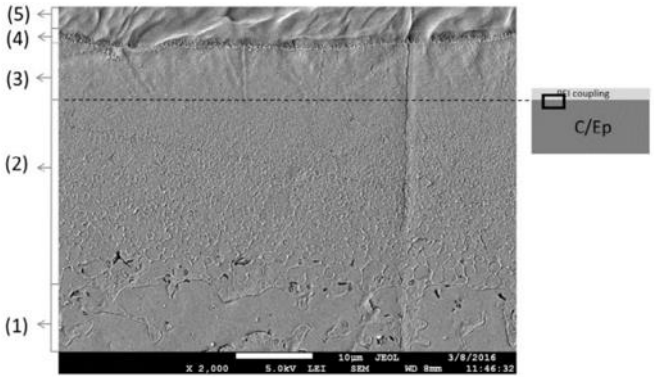

Figure 2.13. The interphase between pure PEI and a PEI toughened epoxy system [56].

Due to the dependence of diffusivity on temperature, the morphology is highly dependent on the applied temperature history. Voleppe et al [60] joined RTM6 epoxy resin with PEI thermoplastic under temperature histories with different temperature ramp rates. Faster ramp rates caused interphases with co-continuous and phase inverted morphologies. Slower ramp rates produced a sharp interface, a sea-island morphology and no evidence of PEI swelling. Due to viscosity having a greater sensitivity to temperature than reaction rate [38], with a slower temperature ramp a higher degree of cure is reached before the viscosity is sufficiently low for significant interdiffusion to occur. The difference in the resulting toughness increase between the two morphologies was marked. Compared to neat RTM6, with a high ramp rate there was 5 times increase in toughness compared to a 2 times improvement with the slower ramp rate.

2.1.3.2 Thickness

Another feature of the interphase that is subject to large amounts of variability is thickness, that is the extent to which interdiffusion has occurred. This area has been the subject of fewer studies than morphology, as it is not directly applicable to thermoplastic/thermoset blends. Generally, the final thickness of the interphase is driven by the competition between the rate of cure and phase separation [61] or the rate of cure and diffusivity [62].

The potential for variability in interphase thickness is shown by the range of values in Table 2.1, which compares results from different publications at the aerospace standard 180 °C cure temperature where possible. The examples in Figures 2.12 and 2.13 [26, 56] differ in thickness by an order of magnitude. Given that the same Ultem 1000 PEI was used in both cases, this disparity in thickness is believed to be due to processing conditions and the epoxy systems, both of which differ significantly [56].

Villegas et al [56] used a B-stage tetra-functional epoxy and Lestriez at al [26] used an A-stage di-functional epoxy. The viscosity of the higher functionality B-stage epoxy reduced the diffusion rate and the proximity to phase separation reduced the diffusion time. It was also suggested that the lower diffusion speed caused by the PEI toughening agent and the obstructing effect of the fibres in the prepreg material also contributed [56]. Another significant factor was the large difference between the cure cycle parameters, particularly time and temperature which have been shown to be highly influential over the final interphase [61, 91].

When measuring gel layer thickness between an epoxy system consisting of TGMAP, DGEBF and DDS, and PEI at different isothermal curing temperatures, Teuwen et al [62] observed a positive correlation between temperature and thickness, demonstrating thickness can be controlled through the curing process [61]. An interphase was first observed at 120 °C, thicknesses increased with temperature until peaking at 170 °C. This trend was attributed to reactivity becoming more sensitive to temperature changes than diffusivity at around 170 °C. This change was described by Farooq et al [61] as interphase thickness going from phase separation controlled to cure rate controlled. Similar observations by Brauner et al [58] between Cytec 977-2 epoxy resin and PEI supported the increase of interphase thickness with temperature, however no maximum was observed in this case, thickness increased monotonically with temperature over the 120 °C to 190 °C range considered, this was likely due to the different epoxy system.

The importance of the cure cycle and the uncertainty regarding the effect of the epoxy system is illustrated by noting results from Vandi et al [92], who observed a comparable interphase thickness to Villegas et al [56] despite using a very different, A-stage epoxy system that contained: bi-, tri- and tetra- functional epoxies, but a cure cycle that was largely the same except for the lack of applied pressure. The relevance of this comparison is increased when it is noted that Heitzmann et al [90] observed that for interphase formation, the influence of pressure during cure is negligible compared to that of the temperature profile.

Despite using an apparently identical material combination and final cure dwell, Heitzmann et al [90] produced an interphase that was a third of the thickness of that produced by Villegas et al [56] due to the reduced miscibility of the higher molecular weight epoxy [77] brought about by the inclusion of a 1-hour pre-dwell at 80 °C. Due to viscosity having a greater sensitivity to temperature than the rate of reaction, low temperature pre-dwells have been

shown to be detrimental to the final size of the interphase as the weight of the epoxy can increase significantly while a negligible amount of interdiffusion takes place [25, 38, 54, 75].

The interphase thickness measurements in this work are unique in that both the thermoset and thermoplastic are prepreg. This includes an extension of the effect of initial degree of cure on interphase thickness considered by Lestriez et al [26] to the laminate level. A model derived from hot-stage microscopy thickness measurements is used to predict the relationship between initial degree of cure and thickness.

Multiple thickness measurements are taken across the interface to give a more representative value and an indication of variability. Consideration of thickness variability has not been observed in the literature.

Table 2.1. Interphase thicknesses for a range of epoxy-PEI combinations and cure cycles.

Authors	**Cycle**	**Thermoset**	**Thermoplastic**	**Thickness (µm)**
Lestriez et al [26]	135 °C 7 hours 220 °C 2 hours 240 °C 2 hours	DGEBA - MCDEA resin	Ultem 1000 PEI film	330
Vandi et al [92]	2 °Cmin^{-1} ramp 180 °C 2 hours	TGDDM, DGEBF - DDS resin		~167
Farooq et al [61]	180 °C isothermal	TGMAP, DGEBF – DDS resin		~70
Zweifel et al [63]	180 °C isothermal	TGMAP (14%), DGEBF (50%) - DDS (36%) resin		~45
Villegas et al [56]	180 °C dwell (6 bars)	Hexply M18/1 (1/4 twill weave): TGMDA (34%), PEI (20%) - MBDA, MBIMA & DDS (34%) prepreg		30
Heitzmann et al [90]	80 °C pre-dwell 180 °C dwell (2 & 6 bars)			~10

2.1.4 Suitable Materials

2.1.4.1 Thermoplastic

Many thermoplastics are not suitable for joining with thermoset materials through interdiffusion. Tsiangou et al [57] presented two criteria a thermoplastic must fulfil to be suitable for this process, these help to guide the selection of materials. The criteria state that the thermoplastic must be at least partially soluble in the thermoplastic and have a T_g that exceeds the processing temperature [57]. The former allows the thermoplastic to be

dissolved and undergo interdiffusion with the thermoset under the action of osmotic pressure [26], the latter enables the thermoset monomers to swell and dissolve the thermoplastic.

Thermoplastics used as toughening agents in epoxy systems have proven compatibility, some common examples of these are: PEI, Polysulfone (PSU) and Polyethersulfone (PES) [35, 38, 47, 86], all of which are amorphous. Semi-crystalline thermoplastics are not suitable due to low surface polarity and crystallinity preventing dissolution into epoxy. The second criterion also points towards the suitability of amorphous thermoplastics, they are characterised by significantly higher T_g than semi-crystalline materials, for example the T_g of PEI exceeds that of PEEK by 77 °C. Crucially PEI has a T_g of 217 °C which exceeds the 180 °C temperature typically used to process aerospace grade epoxy resins. PEEK has a T_g of 140 °C, hence by the given criteria it is not suitable.

Support for these criteria can be found in the literature. Brauner et al [58] cured Cytec 977-2 epoxy with PEEK, PPS, PEI and Polyvinylidene fluoride (PVDF) at isothermal temperatures from 120 °C to 190 °C. Of these thermoplastics, only PEI is both amorphous and has a T_g above the temperature range considered. In accordance with [57], dissolution-diffusion was only identified with PEI.

In the literature related to thermoplastic-thermoset blends and bonding, PEI features significantly in combination with epoxy resins [26, 56, 57, 62, 90]. This particular material combination has been shown to be highly effective [58]. In addition to having the general amorphous properties that are advantageous for compatibility with thermosets, PEI has superior mechanical properties to the other suitable polymers for high performance applications, having been described as having similar characteristics to PEEK [47]. The chemical structure of PEI (Figure 2.14) is defined by the aromatic rings that provide excellent mechanical and thermal properties [93]. The ether linkages allow the good melt processability needed for fusion bonding, addressing a general deficiency of polyimides [93]. From the above literature review, it was clear PEI was the most suitable thermoplastic for this project.

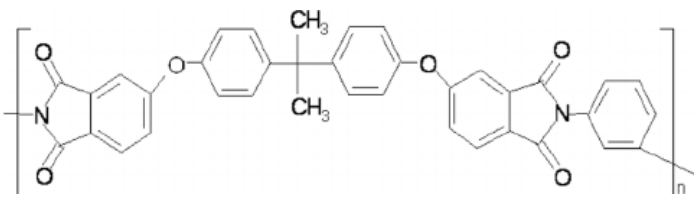

Figure 2.14. The chemical structure of Polyetherimide (PEI).

2.1.4.2 Epoxy System

The selection of an epoxy for this project was motivated by the wide usage in the supporting literature and in the aerospace industry. The versatility of epoxies provides a diverse selection of systems, previous work gave suggestions as to what makes a suitable choice.

Functionality is a key feature of an epoxy. Critically for diffusion, the viscosity of higher functional epoxies is both greater before cure and increases faster during cure [6]. The influence of epoxy functionality on interactions with thermoplastics is not well documented. Results from Ma et al [6] with epoxy/PEI suggested functionality did not affect the type of morphology for a given PEI concentration, but the size of the discontinuous phase. A higher functionality produced smaller particles, both in sea-island morphology at low PEI content (5 wt%) and phase inverted morphology at high PEI content (20 wt%). This was attributed to the greater viscosity and cross-link density of the higher functional epoxy impeding thermoplastic diffusion. The smaller particles were shown to result in lower fracture toughness due to less shear banding [6].

Curing agents can have an influence on how an epoxy system interacts with thermoplastics. A common example in this context is the contrasting effects of the two aromatic diamines MCDEA and DDS in epoxy/PEI blends. MCDEA acts to improve the compatibility with the thermoplastic, while DDS has the opposite effect [64, 94]. The result of this being, all other conditions being equal, phase separation will occur at a lower epoxy conversion with a DDS hardener than with no harder, and with no hardener than with a MCDEA hardener [64]. A complication arises from the fact that the effect of a hardener can change depending on the thermoplastic, for example in contrast to with PEI, MCDEA reduces the miscibility between epoxy and PES, causing a quicker onset of phase separation [64].

Naturally, the focus of this project on thermoplastic-thermoset adhesion required a material combination that would adhere. Stud pull testing was performed between PEI and a selection of epoxy resin systems, including: Solvay EP2410, and di-, tri- and tetrafunctional epoxies with a DDS hardener. The results indicated superior adhesion between PEI and Solvay EP2410 than with the other epoxy systems. The details of these tests are outlined in Appendix A.

Solvay EP2410 [95] was seen as a suitable choice, not only did it consistently produce the greatest adhesion with PEI, but it had prior use at the university, meaning it was readily accessible and the associated safe handling and manufacturing procedures were understood.

Furthermore, as an industrial epoxy system, results with EP2410 would be more relevant to aerospace structural applications than the model epoxy systems considered. EP2410 is a commercial resin hence the details of the chemical composition are not publicly available. Please see [95] for the safety data sheet of this resin system.

2.1.5 State of the Art Summary

Table 2.2. Key contributions to the thermoplastic-thermoset co-curing literature.

Contribution	Contributor	Summary
Diffusion is possible post the onset of phase separation.	Farooq et al [61]	Due to fractionation effects, degree of cure of diffused epoxy, is lower than the bulk.
Independent characterisation of epoxy and thermoplastic diffusion.	Zweifel et al [63]	The epoxy diffusion was Case II, the PEI diffusion was Fickian. PEI diffusion was around 2/3 of the interphase thickness. A novel combination of in-situ optical microscopy and Ramen spectroscopy was used.
Temperature has a strong influence on interphase formation between a thermoplastic and thermoset.	Teuwen et al [62]	The degree of cure at the onset of phase separation and interphase thickness increase with temperature.
Initial degree of cure affects the nature of the interdiffusion between thermoplastics and thermosets.	Lestriez et al [26]	As initial degree of cure increases, ratio of swelling rate to diffusion rate decreases. No interphase is formed at initial degrees of cure past the onset of phase separation.
Nature of crack propagation through the thermoplastic-thermoset interphase.	Voleppe et al [60]	Cracks can become trapped in the interphase by higher toughness pure thermoplastic on one side and a higher strength thermoset on the other.
Interphase thickness is reduced in a prepreg epoxy system compared to an A-stage model system	Villegas et al [56]	The smaller interphase when an epoxy prepreg was co-cured with a PEI film was attributed to the higher initial degree of cure, fibres and plasticiser
Negative effect of time at low temperature on interphase growth	Voleppe et al [60], Heitzmann et al [90]	Decreasing ramp rate or including a low temperature pre-dwell decreases thermoplastic swelling and interphase growth. Decreasing fracture toughness.

It has been shown that the interdiffusion process during thermoplastic-thermoset co-curing is dependent on multiple phenomena. Diffusion parameters such as rate, duration and termination are dependent on temperature and degree of cure. These are rooted in the transfer

of applied heat from the surroundings into and through the part, and the cure kinetics of the thermoset. To achieve a better understanding of the interdiffusion process, it is important that the interplay between these processes is understood. An established way of achieving this is through numerical modelling based on multiphysics simulation.

2.2 Numerical Modelling

2.2.1 Cure Kinetics

A cure kinetics model establishes the relationship of key parameters during the curing process. They are often empirical or mechanistic in nature. Empirical models are typical, often based on Differential Scanning Calorimetry (DSC) data via some form of regression method. Assuming suitable parameter values can be derived, these models provide a powerful tool for determining the rate of cure as a function of temperature and degree of cure. Numerous cure kinetics models have been formulated, the applicability of each to a particular curing process is dependent on the nature of the thermoset system and the cure cycle being considered [96]. The models are ordinary differential equations that are first order in time, where the required initial condition is defined as the initial degree of cure of the resin.

The simplest form of cure kinetics equation is the nth order model shown in Equation (2.3),

$$\frac{d\alpha}{dt} = k(1-\alpha)^n \tag{2.3}$$

Where α is the degree of cure, n is the reaction order and k is the reaction rate constant which is characterised by the Arrhenius temperature dependence shown in Equation (2.4).

$$k = Aexp\left(\frac{-E_a}{RT}\right) \tag{2.4}$$

Where A is the pre-exponential factor, E_a is the activation energy of the reaction, R is the universal gas constant and T is the absolute temperature. Nth order models are suited to curing processes with no autocatalytic phenomena and a simple reaction mechanism [97], especially under isothermal conditions.

Curing reactions that exhibit autocatalytic characteristics, that is the reaction products are catalysts to the curing process, require additional complexity of the model to capture this effect. Kamal and Sourour [98] achieved this through the addition of a second reaction order m as in Equation (2.5), enabling the prevalence of the different reaction mechanisms to be captured as the degree of cure advances. With $\alpha \leq 1$ and $m > 0$ the result is a rate of reaction prediction that is never greater than the nth order model with the same n.

$$\frac{d\alpha}{dt} = k\alpha^m(1-\alpha)^n \tag{2.5}$$

In reality, a large number of epoxy systems exhibit complex curing characteristics, furthermore, the majority of practical cycles contain some form of dynamic element. Consequently, characteristics captured by both the above equations are often required. For example, in an epoxy-amine system the nth order element is required to capture the complexity of the system, while the autocatalytic effects of the hydroxyl group cure products necessitate additional reaction orders [97] as in Equation (2.5). The simplest form of a combined nth order autocatalytic equation is simply the sum of Equations (2.3) and (2.4) as shown in Equation (2.6).

$$\frac{d\alpha}{dt} = (k_1 + k_2\alpha^m)(1-\alpha)^n \tag{2.6}$$

Where k_1 and k_2 are the reaction constants for the non-autocatalytic and autocatalytic reaction components respectively. This model can be extended to account for rate limiting diffusion phenomena caused by the reduced mobility of reactive functional groups post vitrification [99]. This restricted mobility of reactants inevitably leads to incomplete curing processes. Cole et al [100] defined a diffusion factor for epoxy amines to incorporate this effect which when applied to Equation (2.5) has been found to be effective at modelling curing reactions where these phenomena are present [101], this augmented equation is shown in Equation (2.7).

$$\frac{d\alpha}{dt} = \frac{(k_1 + k_2\alpha^m)(1-\alpha)^n}{1 + \exp\left(D\left(\alpha - (\alpha_{CO} + \alpha_{CT}T)\right)\right)} \tag{2.7}$$

Where D is a constant that represents the rate at which diffusion phenomena become significant, α_{CO} is the critical degree of cure at absolute zero and α_{CT} determines that rate the critical degree of cure increases with temperature. The relationship is established such that the exponential term becomes more significant with increasing degree of cure, the movement of the denominator away from unity representing the increasing influence of the diffusion-controlled effects. This model was found to provide a good representation for the cure kinetics of Solvay EP2410 [102], considered in this project.

The basic form of the combined nth order autocatalytic model can be extended to capture greater complexity by adding a third reaction order as shown in Equation (2.8). Karkanas and Partridge [96] applied Equation (2.8) to achieve a better fit to dynamic DSC data for

RTM6 after the simpler form of the combined model failed to accurately capture the latter stages of the reaction.

$$\frac{d\alpha}{dt} = k_1(1-\alpha)^{n_1} + k_2\alpha^m(1-\alpha)^{n_2} \tag{2.8}$$

Further adaptions can be made to the model to account for diffusion rate limiting phenomena, this can be achieved by including a diffusion dependent term into the rate reaction constants, making them a function of temperature and diffusion as shown in Equation (2.9).

$$\frac{1}{k_i} = \frac{1}{k_{iC}} + \frac{1}{k_D}, i = 1,2 \tag{2.9}$$

Where k_i is the reaction rate constant of the ith reaction, k_{iC} is the Arrhenius temperature dependent rate constant as defined in Equation (2.4) and k_D is the diffusion dependent rate constant defined in Equation (2.10).

$$k_D = A_D \exp\left(\frac{-E_D}{RT} - \frac{b}{f}\right) \tag{2.10}$$

Where A_D is the pre-exponential factor, E_D is the activation energy, b is a fitting constant and f the equilibrium fractional free volume given in Equation (2.11).

$$f = w\left(T - T_g\right) + g \tag{2.11}$$

Where w and g are constants and T_g is the glass transition temperature. Hence, a prediction of the cure dependence of T_g is necessary to capture diffusion control effects [97]. Di Benedetto's equation (Equation (2.12)) is typically used, assuming a one-to-one relationship with degree of cure is applicable.

$$T_g = T_{g0} + \frac{(T_{g\infty} - T_{g0})\lambda\alpha}{1-(1-\lambda)\alpha} \tag{2.12}$$

Where T_{g0} and $T_{g\infty}$ are the glass transition temperatures of the uncured and fully cured resin respectively and λ is a fitting parameter. Hexply M21 epoxy prepreg featured in this project as representative aerospace composite. Mesogitis et al [103] found this model to be capable of capturing the cure reaction of M21 under both isothermal and dynamic heating conditions.

2.2.2 Heat Transfer

Heat transfer models are generally constructed around the heat equation. The energy balance, assuming no flow of material, produces the following form of the heat equation,

$$\frac{\partial}{\partial x_i}\left(k_i \frac{\partial T}{\partial x_i}\right) + q = \rho c_p \frac{\partial T}{\partial t} \tag{2.13}$$

if the directions x_i are aligned with the conductivity tensor, k_i and $\frac{\partial T}{\partial x_i}$ are the conductivity and temperature gradient in the corresponding direction respectively, q is internal heat generation, ρ is density, c_p is specific heat capacity and $\frac{\partial T}{\partial t}$ is the heating rate. This is a parabolic partial differential equation that is first order in time and second order in space.

In composites, fibres have a significantly higher conductivity than the polymer matrix. Nonetheless, in-plane dimensions are often much greater than the thickness. Consequently, in-plane temperature gradients are often sufficiently low to assume no heat transfer in this direction. Consequently, a lot of implementations of the heat equations in this context are 1D, focusing only on transverse heat transfer [103].

The cross-linking process that takes place during the curing of thermoset materials is exothermic [5]. The low transverse conductivity of thermoset composites means that if the thickness is sufficient, heat due to these exotherms can quickly accumulate. The curing reaction is highly temperature dependent, hence the exothermic heating can drive reaction rate in a self-sustaining cycle. Therefore, to capture the process accurately it is necessary, as proposed by Loos and Springer [104], to couple the heat transfer model with the cure kinetics model. For the cure kinetics model this is naturally achieved by using the temperature values produced by the heat transfer model. To go the other way, an exotherm term can be added to the heat transfer equation, this is the product of the volumetric heat capacity and the rate of reaction. Volumetric heat latent heat can be computed as the product of total heat of reaction, resin density and resin volume fraction.

As described above, the heat transfer equation is first order in time and second order in space, thus one initial condition and two boundary conditions (in each direction) are required to solve it. The initial condition is typically a constant temperature across the thickness as this is representative of a part starting at ambient conditions. A range of boundary conditions can be defined, the Dirichlet and Neumann boundary conditions are the most common. The Dirichlet boundary condition is arguably the simplest, it can take the form of a prescribed temperature being applied directly at the boundary, for example the chosen temperature history. The Neumann boundary condition is more conducive to representing how heat is transferred at the boundary, it involves applying a flux, this can be defined using Newton's law of cooling, defined,

$$q = h(T - T_\infty) \tag{2.14}$$

where q is the heat flux exchanged at the boundary, h is the local heat transfer coefficient, T the surface temperature of the part and T_∞ is the ambient temperature. Again, the ambient temperature can be defined as the temperature history, however, the inclusion of the local heat transfer coefficient in this case enables the conditions to better reflect the conditions within the autoclave/oven.

Like the cure kinetics model, the parameters in the heat equation such as conductivity and specific heat capacity are typically derived from empirical observations. The empirical observations are used to compute fitting parameters in sub-models which enable the thermal properties in the heat transfer model to be updated as the degree of cure and temperature change.

Laser flash analysis (LFA) is often used to measure the thermal diffusivity of composites from which the thermal conductivity is derived. LFA allows the conductivity of the prepreg to be obtained during cure under isothermal conditions, capturing this degree of cure dependencies is highly desirable when modelling the curing processes. A model for thermal conductivity is obtained by fitting the measurement to an appropriate model, for example Metogitis et al [103] used multivariate regression to fit sets of isothermal LFA data to Equation (2.15).

$$K_{33} = A_{kr}T\alpha + B_{kr}\alpha + C_{kr}T + D_{kr} \tag{2.15}$$

Where A_{kr}, B_{kr}, C_{kr} and D_{kr} are the fitting parameters. The linear dependence of thermal conductivity on temperature and degree of cure assumed by this model was shown to have a good agreement with the LFA data [103].

The simplest approach to computing density of the prepreg is to use the rule of mixtures based on constant densities for the fibres and matrix, and the fibre volume fraction as shown in Equation (2.16).

$$\rho = v_f\rho_f + \left(1 - v_f\right)\rho_m \tag{2.16}$$

Where ρ_f and ρ_m are the densities of the fibres and matrix respectively and v_f is the fibre volume fraction. The main issues with this approach are that it neglects the presence of voids and does not account for changes in density or void volume fraction during the curing process. The second issue can be addressed by characterising the development of matrix density as it cures, this is made easier by the an independence from cure temperature [105].

The progression of specific heat capacity in the fibres and matrix occur differently due to the phase change that occurs in the matrix, as such two separate sub-models are often used. The heat capacity of the fibres has been shown to follow a linear relationship with temperature [106]. Away from glass transition, the specific heat capacity of the matrix can also be captured as a linear function of temperature [103]. At glass transition a step change occurs, the specific heat capacity of the matrix abruptly decreases, hence the model must also be dependent on the degree of cure [103]. The parameters of the sub-model are typically derived by fitting the appropriate equation to DSC data, Equation (2.17) is an example.

$$c_{pm} = A_{mc_p}T + B_{mc_p} + \frac{\Delta_{mc_p}}{1 + \exp\left(C_{mc_p}\left(T - T_g - s\right)\right)} \tag{2.17}$$

Where $A_{mc_p}$and B_{mc_p} are fitting parameters that capture the linear dependence away from glass transition, Δ_{mc_p}, C_{mc_p} and s refer to the strength, breadth, and temperature shift of c_{pr} around glass transition [103]. As in the cure kinetics model, T_g is computed using Di Benedetto's equation (Equation (2.12)), this is where the dependence on degree of cure is introduced. The specific heat capacities produced for each component are combined by rule of mixtures based on the fibre weight fraction, defined in Equations 2.18 and 2.19 respectively.

$$c_p = w_f c_{pf} + \left(1 - w_f\right)c_{pm} \tag{2.18}$$

$$w_f = \frac{v_f \rho_f}{\rho} \tag{2.19}$$

Where w_f is the fibre weight fraction, the other variables and constant are defined as before.

2.3 Gaps in the Literature

The significant uncertainty arising from the many sources of variability in composite manufacturing has been made apparent [27, 28]. Given the large number of sources, it would be beneficial to know which are the most influential and hence which would be the most beneficial to address. Studies have focused on specific areas such as the role of uncertainty in process induced deformations [107], or the effect of cure kinetics uncertainty on the curing process [30]. However, no study could be found that compared the influence of parameters from all aspects of the process on the curing reaction. To address this, an objective of this work is to identify the most influential parameters on epoxy curing by establishing a hierarchy based on sensitivity analyses.

Several studies have characterised the curing environment within autoclaves [108-110]. However, given the increasing use of ovens for composite curing, they must be included in an overview of curing vessels for it to be comprehensive. The current absence of oven characterisation in the literature does not support a smooth adoption of oven curing. Furthermore, the greater influence of process environment variability at lower pressures [108] makes understanding it particularly important in ovens. In addition to characterising oven curing environments, given the heritage of autoclave manufacturing, a comparison of variability in the two vessels and the effects on the curing process would be helpful for adapting established curing practices. Through combining an analysis of thermocouple measurements from industrial-scale ovens and autoclaves with a model of composite curing, this study aims to address this.

Much of the literature regarding thermoplastic-thermoset interphase formation uses neat resins and model epoxy systems. This has proven effective at characterising the interdiffusion process, however, the results produced are not directly applicable to structural usage. Most work that has used epoxy prepreg with representative, plasticiser containing systems have used thermoplastic films [56, 90, 111]. The one study to our knowledge to consider thermoplastics and thermosets laminates provided lap shear results, optical and scanning electron microphase [57]. However, it was used as a reference case, hence was not the focus of the study. Given the potential structural application of thermoplastic-thermoset structures, this scarcity in the literature motivated this work to consider interphase formation at the laminate level.

With thermoset-thermoset co-curing, semi-curing one of the adherends has been shown to increase handleability and reduce the need for complex tooling [13]. As the majority of the work on thermoplastic-thermoset co-curing has considered resins, this has been beyond the scope of most of the literature. Lestriez et al [26] presented the only direct comparison of different initial degrees of cure, however, using resins these results were limited to morphological observations. Furthermore, a model resin system was considered, hence the results were not directly applicable to industrial resins. The absence in the literature, motivated the objective to extend the work to the laminate level, thus, enabling the trade-off between adhesion and increasing initial degree of cure to aid manufacturing to be considered.

Chapter 3 Forword

A large quantity of parameters is required to capture the complexity of composite processing. However, the influence of these parameters on the process is not equal. The manufacturing process can be refined efficiently by optimising the most influential parameters. This chapter addresses Objective 1, identifying the most influential parameters on aerospace epoxy curing. This enabled later research to focus on the parameters of consequence.

Parameter variability is liable to propagate through the process, causing uncertainty in key aspects such as the time required to reach a desired degree of cure. This is problematic for the condition sensitive processes considered in this thesis. Semi-curing, where a particular degree of cure is targeted, and thermoplastic-thermoset co-curing, where the underlying interdiffusion is sensitive to material properties and process conditions. The ability to identify and mitigate the most influential parameters would be highly beneficial for the success rate of these processes.

Parameter influence can be determined numerically. Coupled cure kinetics and heat transfer models can accurately model the processing of a composite part [104]. Models have been validated for a variety of materials. Sensitivity analysis applied to these model reveals the most influential parameters. The widespread use of the Kamel and Sourour model [98] has shown many materials follow similar processes, hence the results of a sensitivity analysis have reasonable generality for similar materials.

Given the objective of this research and the abundance of existing models, there was no need develop a new model. A model validated on an aerospace composite consisting of Hexply M21 epoxy resin reinforced with IMA carbon fibres [103], was used. In addition to being relevant to aerospace materials, the completeness of the model motivated the selection. The model includes temperature and degree of cure dependent thermal conductivity and specific heat capacity and captures diffusion-controlled cure kinetics. Furthermore, the datasets used to derive the parameter values were available, allowing the variabilities to be calculated.

This chapter is based on an article published in Composites Communications [112]. As the first author, my contributions were: conceptualisation, methodology, formal analysis, Writing – original draft, Writing – review & editing, visualisation.

3 The Influence of Key Processing Parameters on Thermoset Laminate Curing

Adam Fisher[a,b] , Arthur Levy[b] , James Kratz[a,*], Arjun Radhakrishnan[a]
[a]Bristol Composites Institute, University of Bristol, Queen's Building, University Walk, Bristol BS8 1TR, United Kingdom
[b]Nantes Université, CNRS, Laboratoire de thermique et énergie de Nantes, LteN, UMR 6607, F-44000 Nantes, France
Email address: james.kratz@bristol.ac.uk

Abstract

The many uncertainties in thermoset composite laminate processing can have undesirable consequences. It is impractical to address the uncertainties individually. A methodology is introduced that ranks parameters by an influence metric to give insights into how to reduce variability in cure time most effectively. The presented example considers a range of parameters from the material, geometry, and processing conditions within a thermochemical model of a representative aerospace laminate system. Due to the nonlinearities in the process, the influence metric must include representative parameter uncertainty. In the example, dwell temperature and diffusion terms in the cure kinetics model were most influential. This was a result of a long dwell period and a post-vitrification final degree of cure.

Keywords: Thermoset laminate, curing, sensitivity analysis, variability, processing

3.1 Introduction

The demand for composite materials within the aerospace industry has exploded in recent decades, with a trend of replacing metallic primary structures with high-performance thermosetting epoxy composites. In thermoset composite processing it is common for conditions to differ from those assumed/prescribed, this can occur in both the materials and the processing environment. This variability can cause higher scrappage, reducing efficiency and increasing costs. Potter [28] introduced a taxonomy of offending variability sources, listing more than sixty that are present during composite manufacturing. Given the high number of variables identified, it may not be practical to address them all and no method was given to determine which to prioritise.

Sensitivity analysis coupled with numerical simulation provides an effective tool for determining which parameters have the most influence on a given process. Loos et al [104] showed that a thermochemical model coupling heat transfer and cure kinetics was capable of modelling composite curing. Building on these concepts, sensitivity analysis has been used on a cure kinetics model to determine which parameters to consider in more detail [103], efficiency was improved by only selecting the most influential parameters. This approach

can be extended to consider parameters of the whole process, by applying sensitivity analysis to a suitable thermochemical model.

In this study, a methodology is presented to give a qualitative indication of which parameters to prioritise to increase the robustness of thermoset laminate processing. The parameters are ranked by an influence metric, similar to sensitivity, but accounts for real-world uncertainty. Values of the metric, based on the time to reach a degree of cure, are derived from a Finite Elements (FE) solution to coupled 1-Dimensional (1D) through thickness transient heat transfer and cure kinetics equations. Uniquely, the analysis considers the influence of key parameters, from the process, the material, and the geometry on composite curing. The numerical element of the approach is demonstrated by considering a flat plate, representative of epoxy laminate processed by vacuum bag moulding in an oven. Recommendations are provided based on the results.

3.2 Method

3.2.1 Predicting Parameter Influence

The metric of influence considered the rate of change of cure time with respect to the parameters listed in Table 3.1. Where, cure time was defined as the time for a degree of cure to be passed at every location through the thickness [104]. The parameters were classified as related to the process, geometry, or material, as well as cure kinetics, conductivity, and specific heat capacity fitting parameters. To accommodate the different units among the parameters, each gradient was multiplied by the standard deviation of the corresponding parameter, giving the influence metric the units of cure time.

Using the standard deviations as the step size for the gradients, the influence metric represented parameter variability in addition to the sensitivity of cure time. Given the standard deviations were not infinitesimally small, the influence metric approximates the gradient of the secant about the nominal cure time. This corresponds to the average rate of change over the interval. By combining sensitivity and variability, the influence metric indicates the likely cure time variability each parameter will cause.

Where possible the standard deviations were derived from data available in-house or in the literature. The dwell temperature, heat transfer coefficient and ramp rate from measurements in an industrial oven [113], fibre volume fraction from acid digestion of Hexply IMA/M21 composite panels (see Appendix B), part thickness from measurements of IMA/M21 prepreg thickness [114] and the cure kinetics parameters from the fitting of Differential Scanning

Calorimeter (DSC) data [103]. The two curves created by the conductivity model when the values of the fitting parameters were simultaneously shifted by 6%, up and down, bounded 68.2% of the laser flash analysis data points used to fit the model [103], corresponding ±1 standard deviation from the mean. The same procedure was applied to the specific heat capacity fitting parameters, giving standard deviations equal to 5% of the parameter values. Manufacturer data suggested a 0.35 mm tolerance is typical for a 6 mm thick metal sheet [115], assuming a normal distribution, the standard deviation for tool thickness was derived from a distribution with a 95% confidence interval of ±0.35 mm from the mean.

An approach analogous to the central difference method, with step size equal to one standard deviation, was used to calculate the average rates of change. The matrix of influence metric values (unit corrected average rates of change) was written as,

$$\boldsymbol{S}^* = \boldsymbol{S}\boldsymbol{\sigma} \tag{3.1}$$

where **S** is the matrix of average rates of change for a given degree of cure and $\boldsymbol{\sigma}$ is a diagonal matrix containing the standard deviations. Each element of $\boldsymbol{S}^*$ took the form,

$$S_i^* = \sigma_i S_i = \sigma_i \left[\frac{t_c(\Phi_i + \sigma_i) - t_c(\Phi_i - \sigma_i)}{2\sigma_i}\right] = \frac{t_c(\Phi_i + \sigma_i) - t_c(\Phi_i - \sigma_i)}{2} \tag{3.2}$$

where t_c is the cure time, and Φ_i is the nominal parameter value. The values of Φ_i and σ_i for each parameter are shown in Table 3.1.

It should be noted that the objective of the proposed approach was to give a qualitative indication of the most influential parameters on curing. As such, techniques such as T-tests were not used to determine the statistical significance of the levels of influence observed. This decision was taken as a ranking alone provides a simplified way to determine which parameters to prioritise. Given the variety of data sources, it could be misleading to impose a quantitative influence threshold. Additionally, given the large number of parameters, it would likely be impractical to address all those above such a threshold.

To enable the influence of a large of range of parameters to be considered in a practical time frame, each parameter was considered without consideration of coupling between parameters. However, the results could be built upon to enable a more time efficient coupled analysis, limiting the scope to the parameters that have been shown to have the greater influence.

Table 3.1. Parameters with description, units, nominal values and standard deviations.

Parameter	Description	Units	Nominal Value Φ_i	Standard Deviation σ_i
A_1	Cure kinetics	s^{-1}	420615	333
E_1	Cure kinetics	$Jmol^{-1}$	78890	355
A_2	Cure kinetics	s^{-1}	57440	33
E_2	Cure kinetics	$Jmol^{-1}$	68978	1086
A_D	Cure kinetics		2.60E+20	2.80E+17
E_D	Cure kinetics	$Jmol^{-1}$	87455.74	419
m	Cure kinetics		0.6	0.0032
n_1	Cure kinetics		0.8	0.026
n_2	Cure kinetics		3.2	0.031
b	Cure kinetics		1.98	0.014
w	Cure kinetics		1.65E-04	7.40E-07
g	Cure kinetics		0.058235	3.80E-04
Dwell temperature	Process	K	453.15	5
Ramp rate	Process	$Kmin^{-1}$	2	0.16
Heat transfer coefficient	Process	$Wm^{-2}K^{-1}$	50	4
Total heat of reaction	Material	Jkg^{-1}	4.15E+05	11602
Fibre volume fraction	Material		0.6	0.008
Part thickness	Geometry	m	0.005	0.00023
Tool thickness	Geometry	m	0.006	0.00018
A	Heat capacity	$Jkg^{-1}K^{-1}$	2.9	0.15
B	Heat capacity	$Jkg^{-1}K^{-1}$	1840	92
C	Heat capacity	JK^{-1}	0.15	0.0075
Δ	Heat capacity	$Jkg^{-1}K^{-1}$	-260	-13
s	Heat capacity	°C	0.65	0.033
A_r	Conductivity	$Wm^{-1}K^{-2}$	-1.50E-03	-7.5E-05
B_r	Conductivity	$Wm^{-1}K^{-1}$	0.392	0.020
C_r	Conductivity	$Wm^{-1}K^{-2}$	-1.00E-03	-5.00E-05
D_r	Conductivity	$Wm^{-1}K^{-1}$	0.734	0.037

3.2.2 Numerical Implementation

The process of calculating the sensitivity metric was performed in Matlab using COMSOL LiveLink. For each parameter, the nominal value was shifted up and down by 1 standard deviation within a for loop. The simulation for each loop was performed in COMSOL. The cure times were produced for degrees of cure between 0 and 0.95 at intervals of 0.05 from the results by interpolation, the sensitivity metric values were computed from these cure times using Equation (3.2).

Coupled cure kinetics and transient heat transfers equations were solved in 1D using FE in COMSOL Multiphysics. The 1D assumption was based on the high conductivity of the fibres causing a much lower Biot number in-plane than through the thickness, this assumption has

been shown to produce reliable results [103, 104]. The modelled material was based on HexPly M21/IMA, a broadly representative aerospace grade epoxy prepreg, with thermoplastic interleaf, for details please see [116]. The cure kinetics for the M21/IMA prepreg with 13 fitting parameters, developed my Mesogitis et al [103], was implemented as a distributed ordinary differential equation in COMSOL. The cure kinetics model had both kinetic and diffusion terms (Equations (3.5) and (3.6)) because this specific material vitrifies, i.e., the glass transition temperature of the resin will exceed the process dwell temperature. The cure kinetics model is given in Equations (3.3) – (3.7). A non-zero value for initial degree of cure was required to escape the singular stationary point of the model; a convergence analysis showed negligible changes in cure time at values below 0.0001.

$$\frac{d\alpha}{dt} = k_1(1-\alpha)^{n_1} + k_2\alpha^m(1-\alpha)^{n_2} \tag{3.3}$$

$$\frac{1}{k_i} = \frac{1}{k_{iC}} + \frac{1}{k_D}, \qquad i = 1,2 \tag{3.4}$$

$$k_{iC} = A_i e^{\left(\frac{-E_i}{RT}\right)}, \qquad i = 1,2 \tag{3.5}$$

$$k_D = A_D e^{\left(\frac{-E_D}{RT}\right)} e^{\frac{-b}{f}} \tag{3.6}$$

$$f = w\left(T - T_g\right) + g \tag{3.7}$$

Heat transfer was modelled using the 'Heat Transfer in Solids' physics in COMSOL. The cure cycle was the recommended cycle for M21 [116], a 2 °Cmin^{-1} ramp from 20 °C to a dwell at 180 °C which continued until 95% cure. The part and tool were assumed initially to be at 20 °C. Figure 3.1 shows a schematic of a curing assembly, the dotted line highlights the simplified form assumed in the model. Under the applied vacuum, it was assumed the contact resistance between the elements was negligible. The properties of the consumables were from [117] and the thicknesses from [118]. The same convective boundary condition was applied to each end, with a heat transfer coefficient of 50 Wm^{-2}K^{-1}, representative of an industrial oven [113].

A 60% fibre volume fraction was assumed for the composite laminate. The thermal properties in the composite domain were representative of the through thickness direction. The density and specific heat capacity were homogenised using rule of mixtures according to fibre volume fraction and fibre weight fraction respectively [103]. The specific heat capacity model for the resin, with 5 fitting parameters, is shown in Equation (3.8). The thermal

conductivity model (Equation (3.9)), has 4 fitting parameters [103]. All the fitting parameter values are given in Table 3.1.

$$c_{pr} = A_{rc_p}T + B_{rc_p} + \frac{\Delta_{rc_p}}{1 + \exp\left(C_{rc_p}(T - T_g - s)\right)} \tag{3.8}$$

$$K_{33} = A_{kr}T\alpha + B_{kr}\alpha + C_{kr}T + D_{kr} \tag{3.9}$$

The described model conditions are typical of aerospace composite manufacturing. The results give an indication of the parameters likely to be most influential.

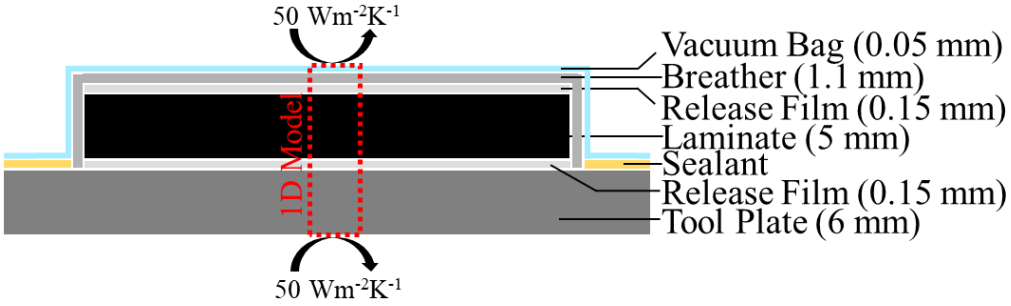

Figure 3.1. The layup schematic assumed in the Finite Elements model, including thicknesses and boundary condition.

3.3 Results and Discussion

Figure 3.2 shows how the absolute value of the influence metric depends on the final targeted degree of cure. The parameters are ranked by the absolute value of the influence metric at 0.95 degree of cure, a typical end point when targeting full cure. For clarity, the results have been separated into subplots with similar values. Presenting the metric value versus targeted degree of cure is relevant for preliminary cure steps, such as those prior to co-curing and co-bonding where the level of partial cure effects the adhesion [13, 102].

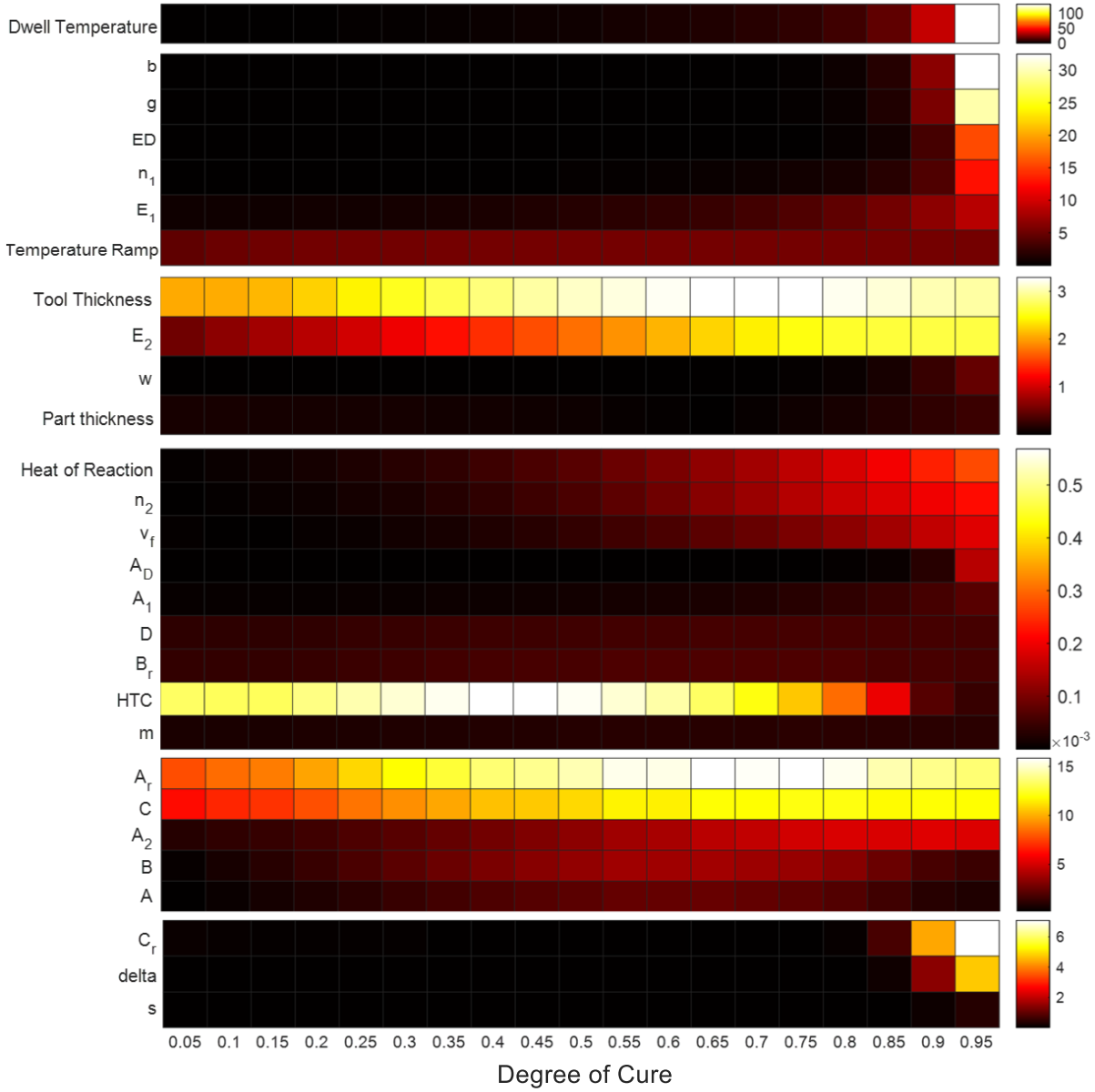

Figure 3.2. The absolute influence metric value for each parameter for degrees of cure up to 0.95. The parameters are ranked by the metric values at 0.95 cure.

Figure 3.3 focuses on the influence of dwell temperature, ramp rate and heat transfer coefficient. Dwell temperature has non-zero influence before the dwell is reached, because for a given temperature ramp rate, dwell temperature influences the duration of the ramp. The high 180 °C dwell temperature and slow 2 °Cmin^{-1} ramp rate in this example resulted in an influence that grew slowly during the initial stages of the process, but increased rapidly at high degrees of cure, as the dwell became a more significant proportion of the cure cycle. As shown in Figure 3.3, beyond a degree of cure of 0.6, dwell temperature surpasses temperature ramp rate as the dominant influence on cure time. A similar trend is expected for other aerospace grade epoxies, among which 180 °C dwell temperatures are common. For lower

temperatures or higher ramp rates, the influence metric for dwell temperature would be more significant earlier in the process.

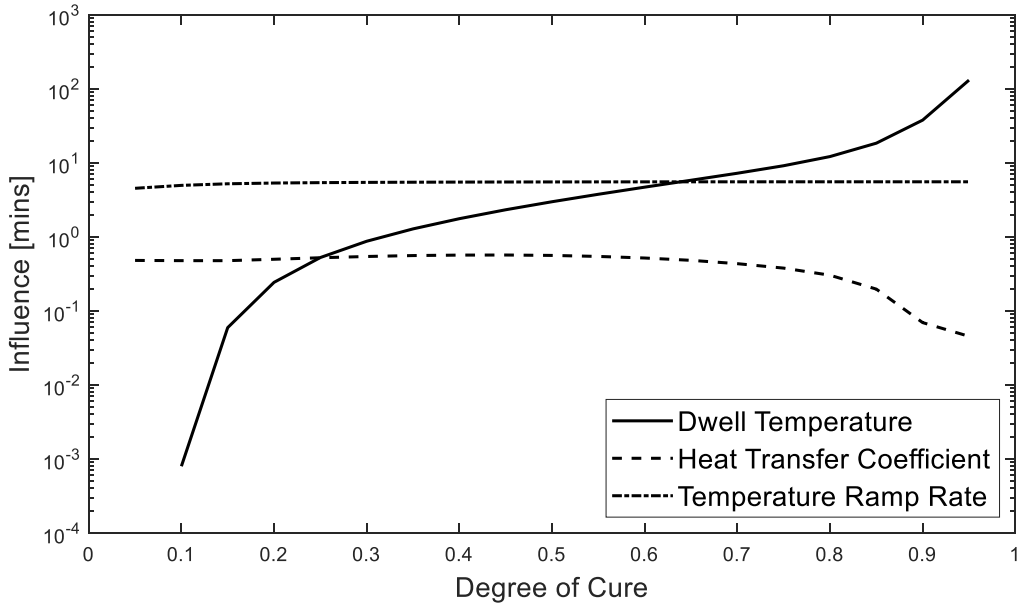

Figure 3.3. The absolute gradients values for the process parameters during the curing reaction.

Dwell temperature can be used to illustrate the need for case specific nominal values. Figure 3.4 shows that cure progresses as a sigmoid function of time, the rate starts to slow around gelation, the plateau coincides with vitrification [78], these occur at degrees of cure of approximately 0.7 and 0.9 respectively for M21 at 180 °C [103]. At a higher dwell temperature vitrification occurs earlier in the plateau, so in terms of degree of cure, cure rate remains higher for longer, as demonstrated in Figure 3.4. Therefore, for cases such as this, where final glass transition temperature exceeds the dwell temperature, the influence of dwell temperature will be large and may not be representative of the reaction pre-vitrification.

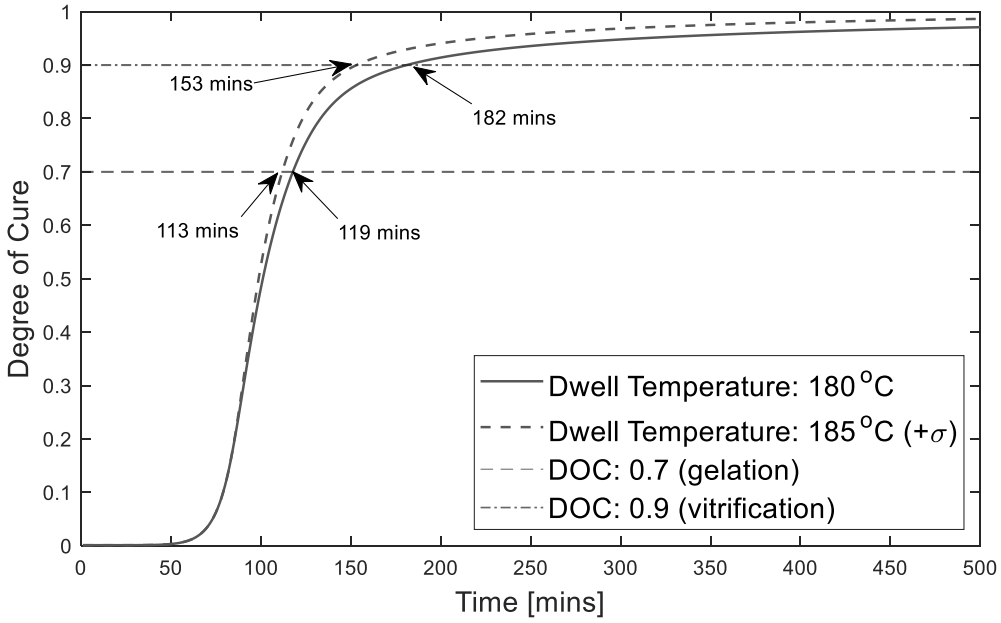

Figure 3.4. Degree of cure (DOC) with time for dwell temperatures of 180 and 185 °C. Arrows mark gel time (0.7 DOC) and vitrification time (0.9 DOC) with the two dwell temperatures.

From Figure 3.2, the influence of the cure kinetics parameters was often highly weighted towards the end of the curing reaction; therefore, the high rankings of these parameters are not applicable to all processes. As shown in Figure 3.5, this is particularly true for the parameters representing post-vitrification diffusion limiting effects (b, g, E_D). Away from a degree of cure of 0.85, the influence of diffusion limiting effects drops more sharply than reaction effects. The results indicate that although accurately characterising DSC measurements is critical for process reliability at high degrees of cure, it becomes less important away from vitrification, for this system, below a degree of cure of 0.85.

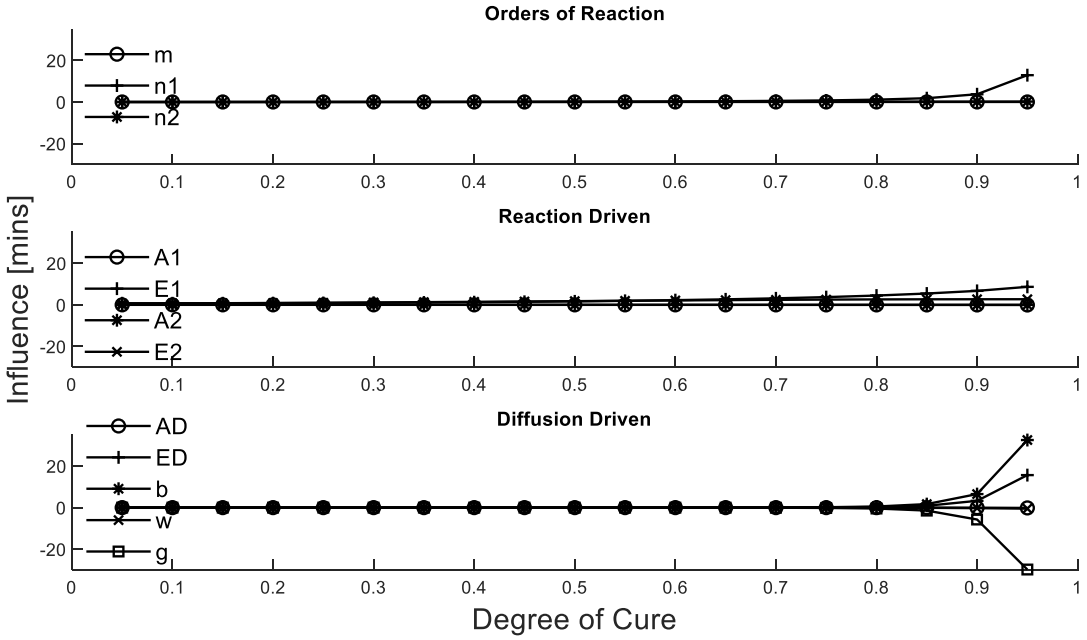

Figure 3.5. Influence metric of the cure kinetics parameters during the cure reaction.

In contrast to dwell temperature and the cure kinetics parameters, the influence of many process and geometry parameters is less concentrated towards higher degrees of cure. Hence, when only considering high degrees of cure the importance of these parameters can be overlooked. This is particularly true for heat transfer coefficient which as indicated by Figure 3.3, is only influential initially, when there is a temperature difference between the geometry and the imposed cure cycle, not applicable to the long dwell in this example. The contrasting distributions of parameter influence illustrates how the most effective parameters for reducing process variability can change with the targeted degree of cure.

3.4 Conclusion

A methodology that ranked parameters by an influence metric, based on cure time, to determine qualitatively which parameters contribute most to variability in thermoset curing processes was presented. The ranking appeared to be dependent on the final degree of cure targeted.

Based on the methodology shown here, the results from the influence study can be used to optimise design and manufacturing processes for composite curing. For example, if material properties dominate, investment in better material characterisation instruments for deriving material models and verifying incoming batches would lead to more consistent parts. If the process equipment drives variability, an oven with more uniform temperature and convection heat-transfer coefficients might be a better investment. For geometry, metrology equipment or

tighter tool tolerances might be the best approach. Based on our analysis, process equipment with temperature uniformity and repeatability is the best investment to minimise variability in curing.

Disclosure statement

The authors report there are no competing interests to declare.

Data access statement

The acid digestion data is available in the supplementary information of the published article (see Appendix B).

Funding

This work was supported by the EPSRC Future Composites Manufacturing Research Hub under Grant EP/P006701/1.

Acknowledgements

The authors wish to thank Dr Vincent Maes of the University of Bristol for proof reading and providing suggestions on formatting.

Chapter 3 Closing Remarks

By revealing the relative influence of a diversity of parameters during the curing reaction, the above work package accomplished Objective 1. The work went beyond the objective by providing a methodology to enable this result for other systems and processes.

Given the significant influence of many cure kinetics parameters in the example case, the importance of accurately characterising the curing reaction is clear. Accurately modelling the degree of cure is essential for the processes central to this thesis. Including achieving a target degree of cure in semi-curing and predicting when interdiffusion will terminate in thermoplastic-thermoset co-curing.

Whereas the cure kinetics parameters remain constant for the chosen material, the processing parameters can vary both during and between processes. Processing parameters are therefore more likely to affect the repeatability of a process adversely. Consequently, Chapters 4–6 focus on the variability of processing parameters, how prevalent they are in industrial vessels, how they can be mitigated and the potential consequence for thermoplastic-thermoset co-curing.

Chapter 4 Foreword

The hierarchy in Chapter 3 showed that dwell temperature and heat transfer coefficient have significant influence during the curing reaction. Chapter 3 discussed how in addition to sensitivity, knowledge of variability is necessary to assess influence. Motivated by these points, the work towards Objective 2, to determine the effect of measured variability, centred on the influence of the thermal environment.

Ovens and autoclaves used to process composites on industrial scales are often large. The following work characterises and compares the thermal environments of different industrial vessels. The same model of HexPly IMA/M21 composite as in Chapter 3 is used to predict the consequences of the measured variability on the processing of a composite part.

This is an article published in the Journal of Composite Materials [113]. As the first author my contributions were: conceptualisation, methodology, formal analysis, Writing – original draft, Writing – review & editing, visualisation.

4 Effects of Heat Transfer Coefficient Variations on Composite Curing

Adam Fisher[a,b] , Arthur Levy[b] , James Kratz[a,*]
[a]Bristol Composites Institute, University of Bristol, Queen's Building, University Walk, Bristol BS8 1TR, United Kingdom
[b]Nantes Université, CNRS, Laboratoire de thermique et énergie de Nantes, LteN, UMR 6607, F-44000 Nantes, France
Email address: james.kratz@bristol.ac.uk

Abstract

Composite laminates are classically manufactured by curing in a vessel. The environment inside the processing vessel dictates the efficiency and ultimately drives the quality of thermoset composite parts.

Experimental measurements of spatial heat transfer coefficients were conducted on industrial scale vessels, including autoclaves and large ovens. The final part quality was investigated using the experimental data as input to a coupled heat transfer and curing model.

Measurements showed that heat transfer coefficients in autoclaves were greater in magnitude and spatial variability. The distribution in the autoclaves followed a pattern common in the literature, in contrast to that in the ovens which varied considerably between devices.

Numerical predictions indicated autoclave measured heat transfer coefficients provide less lag to the imposed temperature history and smaller temperature overshoots. However, the greater robustness to variability at autoclave heat transfer coefficients was offset by the greater variability, resulting in comparable robustness across the ovens and autoclaves.

Keywords: Heat transfer coefficient, curing, variability, autoclave, oven, thermoset laminate.

4.1 Introduction

The central element in processing thermoset laminates is the application of heat, this triggers the curing reaction through which desirable properties are acquired. Historically, aerospace grade thermoset laminates have been processed in autoclaves, where the ability to apply a compaction pressure in addition to temperature provides superior consolidation in the final part [3]. More recently, the desire to produce larger parts with less energy and cost has motivated the use of OOA manufacturing [4]. This work focuses on vacuum bag only oven consolidation, where the available compaction pressure is limited to 1 atmosphere. As will be

discussed, the inability to apply higher pressure can have negative consequences beyond just poor consolidation.

Material manufacturers often provide a recommended set of processing conditions for a material, this will include a temperature and a pressure cycle (the latter if an autoclave is recommended). However, having the processing environment in-line with these recommendations is not sufficient for producing quality parts. In autoclaves and ovens, forced convection is typically the main source of heat transfer into a part, therefore, it also largely controls the rate of chemical and physical transformation during cure [119]. Measurements by Kluge et al [108] showed significant temperature differences across a tool in an autoclave, demonstrating the consequences of HTC variation. Through analysing large quantities of defect data, Wang et al [120] found the failure to achieve a homogeneous cure within a part can induce voids, resin rich regions, pores and delamination, and excessive temperature overshoots have also been observed [109].

The effectiveness of convective heat transfer from the vessel gas to the part is classically modelled using the convective heat transfer coefficient h_{con} (HTC). HTC is defined as;

$$h_{con} = \frac{q}{T_s - T_\infty} \tag{4.1}$$

where q is the heat flux across the boundary in $Wm^{-2}K^{-1}$, T_s is the surface temperature and T_∞ is the surrounding gas temperature.

Given the importance of convective heat transfer, studies have been conducted to understand how the value of HTC can vary within an autoclave, Ghamlouch [119] presented a comprehensive overview. This analysis routinely involves lumped mass calorimeters. The use of plate calorimeters is common, these are typically insulated at the edges to allow the assumption of 1-dimensional (1D) heat transfer, the validity of these assumptions was demonstrated by Bohne et al [121] using Finite Elements (FE). Measurements are taken using thermocouples at locations along the length of the plate. Slesinger et al [109] demonstrated that calorimeters consisting of a cylindrical metal rod could produce similar results to a plate, which is advantageous due to the much smaller size. It was through measurements made in this fashion that the connection was demonstrated between the local velocity field and the value of HTC [119, 122], the typical lack of uniformity in autoclave gas flow fields [109] explaining the large amounts of observed variability.

A number of studies have focused on providing detailed analysis of the thermal environment within autoclaves [108, 109, 123-125]. Studies mapping the distribution of HTC within an autoclave consistently found large spatial variations. For example, Slesinger et al [109] found a variation from 60 to 200 $Wm^{-2}K^{-1}$ in a 1.5 m long autoclave with a 1.15 m diameter and Bohne et al [121] found a variation from 70 to 110 $Wm^{-2}K^{-1}$ in a 2 m long autoclave with a 1 m diameter. In the study by Kluge et al [108], it was noted spatial HTC values appear to depend on the configuration of the autoclave, increasing pressure or flow velocity augments them while maintaining the existing pattern.

Autoclave layouts generally vary little from that shown in Figure 4.4.1, as such there has been an agreement between the HTC distributions reported by different studies, higher values are found at the front and decrease towards the back as the high velocity inlet air recirculates off the door and flows to the recirculating fan at the back of the vessel [119, 126]. This deduced flow pattern has been confirmed using CFD analysis [109]. Johnston [110] demonstrated the need to consider multiple devices to deduce general relationships, when one of the three autoclaves considered showed a contradictory decrease in HTC at higher pressures, this was attributed to insufficient fan power to accommodate the resulting air density increase.

Despite the increasing use of ovens for processing composites, there appears to be no analysis of the HTC distribution within ovens analogous to the autoclave examples given above. This is surprising given the lack of applied pressure causes variability in the processing environment to have more influence on the properties of the final part. This was demonstrated by Kluge et al [108], when applying the same temperature history with and without applied pressure it was found that the application of pressure significantly reduced the front-back temperature difference in the tool. The greater sensitivity of HTC to pressure compared to the temperature history in autoclaves has been widely reported [110, 121].

Motivated by this absence in the literature, the first part of this study includes the analysis of HTC in ovens. The work presented shows the dependence of HTC on internal geometry and the gas circulatory system [119]. To verify this for ovens, a range of oven sizes is considered, and particular attention is given to the influence of features such as shape, size, inlet, and exhaust locations. For comparison, the HTC distributions inside two autoclaves are also considered. Mapping the devices under the same conditions enables any common trends and differences to be identified, allowing a distinction to be made between what can be assumed to be generally applicable and what must be considered on a case-by-case basis.

The resulting properties of a part manufactured in such a vessel are linked to the mechanics during the curing process [5]. At gelation, the degree of cure (DOC) the resin transitions between a viscous and a rubbery state, there are significant changes in material properties, including shrinkage and the ability to sustain stresses [127]. For a given resin system chemistry, the time for gelation to occur depends on temperature history [2], hence temperature gradients can lead to non-uniformities through the material [128, 129]. Thus, to fully understand the effect of heat transfer variability on the final part, cure kinetics must be considered. Given the cure kinetics are driven by heat transfer in the material, a coupled approach, first proposed by Loos and Springer [104], is required to predict the phenomena.

To understand the consequence of HTC nonuniformity on the curing reaction, in the second part of this study, an FE model will be used to solve coupled heat transfer and cure kinetics equations. Laminate thickness is typically much smaller than the in-plane dimensions, enabling an efficient 1D modelling through thickness. Five indicators shall be considered to capture the influence of HTC variability on the curing process, two refer to the transverse temperature distribution in isolation, the other three take cure kinetics into account.

In consideration of heat transfer, the lag between the imposed conditions and those in the laminate, and the uniformity of conditions within the laminate shall be studied. In consideration of cure kinetics, processing efficiency, the likelihood of residual stresses, and excessive temperature will be the focus. Measured HTC data from the different vessels is used in the FE model to investigate the distinctions between curing in an oven and an autoclave.

4.2 Experimental Mapping of HTC in Ovens and Autoclaves

4.2.1 Methods

4.2.1.1 Temperature Measurements

Calorimeter measurements were taken in seven vessels: five ovens and two autoclaves. Descriptions of each vessel and the measurement conditions are provided in Table 4.1. Figure 4.1 shows examples of how measurements were taken in the ovens and autoclaves, the images demonstrate the arrays of calorimeters used to take temperature measurements at fixed sets of locations within the volumes of each vessel, apart from which they were empty. Note that although this indicated the expected level of variability within the vessels, in practice the moulds and parts will have a strong influence on the flow conditions [110], which is not captured here.

Table 4.1. Descriptions of the curing vessels studied.

Vessel	Dimensions (m)	Temperature history	Pressure Profile	Airflow Description
Oven 1	0.50x0.58x0.75			Top and bottom inlets on right, to left wall, to right wall exhaust
Oven 2	0.62x1.24x0.62			Rear left inlet to central right wall exhaust
Oven 3	1.30x1.30x1.35	Ramp: 2 ºCmin^{-1} Dwell: 155 ºC 10 min	Ambient	6 fans on rear wall, volume divided by 3 densely meshed shelves
Oven 4	20x5x5			From right wall inlets to left wall exhausts
Oven 5	5x5x5	Ramp 1: 5 ºCmin^{-1} Dwell 1: 120 ºC 30 min Ramp 2: 1 ºCmin^{-1} Dwell 2: 180 ºC 60 min		4 left inlets, 4 right inlets, to centre top exhaust
Autoclave 1	2x3	Hu Ramp: 2 ºCmin^{-1}	Ramp: 0.3 bar/min	Bottom inlet to door to rear exhaust
Autoclave 2	2.6x4.5	Dwell: 155 ºC 10 min	Dwells: 3 & 7 bars	Top and bottom inlets to door to rear exhaust

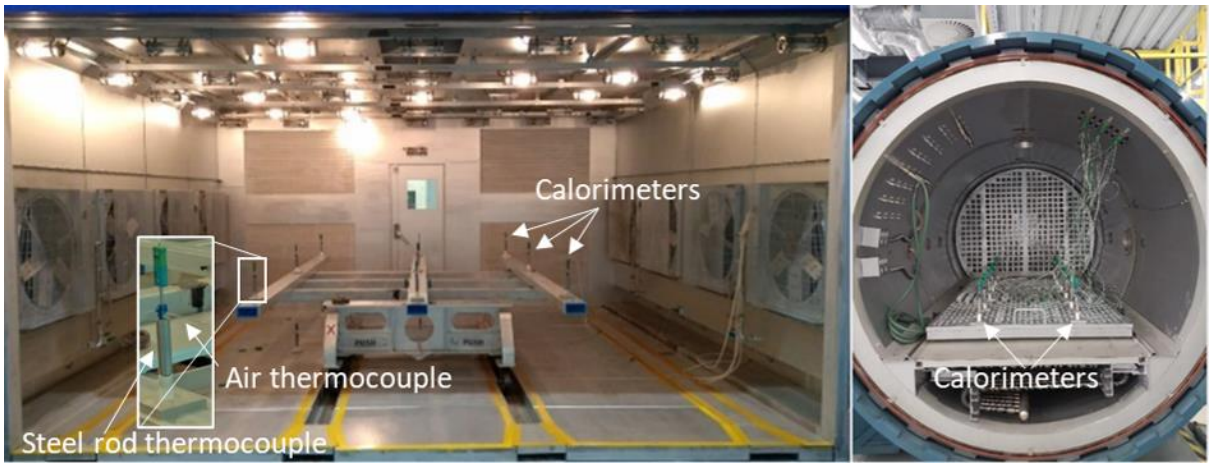

Figure 4.1. Images of two of the studied vessels, oven 5 (left) and autoclave 1 (right).

4.2.1.2 Heat Transfer Coefficient Estimation

The calorimeters, assumed to be lumped masses, consisted of two K-type thermocouples, one inside a stainless-steel 304 rod of length 0.1 m and diameter 0.025 m, the other on the outside to measure the local air temperature. The temperature measurements from the two thermocouples enabled a global calorimeter HTC to be estimated through the following procedure.

Total heat $\dot{Q}$ input in the calorimeter can be determined for a given temperature increase $\dot{T}_c$ as

$$\dot{Q} = \iiint \rho_c C_{p_c} \dot{T}_c \, dV \tag{4.2}$$

where ρ_c is the density, C_{p_c} is the specific heat capacity and T_c is temperature of the calorimeter. Temperature was considered uniform in the calorimeters, the integral became equivalent to

$$\dot{Q} = \rho_c V C_{p_c} \dot{T}_s \tag{4.3}$$

where V is the calorimeter volume and for convention, T_s is the calorimeter surface temperature. Substituting this simplified form into Equation (4.1) yielded the expression that was used to compute the HTC from the experimental data

$$h_{con} = \frac{\rho_c V C_{p_c} \dot{T}_s}{A_s (T_s - T_\infty)} \tag{4.4}$$

where A_s is the calorimeter surface area. The temperature data (T_s, T_∞) used to calculate the HTC was limited to that of the thermocouples during the ramp up. During this sliding regime, $T_s - T_\infty$ was approximately constant for all calorimeters, with the standard deviations typically around 2 ºC. The reported value of HTC for each set of calorimeter measurements was the mean of all the values computed during this period. Assuming noise to be random, this approach helped to reduce the influence of the noise from the thermocouple measurements. In the case of oven 5, the measurements from the first ramp (Table 4.1) were used due to the superior quality of the recorded data.

4.2.1.3 Validating the lumped mass assumption

Biot number is defined as

$$Bi = \frac{h_{con} l}{k} \tag{4.5}$$

where h_{con} is HTC, l and k are the characteristic length and thermal conductivity of the object. The characteristic length can be taken as the ratio of volume to surface area, for a cylinder this is equal to half the radius. The horizontal surfaces of the cylinders were partially obscured, to be conservative, they were not accounted for. The cylinders had radii of 0.0125m and thermal conductivities of 14 $Wm^{-1}K^{-1}$, this gave a Biot number of roughly $0.00045h_{con}$. For Biot numbers below 0.1 a uniform temperature assumption is valid [130]. This gave a maximum allowable HTC of 224 $Wm^{-2}K^{-1}$. Given the greatest measured HTCs of 203 $Wm^{-2}K^{-1}$ and 62 $Wm^{-2}K^{-1}$ in the autoclaves and ovens respectively, the assumption was valid in both vessels.

4.2.1.4 Checking for Negligible Radiative Heat Transfer

Radiative heat transfer is computed according to the Stefan-Boltzmann law of radiation

$$q_{rad} = \varepsilon\sigma\left({T_{wall}}^4 - {T_{cal}}^4\right) \tag{4.6}$$

where q_{rad} is the heat flux into the calorimeter, ε is the calorimeter emissivity, T_{cal} and T_{wall} are the temperatures of the calorimeter and wall respectively, and σ is the Stefan-Boltzmann constant. When the mean (T_m) of T_{cal} and T_{wall} is much greater than the difference between them (ΔT) (i.e. $(\Delta T/T_m)^2/4 \ll 1$), which is the case here, Equation (4.6) can be linearised into the same form as Equation (4.1) [131]. As the calorimeters are much smaller than the vessels, the view factor can be omitted and the resulting coefficient of radiative heat transfer writes

$$h_{rad} = 4\sigma T_m^3 \varepsilon \tag{4.7}$$

The calorimeters were stainless steel 304 which has emissivity between 0.32-0.38 [132, 133]. To be conservative, the upper bound, $\varepsilon = 0.38$, was assumed.

To be conservative, T_{wall} was assumed equal to the air temperature. The ratio of h_{con} to h_{rad} was between 3 and 15 in the ovens and between 160 to 650 in the autoclaves. In line with the literature for similar ratios [134], it was deemed acceptable to assume h_{con} was the sole contribution to HTC (h) in both sets of vessels.

4.2.2 Experimental Results

4.2.2.1 HTC Variability Between the Vessels

The temperature and pressure dependence of HTC in turbulent flow is [110]:

$$h \propto \left(\frac{p}{T}\right)^{\frac{4}{5}} \tag{4.8}$$

This indicates the results from oven 5 are not directly comparable to the others due to the different temperature history used, they are included as a further example. Conversely, literature [110, 121] suggests when the relative change in pressure is much greater than temperature, as in the autoclave cycles, HTC can be approximated solely as a linear function of pressure, the dependence on temperature and heating rate being minor.

The measured HTC values in addition to data from Slesinger [109] are summarised in Figure 4.2, the plotted values are the means, and the error bars represent the standard deviations taken over the calorimeters in each vessel. The error bars at 1 and 7 bars represent the standard deviation of HTC for all the vessels at these pressures to aid visualisation. The pressure dependence of HTC described in Equation (4.8) is shown to follow the general trend of the measurements. A fitting coefficient of 29.3 was found to minimise the mean squared error between Equation (4.8) and the measurements.

The results showed little difference between the mean HTC in each trial for all vessels. This result reflects the conclusions from autoclave measurements in the literature which showed little change under constant pressure [121]. Run-to-run variability is lowest in the ovens followed by the autoclaves at 3 and 3.5 bars. In all autoclaves the run-to-run difference increased at 7 bars. This trend can be interpreted using the link between the gas flow and HTC. Air density increases with pressure, Reynolds number is proportional to density, therefore, the less repeatable HTC distributions at elevated pressure result from greater turbulence in the gas flow.

The effect of applied pressure is clear when the mean HTC values from the ovens are compared with those from the autoclaves. The autoclaves have greater values in all cases, particularly when operated at 7 bars. This trend is to be expected given Equation (4.8); however, the results suggest this relationship has a tendency to overpredict the influence of pressure. When scaled accordingly, the HTC predicted for the oven data consistently exceeded the values measured in the autoclaves, indicating the presence of other influential factors, for example the more significant radiative contribution to the oven measured HTC. The greater HTC in the large ovens is likely due to more powerful gas circulatory systems providing higher air speeds.

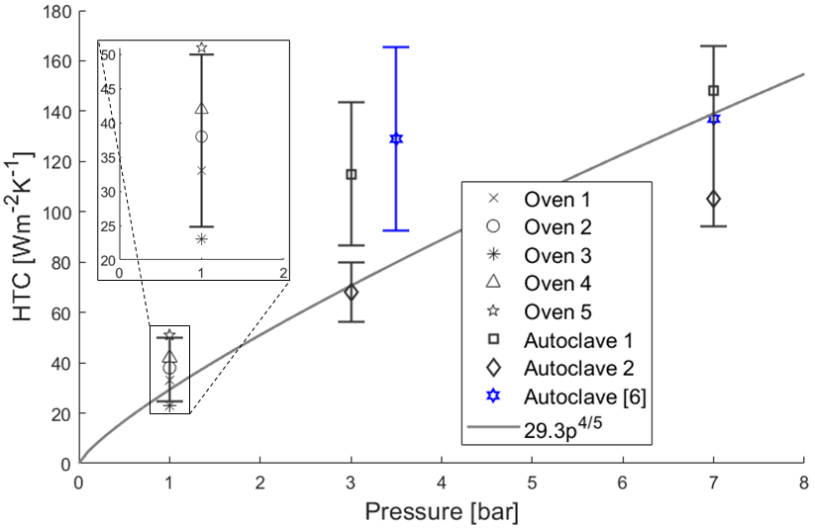

Figure 4.2. Spatial means of HTC measurements in each vessel during the two trials along with autoclave data from Slesinger [109]. Equation (4.8) model fit is also plotted. The error bars signify the standard deviations of the measurements. At 1 and 7 bars respectively, the error bar is the standard deviation of all the oven and autoclave data centred at the mean HTC.

4.2.2.2 Spatial HTC Variability Within the Vessels

The standard deviations displayed in Figure 4.2 represent the spatial variability in HTC during the two trials. Interestingly, in the oven data, there is no clear relationship between size and the level of spatial variability, the second smallest oven produced the lowest standard deviation, yet the largest oven displayed a lower value than the smallest oven. The absence of a standard configuration among ovens likely contributed to the lack of consistency. The large value for Oven 5 was due to a single extreme measurement, which was attributed to the proximity of the calorimeter to the exhaust, discounting this gives the more reasonable standard deviation of 4.1 $Wm^{-2}K^{-1}$. Among the three autoclaves in Figure 4.2, there is a trend towards decreasing spatial variability with increasing size.

There is a noticeable difference between the observed spatial variability in the ovens compared to the autoclaves. This difference can likely be attributed to the techniques used to achieve high HTC in the autoclaves. In addition to elevated pressure, HTC and Reynolds number are positively correlated with air velocity, motivating high inlet air speeds. Due to the way air flows are generally setup in autoclaves [119] this causes a big contrast in the airspeed at the front to that at the back, producing the high spatial variability in HTC.

To provide a summary of the spatial HTC variability within the ovens and autoclaves more generally, Figure 4.3 presents a boxplot of the measurement grouped by vessel type. The autoclave measurements at the different pressures are treated separately due to the strong

influence of pressure on HTC. The large range of values measured in the autoclaves is consistent with the literature [109, 121]. The largest HTC values occurred around the front and the smallest at the back in accordance with the air flow pattern discussed above. When comparing the oven results with the autoclave results, and the 3 bars autoclave with the 7 bars autoclave results, an apparent trend emerges with greater pressure resulting in a broader range of measured values. Despite this, in the autoclaves, the spatial variability represented by the inter-quartile range appears to be unaffected by the change in pressure, this latter result supports the literature [108, 110] which reported the preservation of patterns in the HTC field with changes in pressure.

The spatial disparities observed in the ovens were generally smaller. The uniquely large maximum HTC of 105 $Wm^{-2}K^{-1}$ in oven 5 (the second largest was 51 $Wm^{-2}K^{-1}$) was the cause of the large variability presented in Figure 4.2. The smaller inter-quartile range of the oven data reflects the low spatial variability measured in the ovens. The skew of the oven data towards higher values is due to the lower values (<24 $Wm^{-2}K^{-1}$) being solely contributed by oven 3, the size of these measurements was attributed to the shelves which would have obstructed the airflow, lowering the velocity. Lacking a standard configuration like the autoclaves, the recorded HTC field patterns varied among the ovens, in practice this necessitates a case-by-case approach to analysis of oven environments.

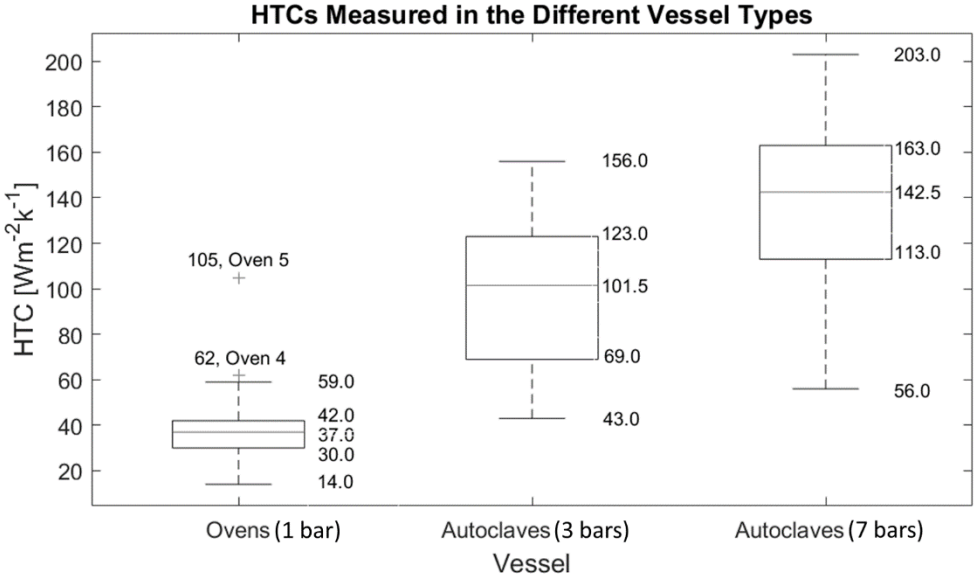

Figure 4.3. Measured HTC values in the ovens at 1 bar, and the autoclaves at 3 and 7 bars.

4.3 Numerical Methods and Results

4.3.1 Numerical Modelling

Coupled cure kinetics and transient heat transfer equations were solved using the FE method to capture the curing process through the thickness of a carbon fibre reinforced thermoset laminate.

4.3.1.1 Numerical Implementation

The curing process of the thermoset laminate was modelled using FE in COMSOL Multiphysics to solve coupled heat transfer and cure kinetics equations. The time dependent solver had a variable step-size which was capped at 60 minutes. The cure kinetics model was derived by Mesogitis et al [103] by fitting differential scanning colorimeter data to an adapted version of the Kamal and Sourour model [98] and was validated against experimental data.

It was assumed that the in-plane dimensions of the laminate far exceeded the thickness, hence the in-plane temperature gradients could be treated as negligible, allowing a 1D approximation of heat transfer [135]. Furthermore, spatial variability in HTC will have a negligible effect on the in-plane temperature gradient compared to the transverse gradient.

The geometry of the 1D model is represented in Figure 4.4, it consisted of a homogenised thermoset composite laminate in ideal contact with a 10 mm thick invar tool. The origin was taken to be at the interface between the two domains, this approach facilitated independent analysis of the two domains. A mesh with 16 uniform elements was sufficient to reliably capture the temperature and cure temperature distributions in all cases.

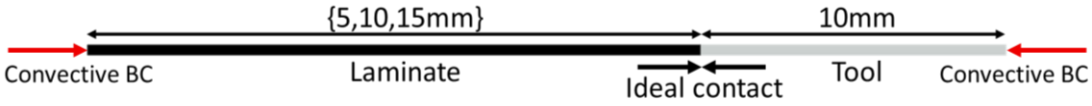

Figure 4.4. The geometry used in the FE model.

The properties of the homogenised laminate were representative of Hexply M21 carbon fibre epoxy prepreg [103, 136]. Simulations were performed with part thicknesses of 5 mm, 10 mm and 15 mm. These specific geometries were considered for illustrative purposes. It is noted that although the trends will be applicable, any such example will lack generality due to the strong influence of geometric parameters such as the laminate and tool thicknesses on the curing process [109].

The heat transfer component of the model was implemented using the 'Heat Transfer in Solids' physics in COMSOL. The heat equation is a first order in time and second order in space partial differential equation, therefore requires an initial condition and two boundary conditions to solve. The initial condition was that the system started at a temperature of 20 ºC. The boundary conditions were convective, applied to the two ends of the geometry. The air temperature history followed by T_∞ during this study was based on the recommended cycle for Hexply M21 [136]. It consisted of a 2 ºC per minute ramp from 20 ºC followed by a dwell at 180 ºC for 2 hours, which is a typical curing cycle for aerospace grade epoxy systems.

The cure kinetics model was implemented in COMSOL as a distributed ordinary differential equation applied to the laminate domain. Computations were performed assuming an initial degree of cure of 0.01 to escape the singular stationary point of the model.

The implementation of the coupled model into COMSOL was validated through a comparison with experimental data [103].

4.3.1.2 Dimensional Analysis

As detailed in Appendix C, the dimensionless forms of the heat equations applied to the laminate and tool domains respectively were

$$\frac{dT^*}{dt^*} = Fo_c \frac{d^2T^*}{dx^{*2}} + P_h \frac{d\alpha}{dt^*} \tag{4.9}$$

$$\frac{dT^*}{dt^*} = Fo_t \frac{1}{A^2} \frac{d^2T^*}{dx^{*2}} \tag{4.10}$$

where Fo_c and Fo_t are the composite and tool Fourier numbers respectively, A is the laminate to tool thickness ratio and P_h is the phase transition number.

The convective boundary conditions applied to the free edge of the laminate and tool domains became

$$\left.\frac{dT^*}{dx^*}\right|_{x^*=1} = -Bi_c[T^*(t) - T^*_\infty(t)] \tag{4.11}$$

$$\left.\frac{dT^*}{dx^*}\right|_{x^*=-\frac{1}{A}} = -Bi_t A[T^*(t) - T^*_\infty(t)] \tag{4.12}$$

where Bi_c and Bi_t are the composite and tool Biot numbers respectively.

The dimensionless cure kinetics equation is given as

$$\frac{d\alpha}{dt^*} = t_c[k_1(1-\alpha)^{n_1} + k_2\alpha^m(1-\alpha)^{n_2}] \quad (4.13)$$

4.3.1.3 Parametric Study

To explore the effect of the observed spatial variability in HTC on the temperature distribution through the thickness of the laminate, FE simulations were performed. Two metrics were used,

i. The time to reach steady state at the imposed dwell temperature through the thickness. A 1ºC margin above was added for robustness.
ii. The absolute difference between the temperature of the hottest and coldest nodes at each time.

These metrics capture the lag between the prescribed temperature and those in the laminate, and temperature inhomogeneity in the laminate itself. HTCs representing low and high oven values, and an autoclave at 7 bars were considered (Table 4.2).

Further simulations were performed to investigate how the curing process of an epoxy composite laminate was affected by HTC. For completeness the HTC range from Figure 4.3 was considered, it is noted the extreme values are outliers. While these values reflect the environment within the devices, it is important to note the absence of a vacuum bag which reduces the HTC seen by manufactured parts.

The influence of HTC on the curing process was characterised using three metrics:

i. Cure time, the time for the DOC to exceed 90% through the thickness.
ii. Temperature overshoot, the greatest positive difference between the predicted temperature and the 180 ºC dwell temperature through the thickness.
iii. Gel time, the time for the DOC to reach gelation (assumed to be 50% DOC) through the thickness.

The simulations were performed with the parameters listed in Table 4.2.

Table 4.2. Parameters used in the coupled heat transfer and cure kinetics simulations [103, 137].

Parameter	**Value**
Effective laminate density	1580 kgm^{-3}
Fibre volume fraction	0.6
Volumetric latent heat	2.12e+8 Jm^{-3}
Tool density	8100 kgm^{-3}
Tool conductivity	15 $Wm^{-1}K^{-1}$
Tool specific heat capacity	515 $Jkg^{-1}K^{-1}$
Part thicknesses	5, 10, 15 mm
HTCs (temperature analysis)	25, 50, 150 $Wm^{-2}K^{-1}$
HTCs (cure analysis)	15 - 215 $Wm^{-2}K^{-1}$

4.3.2 Numerical Results

4.3.2.1 Dimensional Analysis

The Biot number in the nondimensionalised boundary conditions indicated the need to model the temperature gradient through the domains. Figure 4.5 shows Biot number was lowest at the smallest values of HTC and thickness. The value for the laminate never dropped below the 0.1 threshold required to assume lumped capacitance, justifying the need to model the heat transfer within it. The middle plot in Figure 4.5 shows lumped capacitance could only be assumed in the tool for HTCs less than 150 $Wm^{-2}K^{-1}$, hence for consistency across the analyses, the temperature field in the tool was fully computed in all simulations.

Fourier number gives the ratio of the rate of heat transfer to the rate of heat storage. Fourier number is greater with a thinner part, indicating efficient dissipation of exothermic heat, combating the occurrence of severe temperature overshoots. Owing to the much greater conductivity of invar, the tool Fourier number of 176 far exceeded any of the laminate values shown in Figure 4.5. The ability of the tool to transfer heat much faster than accumulating it makes it influential in dispersing exothermic heat. Being significantly greater than unity, the Fourier numbers indicate the need to model conduction $\left(\frac{d^2T}{dx^2}\right)$ in both domains.

Phase transition number gives the ratio of the exothermic heat to the amount of heat available due to the temperature ramp. Values greater than unity indicate the curing reaction is the dominant form of heating during the ramp, suggesting the occurrence of a highly influential exotherm. In this case, the phase transition number was 0.86, below unity, indicating the environment was the primary source of heating, however, its proximity to one indicates the relevance of the exotherm and justified the coupling of the two sub-models.

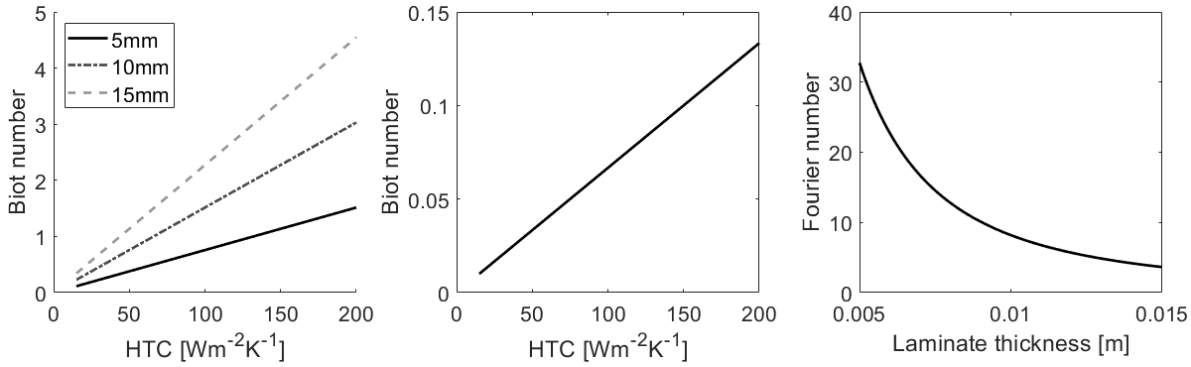

Figure 4.5. Variation of laminate (left) and tool (middle) Biot numbers with HTC, and laminate Fourier number with thickness (right). 90% DOC assumed where applicable.

4.3.2.2 Effect of HTC on Through Thickness Temperature

4.3.2.2.1 Time to reach the prescribed dwell temperature

Figure 4.6 illustrates the effect of HTC on the temperature history in a 10mm thick laminate. With this thickness, the effect of position in the laminate is negligible compared to the effect of the changes in HTC. The difference between the three sets of curves reflects the non-linearity in Figure 4.7, a bigger change occurring with the step from 25 $Wm^{-2}K^{-1}$ to 50 $Wm^{-2}K^{-1}$ compared to from 50 $Wm^{-2}K^{-1}$ to 150 $Wm^{-2}K^{-1}$ despite its smaller size. The reduced time to reach the prescribed temperature with increasing HTC shown in Figure 4.7 is clearly attributed to the smaller temperature lag with the surroundings during the ramp and the smaller temperature overshoot.

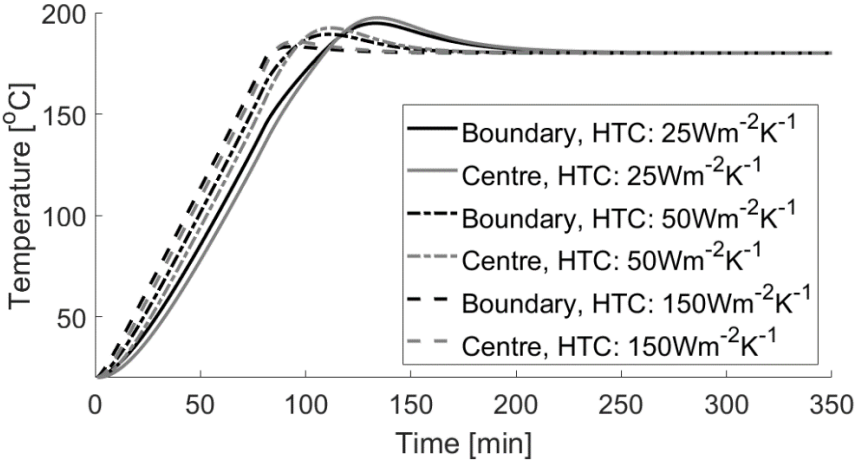

Figure 4.6. Air/laminate boundary and central laminate temperatures during the process. For HTCs of 25, 50 and 150 $Wm^{-2}K^{-1}$ with a 10 mm thickness.

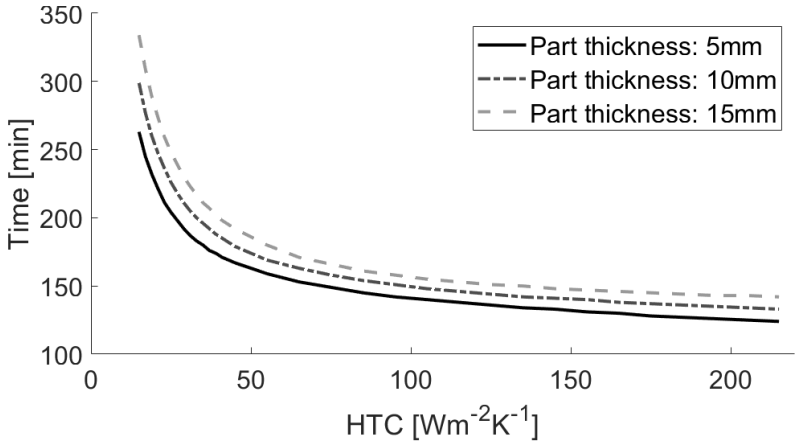

Figure 4.7. Time to reach dwell temperature over the range of observed HTCs for part thicknesses of 5, 10 and 15 mm.

4.3.2.2.2 Establishing through thickness temperature homogeneity

Figure 4.8 shows how the maximum transverse temperature difference changes with time in a 10 mm part. Analogous trends were observed for the other part thicknesses, with values that were scaled in proportion to the thickness, according to the change in Biot number.

The trends in Figure 4.8 are reflective of a higher HTC helping to impose the ramp up and mitigate overheating due to the exotherm. The key points can be explained by considering the heat transfer from the two sources of heat, the environment, and the exothermic curing reaction.

The initial heat input is solely from the environment via convective heat transfer, so the air/laminate boundary is initially the hottest point of the laminate, and the centre the coolest. The increasing temperature difference is due to the low transverse conductivity. The temperature difference peaks at the end of the ramp, beyond this point convective heating from the environment becomes less significant.

The minima represent the points at which the location of highest temperature moves from the boundary into the laminate because of the exotherm. The second maxima represent the peak temperature overshoots, the centre of the laminate is hottest and the boundary the coldest.

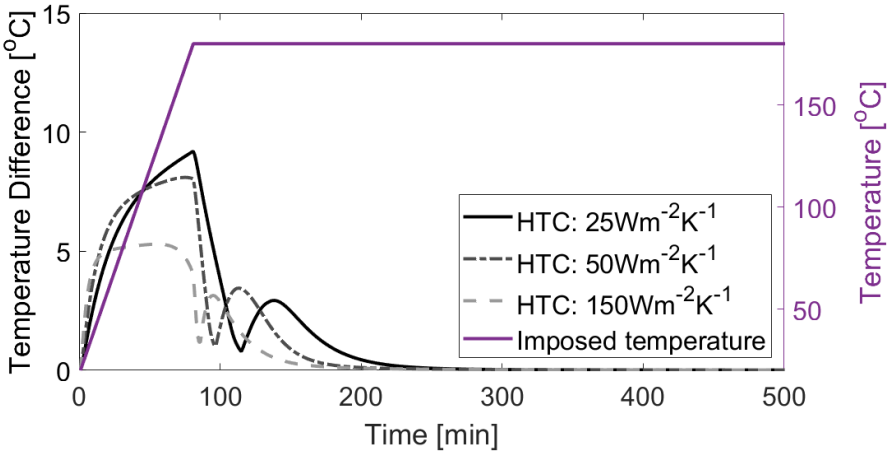

Figure 4.8. Maximum through thickness temperature difference with time for HTCs of 25, 50 and 150 $Wm^{-2}K^{-1}$ with a part thickness of 10mm.

4.3.2.3 Effect of HTC on Cure Through the Thickness

4.3.2.3.1 Cure time

Cure time as defined in Section 4.3.1.3 varied in a non-monotonic fashion as HTC increased. Figure 4.9 illustrates this relationship for the three part thicknesses considered. Initially cure time decreased with increasing HTC, taking a minimum value between 25 and 35 $Wm^{-2}K^{-1}$, before increasing.

This relationship can be explained by considering Figure 4.9. At HTCs below the minima the resistance at the boundary is too great for effective heating. At HTCs above the minima the low resistance at the boundary reduces the influence of exothermic heat. The minima represent a balance of the two effects; however, it is unlikely to be optimal due to overheating.

The error bars represent 95% confidence intervals for the HTCs measured in three types of vessels, assuming normal distributions. To maximise generality, measurements from the ovens and autoclaves were grouped together, as in Figure 4.3. They illustrate the range of cure times possible with a 10 mm thick part.

The lower minimum with increasing part thickness can be attributed to greater temperature overshoot (Figure 4.10). The offsets are due to the higher Biot numbers indicated in Figure 4.5. Cure time depends on the node where cure occurs slowest. As Biot number increases the exothermic heating at the centre has less influence on the boundary. Hence the convergence of cure times beyond the minima.

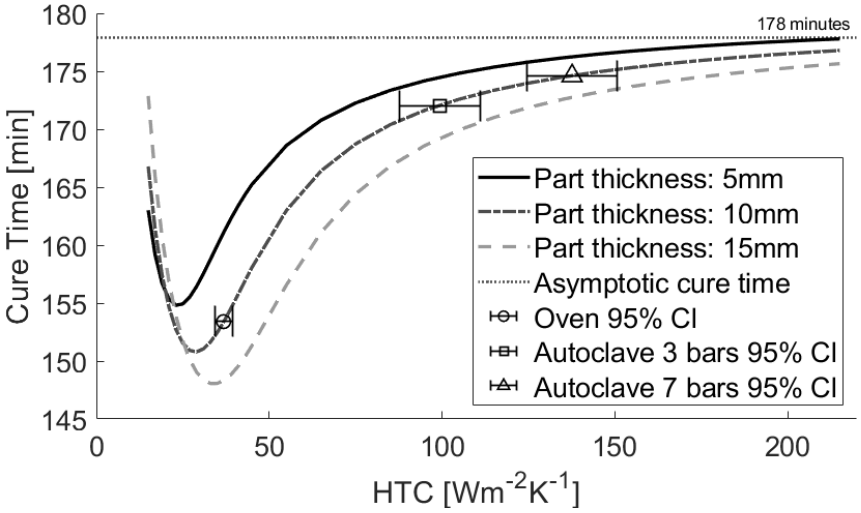

Figure 4.9. Cure time approximated for the geometry over the range of observed HTCs for part thicknesses of 5, 10 and 15 mm. The cure time if the matter followed the cycle is 178 minutes. The error bars mark 95% confidence intervals (CI) for the specific case of HTC measured in the vessels.

4.3.2.3.2 Temperature overshoot

The curves in Figure 4.10 are highly similar, the thickness increases mostly causing a translation. The size of the translation is clearly non-linear, the increasing difference reflecting the change in Fourier number and the Arrhenius temperature dependence of the cure kinetics [103]. The same 95% confidence interval error bars as in Figure 4.10 have been applied to mark the possible overshoot variation in a 10 mm thick part.

As Biot number increases the temperature distribution through the thickness becomes less uniform, the resulting temperature gradient combined with the lower boundary resistance increases the dispersion of exothermic heat in accordance with Fourier and Darboux [138].

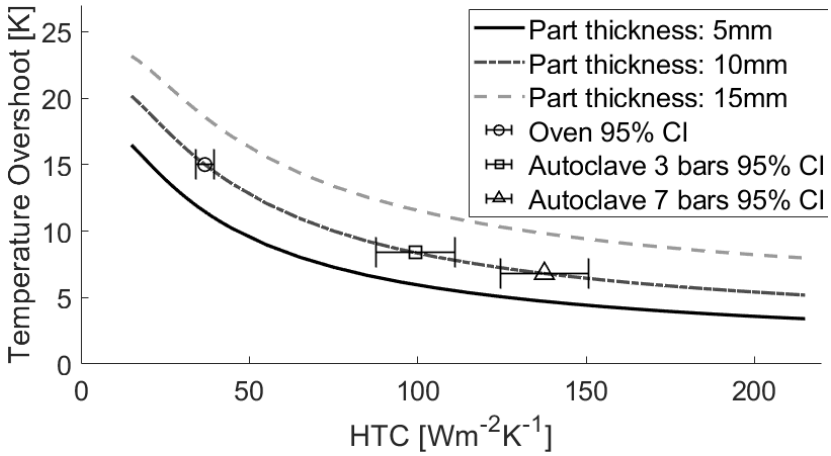

Figure 4.10. Temperature overshoot approximated for the geometry over the range of observed HTCs for part thicknesses of 5, 10 and 15 mm. The error bars mark 95% confidence intervals (CI) for HTC measured in the vessels.

4.3.2.3.3 Gel time

Gel time as defined in Section 4.3.1.3 decreases with increasing HTC as shown in Figure 4.11. As with cure time, at high values of HTC, the gel times for the different thicknesses converge. Again, this is attributed to the increasing dominance of conductive resistance making the reaction at the boundary increasingly dependent on the environment and less dependent on the exothermal heating centred at the middle of the part.

Unlike cure time, gel time decreases monotonically with increasing HTC. The difference is made clear by Figure 4.6, for the HTCs measured, the gel time (when DOC reaches 0.5) elapsed before the temperature overshoot (occurring at DOC of around 0.8). Therefore, the change in gel time due to HTC is only affected by the effective ramp rate in the material which increases with HTC, and not exotherm effects.

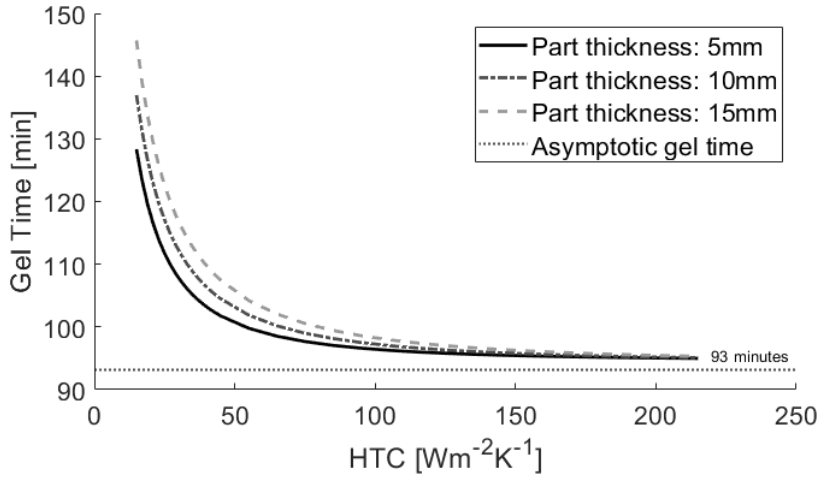

Figure 4.11. Gel time approximated for the geometry over the range of observed HTCs for part thicknesses of 5, 10 and 15 mm. The gel time if the matter followed the cycle is 93 minutes.

4.4 Discussion

4.4.1 Efficiency-Quality Trade-Off

For this combination of configuration and temperature history, none of the ovens have sufficient HTCs (>45 $Wm^{-2}K^{-1}$) throughout to prevent temperature overshoots exceeding 10 ºC for any of the part thicknesses studied here. With the non-linear increase of temperature overshoot with part thickness noted in Section 3.2.3.2, although the 5 mm part can be safely cured in the autoclaves, only autoclave 1 at 7 bars is suitable for the 15 mm part. This level of overshoot is significant for M21 as phase changes have been reported above these temperatures [103].

The flattening of the temperature overshoot-HTC curve in Figure 4.10 highlights the limitations of the curing environment for reducing temperature overshoot. The cure cycle used is representative of one typically used with thinner parts, a relatively high ramp rate (2 $^{o}Cmin^{-1}$) with no pre-dwell. It is clearly not suitable for curing M21 composite parts in oven environments. To reduce the rate of exothermic heating, features such as pre-dwells and slower temperature ramps must be added. However, these features can significantly reduce processing efficiency, hence by operating in autoclave HTC regimes, greater part thicknesses can be processed before such inefficiencies are necessary.

4.4.2 Effect of Spatial Heat Transfer Coefficient Variability

The error bars in Figures 4.9 and 4.10 were used to consider how the spatial variability in HTC could propagate through the curing process, using cure time and temperature overshoot for a 10mm thick part as metrics. The ranges of cure time and temperature overshoot corresponding to the bounds of the error bars for the three types of vessels are shown in Table 4.3.

Table 4.3. Cure time and temperature overshoot corresponding to the bounds of 95% confidence intervals for HTC in each vessel type assuming a normal distribution.

	Ovens	**Autoclaves 3 bars**	**Autoclaves 7 bars**
Cure Time [min]	152.1, 154.8	170.7, 173.0	173.9, 175.2
Temperature Overshoot [^{o}C]	14.5, 15.5	7.8, 9.1	6.4, 7.3

With a mean HTC of 37 $Wm^{-2}K^{-1}$ the oven confidence interval straddles a steep section of the cure time-HTC curve (Figure 4.9). Despite this, the small spatial variability of HTC in the ovens resulted in a narrow range of cure time values. In contrast, the respective means of 99 $Wm^{-2}K^{-1}$ and 138 $Wm^{-2}K^{-1}$ for the autoclaves at 3 and 7 bars were on much shallower sections of the curve. However, due to the greater spatial variability in these vessels, this advantage from the higher HTCs was largely offset. Consequently, the range of cure times predicted for the three types of vessels were similar, the closest ranges being for the ovens and autoclaves at 3 bars, with the autoclaves at 7 bars having the narrowest range. These results show the much greater robustness to HTC variability at higher HTC values.

The more comparable gradients at oven and autoclave HTCs in Figure 4.10 meant the lower spatial variability in the ovens produced a range of temperature overshoots practically indistinguishable from the autoclaves. The oven range was narrower than predicted for the autoclaves at 3 bars and essentially the same as the autoclaves at 7 bars. Hence, for practical purposes, the predictability of overshoot is consistent among the vessels.

In terms of the overshoot values themselves, even the lower bound of the oven was excessive. Whereas both autoclaves had upper bounds below the 10 ºC threshold imposed by the material. This suggests only the autoclaves were capable of curing the 10 mm thick part reliably.

The monotonic nature of Figure 4.10 results in a simpler interpretation for temperature overshoot compared to cure time, where higher HTC values result in a lower mean and greater robustness to HTC variability. Furthermore, the rate of improvement diminishes at a slower rate as HTC increases compared to cure time.

4.5 Conclusion

The curing of composite laminates on a mould, in a vessel (oven or autoclave) is driven by heat transfer. Classically, heat transfer within the part is modelled using a convective heat transfer coefficient (HTC) at the boundaries.

In this study, experimental HTC data from a range of oven sizes, including two large pre-production ovens, was compared to autoclave data. Statistical analysis was conducted to investigate the spatial variability of HTC within the vessels. A coupled Finite Element model was used to propagate the measured uncertainty through the curing reaction to predict the effects on final part quality. The effects were assessed using five indicators, two to consider temperature and three for the cure reaction.

The temperature indicators showed that the temperature history was more successfully imposed with the higher HTCs measured in the autoclaves. This is realised with less temperature lag during the ramp-up and smaller temperature overshoot during exothermic reaction.

The key result was that despite the greater robustness to spatial HTC variability at autoclave HTCs, the larger variability in the autoclave HTC data resulted in similar robustness of the cure reaction indicators across all vessel types.

This study considered a single cure cycle, one recommended for laminate thicknesses of less than 15 mm [136]. Future work could consider the effect of using different cure cycles, for example with different ramp rates and a pre-dwell. These cure cycle parameters could then be optimised for a given combination of vessel and part thickness.

Disclosure statement

The authors report there are no competing interests to declare.

Funding

This work was supported by the EPSRC Future Composites Manufacturing Research Hub under Grant EP/P006701/1. Data collection was supported by Jason Mareo, Stuart Skyes, and Callum Heath at the National Composites Centre through a RCUK Catapult Researchers in Residence award EP/R513568/1.

Data availability

All underlying data to support the conclusions are provided within this paper.

Chapter 4 Closing Remarks

The chapter revealed complications in achieving the objective of quantifying the effect of variability on the curing process. The result that similar process robustness was achieved in ovens and autoclaves, despite far greater heat transfer coefficient variability in the autoclaves reinforces the point made in Chapter 3 about the importance of the nominal value. By presenting the trends between heat transfer coefficient and key cure metrics, the results indicated how the robustness of the process to variability changes with the nominal heat transfer coefficient of a vessel. Having quantified the effect of variability with heat transfer coefficients characteristic of a range of industrial vessels, Objective 2 was addressed.

Chapter 5 Foreword

Having established the effect of variability on the curing process. To address Objective 3, it was desired to see the extent to which the curing environment can be adapted to ensure the targeted cure state is reliably achieved. The desirable cure state varies between applications, in the context of co-curing, a semi-cured state with a positive cure gradient away from the bonding surface is ideal. This maximises stiffness while retaining reactivity at the bonding surface. This shall be targeted by optimising features of the environment, such as tool shape, material, and thickness, and heat transfer coefficient. The following chapter targets Objective 3, proposing manufacturing concepts to achieve the desired degree of semi-cure for co-curing.

This chapter is in the format of a journal article. As the first author my contributions were as follows: conceptualisation, methodology, Writing – original draft, Writing – review & editing, visualisation.

5 Processing Environments to Control Thermoset Composite Cure Gradients

Adam Fisher[a,b] , Arthur Levy[b] , James Kratz[a,*], Arjun Radhakrishnan[a]
[a]Bristol Composites Institute, University of Bristol, Queen's Building, University Walk, Bristol BS8 1TR, United Kingdom
[b]Nantes Université, CNRS, Laboratoire de thermique et énergie de Nantes, LTeN, UMR 6607, F-44000 Nantes, France
Email address: james.kratz@bristol.ac.uk

Abstract

This study used a validated thermochemical model to explore combinations of processing environment parameters to maximise the cure gradient in a thermoset composite part. To create stiff semi-cured parts capable of being co-cured, the aim was to maximise the cure difference between the bonding surface and the rest of the part. This was shown to be possible by having separate tool designs for the two zones. A thick, high diffusivity tool minimised the degree of cure at the bonding surface. A thin, low diffusivity tool maximized the degree of cure away from the bonding surface. A low heat transfer coefficient vessel was significant for a desirable gradient using realistic parameter values. Very large cure gradients were predicted using heat mats positioned away from the bonding surface, outside a curing vessel. The efficiency of this approach was improved by insulating away from the bonding surface.

Keywords: Thermoset composite, cure gradient, co-curing, semi-curing, tooling

5.1 Introduction

Historically polymer matrix composite structures have been assembled using mechanical fasteners and adhesives on fully cured parts [48]. These processes are time consuming and introduce discontinuities to the structure. Mechanical fasteners add mass and produce stress concentrations through the need to drill holes. Adhesives must be cured and with no clear failure criteria, are frequently supplemented with mechanical fasteners [46].

Co-curing presents a more efficient means of joining composite parts. High-quality, discontinuity-free bonds are formed between initially uncured parts when cured in contact. Bond formation is due to cross-linking between thermosets [52] and interdiffusion between a thermoplastic and a thermoset [26]. The inclusion of the bonding process in the curing step has the potential for large efficiency gains.

A disadvantage of co-curing arises from the difficulty in handling low stiffness and tacky uncured thermoset parts. This could be resolved by semi-curing the parts prior to assembly [13]. The stiffer semi-cured parts will make assembly more efficient and the tooling less complex. This is viable providing sufficient reactivity remains to maintain the quality of the

co-cured bond. The adhesion when co-curing thermoset adherends has been shown to be robust to degree of cure until gelation [102]. Thermoplastic-thermoset co-curing is believed to be more sensitive to the initial degree of cure (see Chapter 6).

Progress has been made in adapting the environment within a vessel. Classically fans and applied pressure have been used to control the convective heat transfer coefficient (HTC), as explored in Chapter 4. More recently, research has focused on using tool design to help control the process [139]. For example,

- Self-heating tools that use temperature-controlled water/oil pipes, electrical heaters [140] and electromagnetic induction [139] enable greater efficiency and more localised temperature control than is possible with convective heating.
- Hybrid tools that leverage desirable properties of multiple materials [139].
- Novel materials such as carbon foams with similar coefficients of thermal expansion to composites and high thermal conductivities without the weight penalty of many conventional materials [141].

A potential solution for combining semi-curing with co-curing is to semi-cure parts with cure gradients such that the bonding surface has a significantly lower degree of cure than the rest of the part. This study explores means of adapting the curing environment to promote the desired cure gradient. Based on predictions from a validated thermochemical model [103], with a typical aerospace geometry, an optimal combination of tooling and heating parameters shall be proposed for maximising the cure gradient. The use of heat mats shall be explored with the aim of achieving cure gradients suitably large for both thermoset-thermoset and thermoplastic-thermoset co-curing.

5.2 Method

5.2.1 Geometry

The cross-section of an omega stringer was used as a case study. The geometry of the cross-section was adapted from [142]. Concave and convex configurations were considered, they are presented in Figure 5.1. The geometries were created using Autodesk Inventor. The symmetry of the cross-section allowed half the geometry to be modelled, increasing efficiency. A symmetry boundary condition was applied vertically along the midpoint of the web. The justification for assuming 2-dimensional (2D) heat transfer was the extruded geometry of the stringer and the high aspect ratio, meaning most of the part is unaffected by edge effects.

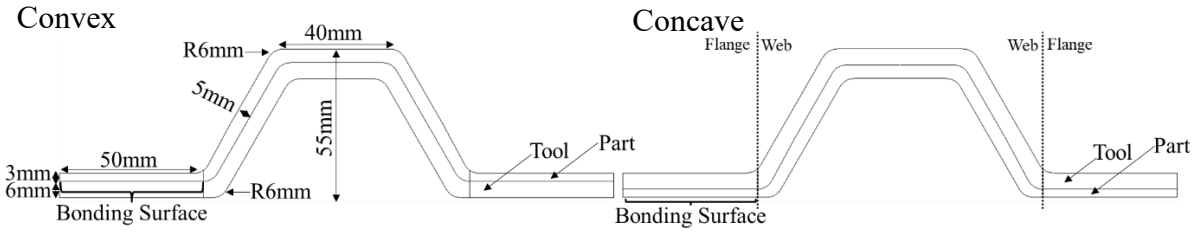

Figure 5.1. The geometry of the convex and concave omega stringers.

Preliminary testing showed the same trends with values of the same order with and without consumables (vacuum bag, breather, and peel plies) in the model. However, the finer mesh size (46793 elements compared to 544) required to capture the small thicknesses of the consumables massively increased the computational intensity. The similarity of the results justified the omission of consumables from the model for the sake of efficiency.

The lower surface of the flange is referred to as the bonding surface, it is the place which will be bonded to a skin, creating an integrated stiffened panel, for example in the fuselage of an aircraft. This is the location of interest, where it is desirable to minimise the degree of semi-cure, to maximise the level of reactivity remaining for co-curing.

As shown in Figure 5.1, the geometry was divided at the end of the bonding surface to allow different boundary conditions and material properties to be applied.

5.2.2 Heat Transfer Model

Coupled cure kinetics and transient heat transfers equations were solved in 2D using Finite Elements (FE) in COMSOL Multiphysics. Heat transfer was modelled using the 'Heat Transfer in Solids' physics in COMSOL.

A 60% fibre volume fraction was assumed for the composite laminate. The thermal conductivity of the laminate was assumed to be orthotropic, with an in-plane and a transverse value. A curvilinear coordinate system was used to enable the material coordinate system to be consistent across the geometry. A linear relationship between fibre volume fraction and in-plane thermal conductivity has been shown to be representative. The relationship, derived by Bard et al [143], gave a conductivity of 3.47 $Wm^{-1}K^{-1}$. Assuming similar conductivity among different carbon fibres and epoxies, this value was used as a prediction for Hexply M21/IMA. The model for transverse thermal conductivity is shown in Equation (5.1) [103].

$$K_{33} = A_{kr}T\alpha + B_{kr}\alpha + C_{kr}T + D_{kr} \quad (5.1)$$

The density and specific heat capacity were homogenised using rule of mixtures according to fibre volume fraction and fibre weight fraction respectively [103]. The specific heat capacity

model for the resin is shown in Equation (5.2). The parameter values and derivation are available in [103].

$$c_{pr} = A_{rc_p}T + B_{rc_p} + \frac{\Delta_{rc_p}}{1 + \exp\left(C_{rc_p}(T - T_g - s)\right)} \tag{5.2}$$

The cure cycle was based on the recommended cycle for M21 [116], a 2 °Cmin^{-1} ramp from 20 °C to a dwell at 180 °C which continued until 95% cure. The part and tool were assumed initially to be at 20 °C.

To simulate processing vessels, convective boundary conditions were applied at each outer surface. Global HTC of 30 and 120 Wm^{-2}K^{-1} were considered, representative of an industrial oven and autoclave respectively [113].

Heat mats were simulated as a boundary heat source applied to the top surface of the web, up to the divide shown in Figure 5.2. The boundary heat source acted in combination with convective boundary conditions applied to the outer surfaces, assuming an HTC of 30 Wm^{-2}K^{-1} and a 20 °C temperature, simulating ambient conditions. To keep cure time within practical limits, the minimum heat mat flux considered was sufficient to make the web gel in 300 minutes.

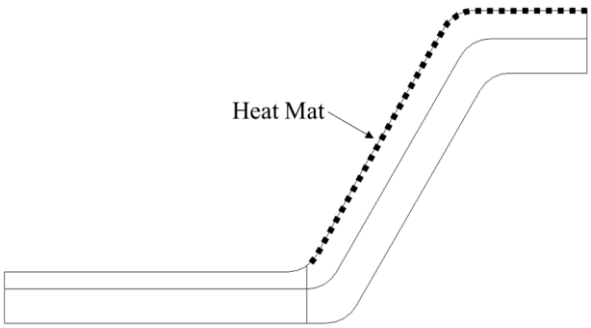

Figure 5.2. Location of heat mat on the convex omega stringer geometry.

5.2.3 Cure Kinetics Model

The cure kinetics for the HexPly M21/IMA prepreg was implemented as a distributed ordinary differential equation in COMSOL [103]. The cure kinetics model is given in Equations (5.3) – (5.7). A convergence analysis showed negligible changes in cure time at values below 0.0001, the initial degree of cure was set to 0.

$$\frac{d\alpha}{dt} = k_1(1 - \alpha)^{n_1} + k_2\alpha^m(1 - \alpha)^{n_2} \tag{5.3}$$

$$\frac{1}{k_i} = \frac{1}{k_{iC}} + \frac{1}{k_D}, \qquad i = 1,2 \tag{5.4}$$

$$k_{iC} = A_i e^{\left(\frac{-E_i}{RT}\right)}, \qquad i = 1,2 \tag{5.5}$$

$$k_D = A_D e^{\left(\frac{-E_D}{RT}\right)} e^{\frac{-b}{f}} \tag{5.6}$$

$$f = w\left(T - T_g\right) + g \tag{5.7}$$

5.2.4 Parameter Space

The means of affecting the degree of cure gradient were tool material, tool geometry and boundary conditions.

Tool material selection was limited to those typical in tool design including, steel, invar, aluminium and thermoset matrix carbon composite [142]. Combining conductivity, specific heat capacity and density, diffusivity was used to characterise the materials. To study the effect of tool diffusivity, aluminium and composite, the materials with highest and lowest diffusivities respectively, were considered. The properties assumed for the materials are presented in Table 5.1.

Table 5.1. Properties of the tooling materials.

Tool Material	**Conductivity ($Wm^{-1}K^{-1}$)**	**Heat Capacity ($Jkg^{-1}K^{-1}$)**	**Density (kgm^{-3})**	**Diffusivity (m^2s^{-1})**
Composite	0.7	800	1550	5.6e-7
Aluminium 6061-T6	170	900	2700	7.0e-5

The gel point, a degree of cure of 0.7 for this material system [103] at 180 °C, was targeted for the web. Gelation represented a level of cure when stiffness was considerably improved, but before the rate of cure had slowed significantly relative to the flange [112].

A metric was defined to quantify the degree of cure difference between the bonding surface and the web. The degree of cure for the web was characterised by the median of the web node values in the model. Extreme values were prone to occur at the ends of the web. By giving less influence to these extreme value than the mean - which could lead to misleading results - the median gave a more reliable indication of the level of cure. The metric value was thus taken when the median degree of cure among the web nodes was 0.7. In this chapter, the onset of gelation in the web refers to the median degree of cure exceeding 0.7.

The degree of cure for the bonding surface was defined by the 90^{th} quantile degree of cure of the nodal values along the bonding surface. The 90^{th} quantile degree of cure was used to be

conservative, while ignoring extreme values. As there were 17 bonding surface nodes, a quantile any larger would have given a single extreme value excessive influence.

From the above, the metric was defined as the difference between 0.7 and the 90th quantile degree of cure along the bonding surface when the median degree of cure in the web was 0.7. A metric value of 0.2 was considered the threshold for reliably achieving a beneficial outcome.

5.3 Results and Discussion

This section will evaluate the ability of each parameter to produce a desirable cure gradient for co-curing and the feasibility of combining them to reach the 0.2 metric threshold.

5.3.1 Geometry

A key part of the configuration was the orientation of the part relative to the tool. In the convex arrangement the bonding surface was at the interface with the tool, in the concave arrangement it was exposed to the convective boundary conditions. The cure distribution, taken at gelation in the web for each configuration with a composite tool and an oven HTC is shown in Figure 5.3.

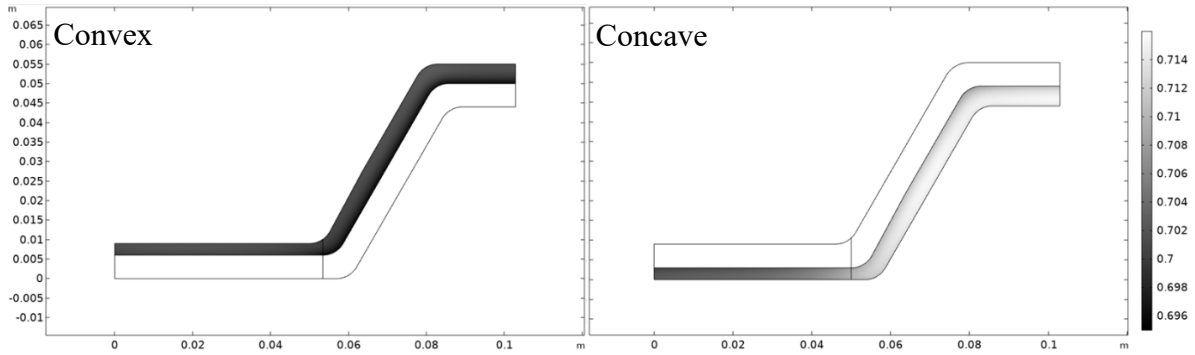

Figure 5.3. Cure distribution in the omega stringer cross-section at the time the metric value is taken with the convex (A) and concave (B) tools.

In the convex configuration the applied heat must be conducted through the part or tool before reaching the bonding surface. In the concave configuration, heat was applied directly to the bonding surface through convection, increasing the rate of cure. Hence, in the convex setup the degree of cure at the bonding surface when gelation occurred in the web was generally lower than in the concave configuration.

The exception to this was when an aluminium tool was combined with the oven HTC. An explanation for this is the exothermic heat from the web being conducted to the flange via the high diffusivity tool. As the bonding surface was in contact with the tool in the convex

configuration, the conductive heating was more significant. This only holds in the oven environment, as HTC increased, Biot number increased signifying the increasing influence of convective heating compared to conductive.

Although the convex configuration generally produced a more favourable cure gradient, in the setups considered, the benefit was minimal and the difference in degree of cure between the flange and the web was minor. For example, in Figure 5.3, the metric value in the convex configuration was 0.012, compared to 0.008 in the concave configuration. The metric values presented would be insufficient to yield manufacturing benefits. Furthermore, the difference could be diminished by processing variability, effecting the reliability of a desirable outcome. Consequently, to achieve a significant cure gradient in the part additional measures must be taken. Shown to be generally superior in this context, further analysis considered the convex configuration.

5.3.2 Material

A high diffusivity tool material aided the redistribution of exothermic heat from the web. Hence with the aluminium tool and oven HTC, the value of the metric was 0.002, lower than with the low diffusivity composite tool and much lower than the 0.2 target.

The results indicated using a single material for the tool was not viable. By having an aluminium tool for the flange and a composite tool for the web, with an oven HTC the metric was increased to 0.030. The aluminium tool acted as a heatsink for exothermic heat from the flange. The more insulating composite tool reduced the rate exothermic heat that could be dissipated from the web into the surroundings and along the tool.

The metric value improvement from mixing tool materials was notable, but at 0.030 the value was still short of the 0.2 threshold. Hence with standard tooling materials, materials alone were not sufficient for the desired cure gradient.

5.3.3 Heat Transfer Coefficient

As shown in Figure 5.4, with all permutations of tool material combinations, the magnitude of the metric increased with a lower global HTC. This included an increase in the magnitude of the unfavourable cure gradient created when the flange tool was composite, and the web tool was aluminium. The larger the metric value, the greater the effect of HTC. This result pointed towards the suitability of OOA environments, such as ovens.

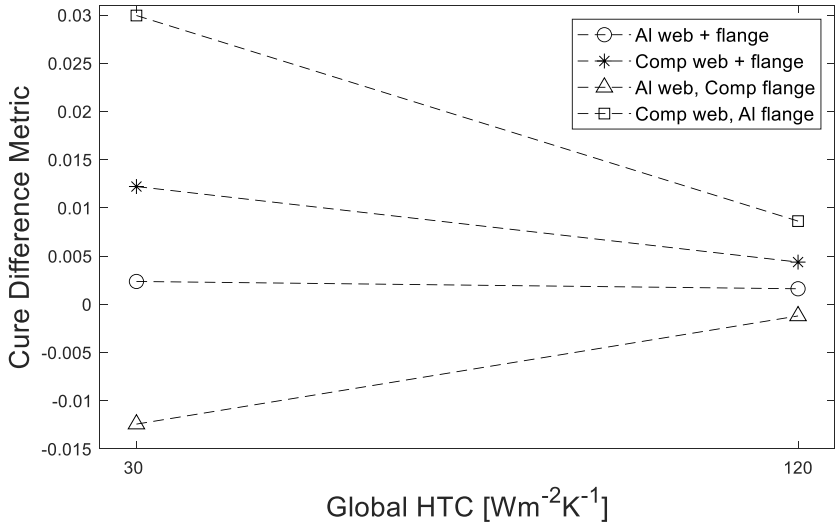

Figure 5.4. The effect of global heat transfer coefficients and tool material on the cure gradient.

5.3.4 Tool Thickness

With a single material tool, increasing tool thickness moved the cure gradient in an unfavourable direction. This trend occurred at both extremes of the HTC range but was less significant at higher values, likely due to increased exothermic heat dissipation from the web.

With an aluminium flange tool and a composite web tool, a thicker tool produced a more favourable cure gradient. Going from the nominal tool thickness of 6 mm to 25 mm with the oven HTC, the metric went from 0.030 to 0.076. A higher HTC increased the robustness of the cure gradient to changes in tool thickness. The same thickness change with the autoclave HTC caused the metric to go from 0.008 to 0.015.

As with tool material a hybrid approach was beneficial, having a different tool thickness for the web and the flange. Continuing with the optimal material combination, a thick aluminium tool in contact with the flange acted as a heat sink, extracting exothermic heat and slowing the rate of reaction. A thin composite tool at the web limited the dissipation of exothermic heat to the surroundings and through the tool, increasing the cure rate.

In the example, with a web tool thickness of 6 mm and the oven HTC, a flange tool thickness of 38.4 mm was required to reach the metric threshold of 0.2. Given how far the other measures were from achieving the threshold, this result showed the effectiveness of tool thickness for achieving the desired gradient. However, the rate of improvement slowly decreased as flange tool thickness increased. It is noted that with the autoclave HTC the asymptotic value of the metric was 0.163, showing the need for a combined approach to achieve the threshold within realistic parameter ranges.

5.3.5 Tool Shape

The findings with tool thickness were extended by considering alternative tool shapes. Changing the shape enables the thermal mass distribution to be altered.

In the case of an omega stringer, having a tool as in Figure 5.1 was beneficial over a tool which was filled in under the web as in Figure 5.5. Due to the shape of the part, when the tool was filled in, there was a lot of thermal mass to cool and isolate the web, slowing the rate of cure relative to the flange. The slow rate of reaction in the web was such that the bonding surface gelled before the web. This is shown in Figure 5.5 with an oven HTC and the optimal tool material combination. The addition of thermal mass above the web only added to this effect. It was shown above that less thermal mass around the web was beneficial for the cure gradient. Indicating a thin, single sided web tool was optimal here.

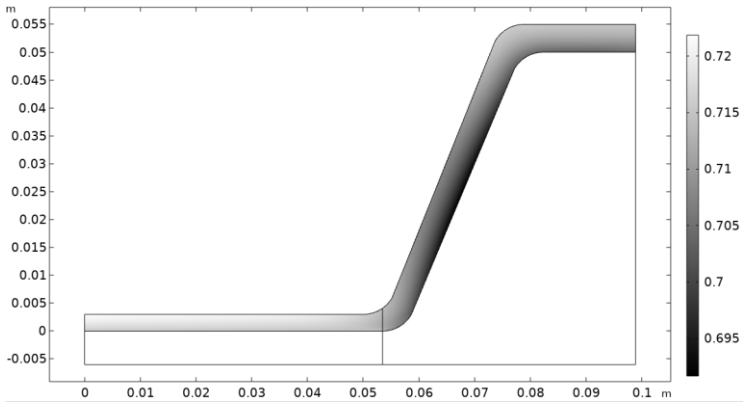

Figure 5.5. Cure distribution at the onset of gelation in the web with a filled-in web tool.

The effect of splitting the thermal mass either side of the flange, for example using a caul plate as shown in Figure 5.6, was investigated. Figure 5.7 shows that for a given total thickness, the metric was greater when a one-sided flange tool was used. As the metric concerns the degree of cure along the bonding surface, maximising the thermal mass directly in contact with it was clearly more effective at slowing the rate of cure. With the caul plate, half the thermal mass was insulated from the bonding surface by the part. The analysis with an aluminium flange tool, a 6 mm thick composite web tool and the oven HTC was repeated with an aluminium caul plate above the flange. The combined thickness required to achieve the 0.2 metric threshold increased to 49.3 mm.

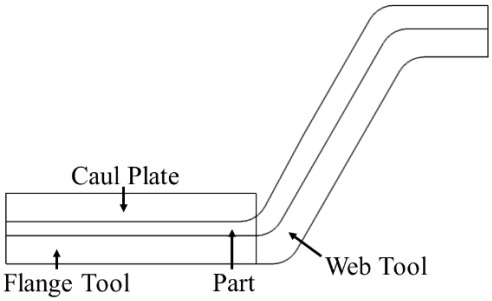

Figure 5.6. Convex geometry with the flange tool thickness split above and below the part.

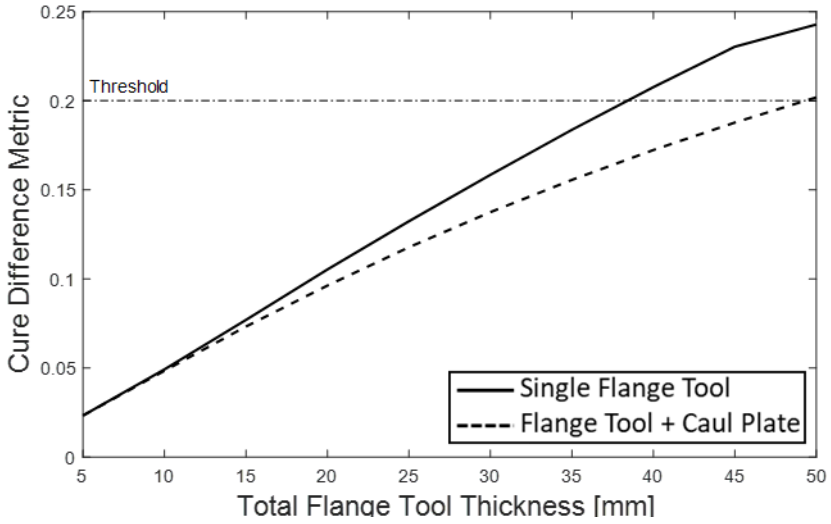

Figure 5.7. Cure difference metric with and without a caul plate of equal thickness to the tool, above the flange.

5.3.6 Heat Mats

When curing through convective heating the objective of tool design was to reduce the amount of heat in the flange and maximise it in the web. This was taken further by applying heat directly to the web using heat mats. This more targeted heat application was motivated by greater cure gradients and in the absence of convective heating, lighter tooling for the flange. A low diffusivity, composite tool across the whole part was used to limit heat flow from the web to the flange. The standard convex geometry shown in Figure 5.1 was used.

With no heat directly applied to the flange, the metric values achievable were much higher than predicted for ovens or autoclaves. From Figure 5.8, with no insulation, a heat mat flux of 7753 Wm^{-2} was necessary for a web gel time comparable to the vessel processing approach, around 115 minutes. This level of flux is in-line with heated tooling in the literature [140]. Figure 5.9 shows there was little sensitivity of the metric value to web gel time, staying at around of 0.68. Given the median degree of cure in the web was 0.7 when the metric was measured, most of the flange was essentially uncured. The very low degree of

cure in the flange suggested the suitability of this approach for thermoplastic-thermoset co-curing, where bonding is sensitive to initial degree of cure (see Chapter 6). According to the simulations, the major advantage of increasing heat mat power was a reduction in web gel time.

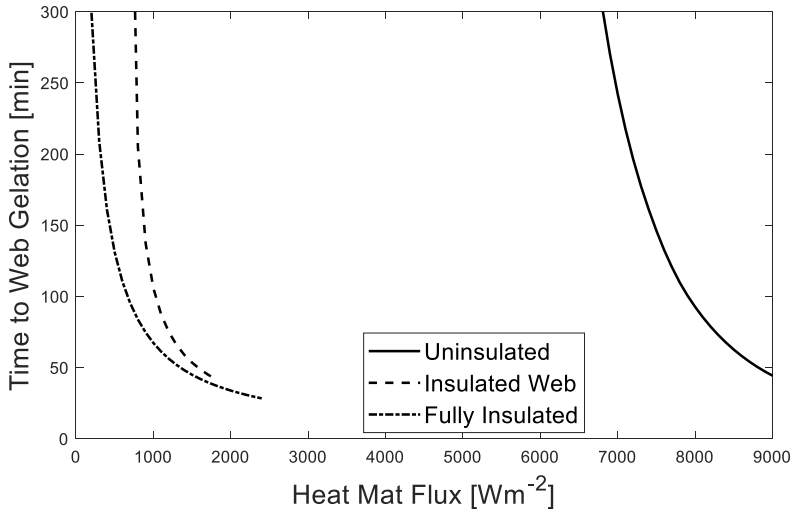

Figure 5.8. The time for the onset of gelation in the web at different heat fluxes for each insulation case.

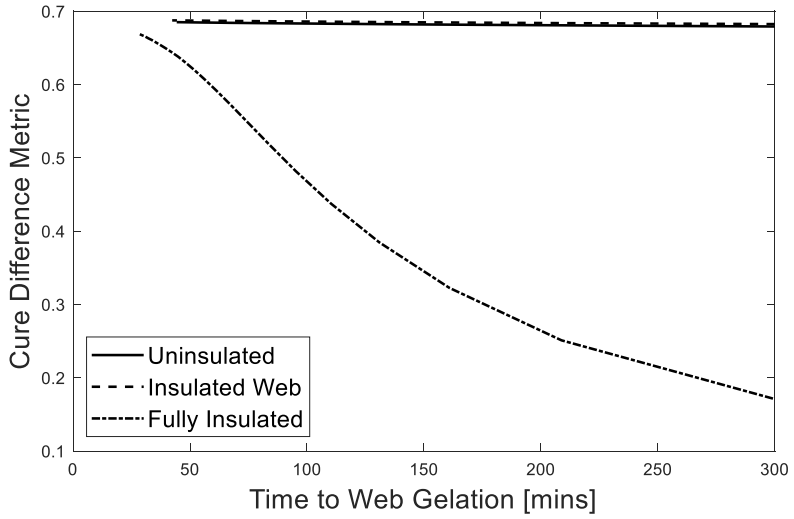

Figure 5.9. The value of the cure difference metric with web gel time for each insulation case.

Given the margin of the metric to the threshold, there was scope to increase efficiency and eliminate the temperature gradient in the web arising from convective heat loss (Figure 5.10C) by applying insulation boundary conditions to the outer surfaces. With insulation applied to all outer surfaces, the applied flux required for a web gel time of 115 minutes, comparable to the vessel approach, dropped significantly to 557 Wm^{-2}. However, with this flux the metric value decreased to 0.425. As shown in Figure 5.9, the metric value increased with decreasing web gel time, but was always less than the corresponding value for the

uninsulated case. Insulating the flange meant that at lower flux levels there was time for the degree of cure along the bonding surface to advance notably, lowering the metric, this is evidenced by the greater degree of cure towards the flange in Figure 5.10A.

Much of the influence of the insulation came from that applied to the web. Figure 5.10B shows that only insulating the web still reduced the cure gradient in the web, but not as significantly as in the fully insulated case, this was reflected in the web-only insulation curve being between the two others in Figure 5.8. As heat could be dissipated from the flange, the rate of cure there did not increase, hence as shown in Figure 5.9 the metric value followed a similar trend to the uninsulated case, staying around 0.68 regardless of web gel time. This gives the option of reducing the power demand without compromising the desired cure gradient. The distinction between the level of cure in the flanges in the two insulated cases is visible when comparing Figures 5.10A and 5.10B. Thus, just insulating the web is predicted to recover the uninsulated metric value with only a small loss in efficiency compared to the fully insulated case.

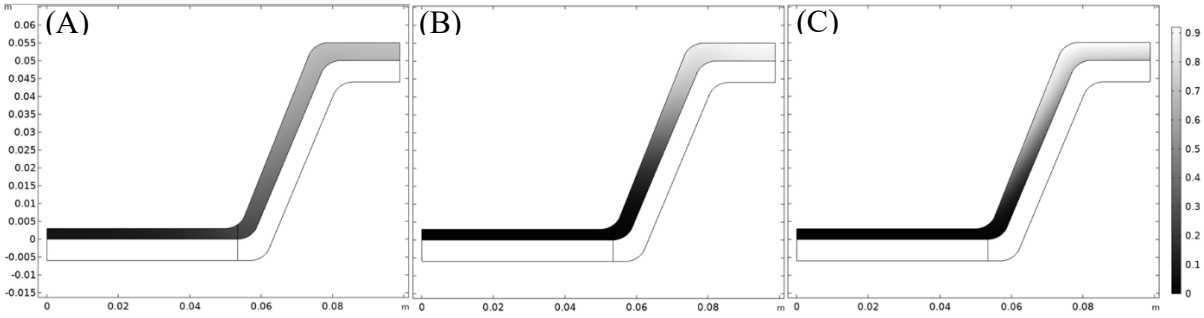

Figure 5.10. Cure distribution with heat mats at the onset of gelation with flux required for the vessel representative 115-minute web gel time in the web with full insulation (A), web insulation (B) and no insulation (C).

From a practical perspective, the reduced cure gradient in the web from applying insulation, shown in Figure 5.10, reduces residual stress and increases geometric stability. The figure also shows the benefit of having the heat mat above the part (shown in Figure 5.2), the part insulated the bonding surface from the applied heat.

5.4 Conclusion

Combinations of tool thickness, tool material, heat transfer coefficient (HTC) and heat mats were considered to maximise the degree of cure difference between the bonding surface and the web in an omega stringer. The aim was to propose a setup that produced semi-cured parts with additional stiffness to aid with handling, while retaining sufficient reactivity on the bonding surfaces for co-curing.

Setups where the bonding surface was at the part-tool interface were found to be more suitable, the insulation from the applied heat reduced the rate of cure there. This was a convex tool shape for the omega stringer considered.

Low and high HTCs were considered, representative of an oven and an autoclave respectively. The low HTC was found to produce a greater cure gradient in all conditions. Indicating the suitability of out-of-autoclave enviroments.

Thermoset matrix composite and aluminium were used to represent low and high diffusivity tool materials respectively. Alone, neither was particularly effective. The benefit was maximised when an aluminium flange tool was combined with a composite web tool. Although the gradient increase was not large in absolute terms, this arrangement maximised the effectiveness of later measures.

Different thicknesses for the aluminium flange tool and composite web tool were shown to significantly influence the cure gradient. A thicker flange tool made it a more effective heatsink, slowing the rate of reaction. A thin web tool was a less effective heat sink for exothermic heat, increasing the rate of cure. Coupled with an oven representative HTC and a 6 mm thick web tool, a flange tool thickness of 38.4 mm was required to achieving the target cure gradient.

It was shown that splitting the thermal mass between the flange tool and a caul plate above the flange was not beneficial. Maximising the thermal mass in direct contact with the bonding surface by using a single-sided tool was the most efficient use of material. Under the same conditions, with the caul plate, the combined thickness required for the target cure gradient increased by 10.9 mm.

Heat mats were used to exclusively apply heat to the web. In ambient conditions, the possible cure gradient increased massively, to the extent the bonding surface had a degree of cure of less than 0.1 at the point the web had gelled. An increase in efficiency was predicted without a loss of cure gradient when insulation boundary conditions were applied to the web. This modification increased cure uniformity in the web, reducing the possibility of residual stress.

The analysis has shown that with the correct combination of tooling parameters it is possible to achieve large cure gradients through passive means. The optimal combination was a thick, high diffusivity tool in direct contact with the bonding surface, a thin, low diffusivity tool in other areas and an oven representative HTC. However, even in the optimal arrangement

described, a significant flange tool thickness was required. Heat mats were shown as a way of achieving very large, potentially thermoplastic-thermoset co-curing compatible cure gradients, with standard tool geometries.

The purpose of this analysis was to show the capability of tooling parameters for influencing the cure gradient. However, it is noted that future work must consider practical issues such as the different coefficients of thermal expansion within a hybrid material tool before these findings can applied to real world processes.

Chapter 5 Closing Remarks

Two approaches have been presented for achieving a desirable semi-cured state for co-curing. Although the analysis was conducted using an example geometry, the methodology was based on the physics and will thus be adaptable. For example, using a thick, thermally diffusive tool to cool the bonding surface and a thin, low diffusivity tool to maximise the temperature in the remaining part.

The use of heat mats to exclusively apply heat away from the bonding surface could be appropriate when very large gradients are required. The effectiveness of creating a temperature difference in the part to control the cure distribution is consistent with the sensitivity analysis in Chapter 3. Chapter 4 supports the result that the cure gradient was enhanced by lower heat transfer coefficients. Having proposed two approaches to achieving the desired cure gradient, Objective 3, to propose manufacturing concepts to achieve the desired degree of semi-cure for co-curing, was addressed.

Chapter 6 Foreword

Considering the extent to which the degree of cure of the bonding surface increased before the rest of the part gelled with the passive approaches in Chapter 5, it was important to see how advancements in degree of cure affect thermoplastic-thermoset co-curing. This addresses the final objective of this work, to investigate the influence of semi-curing on thermoplastic-thermoset adhesion. For thermoset-thermoset co-curing semi-curing was shown to have a minor effect until gelation [13]. For thermoplastic-thermoset co-curing, the morphological effects were explored by Lestriez et al [26] using resins, however, for adhesion relevant to structures, investigations at the laminate level are necessary.

Sensitivity to initial degree of cure has implications for the influence of process variability and the viability of semi-curing before joining. The following chapter explores the effect of initial degree of cure on the interphase and adhesion between co-cured thermoplastic and thermoset laminates.

This chapter has been written in the format of a journal article with the intension of submitting it for publication. As the first author my contributions were as follows: conceptualisation, methodology, formal analysis, Writing – original draft, Writing – review & editing, visualisation.

6 Effect of Pre-Curing on Thermoplastic-Thermoset Interphases

Adam Fisher[a,b] , Arthur Levy[b] , James Kratz[a,*], Arjun Radhakrishnan[a]
[a]Bristol Composites Institute, University of Bristol, Queen's Building, University Walk, Bristol BS8 1TR, United Kingdom
[b]Nantes Université, CNRS, Laboratoire de thermique et énergie de Nantes, LTeN, UMR 6607, F-44000 Nantes, France
Email address: james.kratz@bristol.ac.uk

Abstract

This study considered adhesion between thermoplastic and thermoset laminates through interdiffusion at the interface. The influence of the degree of cure at the start of the process was investigated through mechanical testing and microscopy. Initial degree of cure had a strong influence, decreasing both interlaminar fracture toughness and interphase thickness. The reduction in fracture toughness was shown to be much greater, likely due to the changes in interphase morphology and the level of surface contact at the interface. Guided by the results, a simplified model was developed using existing interphase measurement data to predict the level interdiffusion with increasing initial degree of cure. Compared to thermoset-thermoset co-curing, there was superior bond strength at low initial degrees of cure and a predicted increased sensitivity to initial degree of cure.. Hence, for structural applications, the increased manufacturing efficiency from semi-curing cannot justify the massive reduction in performance.

Keywords: Thermoset laminate, thermoplastic laminate, co-curing, semi-curing, adhesion

6.1 Introduction

Structures that can leverage the advantageous properties of thermoset and thermoplastic polymers promise highly desirable and tailorable characteristics. The combination of the toughness and weld enabling melt processability [50, 51, 111] of thermoplastics with the stiffness of thermosets has numerous potential applications. One such application would be to use thermoplastic composite along the leading edges of wind turbine blades to improve damage and erosion resistance compared with current thermoset solutions [15]. The issue is combining these materials efficiently, without compromising performance.

The issue stems from the incompatibility of the materials, both in terms of the processing conditions and chemical properties. The traditional approach to joining such materials is through mechanical fasteners and adhesive bonding [48]. Beyond the time-consuming nature of these methods [50], they yield interfacial properties that compromise the structure.

Mechanical fasteners introduce stress concentrations [46], fibre damage [47], additional weight [49] and inefficient load transfer [48]. A number of these issues are addressed by adhesive joints [46]; however, the lack of a suitable failure criteria means supplementary fasteners are often required [46].

A potential solution comes from adapting the co-curing method. In co-curing, initially uncured thermoset materials are bonded through chemical cross-linking that develops during cure under a cure cycle [52]. When a thermoset adherend is replaced by a thermoplastic, the formation of bonds has been demonstrated [90]. Although no curing of the thermoplastic is occurring in this process, the term has been used in the literature to cover bond development through interdiffusion across the interface [48].

The interdiffusion process is initiated by thermoset monomers diffusing into the glassy thermoplastic and swelling it [26]. When sufficiently swollen, a glass-to-rubber transition occurs, followed by localised dissolution [26]. The dissolved thermoplastic diffuses into the liquid thermoset. When the thermoset degree of cure advances to the point the two polymers become immiscible, assumed to be gelation, phase separation occurs [26]. For a given temperature, gel layer growth is believed to stop at the onset of phase separation [62], but can be resumed at a higher temperature [61]. Interphase thickness has been used a metric for the amount of interdiffusion [56].

The diffusion of thermoset monomers into glassy polymers during interdiffusion, has been classified as Case II [68]. Case II diffusion is characterised by a sharp, constant velocity penetration front resulting from the difference in the thermoset diffusivity in the swollen polymer behind the front and unswollen polymer ahead [70]. In-situ Raman spectroscopy measurements by Zweifel et al [63] showed thermoplastic diffusion in the thermoset to be Fickian, shown by Figure 6.1(d) to be the dominant contributor to interphase thickness.

Thermoset-thermoplastic interactions during interdiffusion are similar to those in thermoplastic toughened epoxy systems. A morphology forms during phase separation. However, unlike toughened systems, the thermoplastic concentration varies, between pure thermoplastic on one side of the interphase and pure thermoset on the other. As morphology is dependent on thermoplastic concentration, an interphase with a gradient of morphologies is created [26], including some commonly observed in toughened systems.

Figure 6.1 [26] shows an example of an interphase produced by the interdiffusion process [26]. The region of thermoset swollen thermoplastic, Figure 6.1(a)-(b), is known as the gel

layer and is characterised by phase inverted Figure 6.1(a) and co-continuous Figure 6.1(b) morphologies. Both morphologies are effective at increasing toughness [65, 86] and are common among toughened systems. The region of thermoset with diffused thermoplastic, Figure 6.1(d), is the liquid layer.

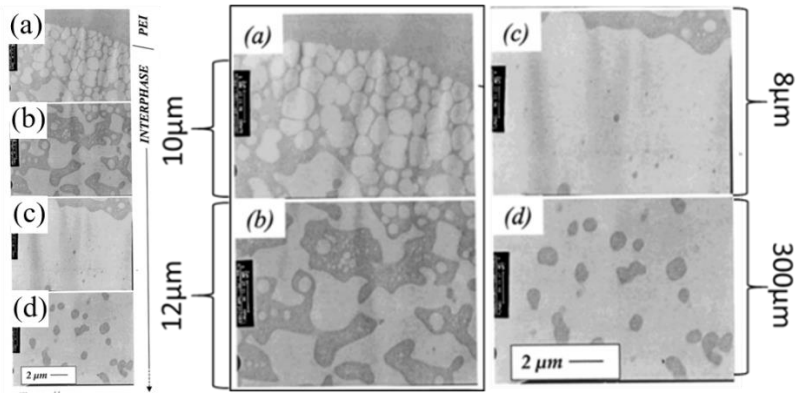

Figure 6.1. The morphology of an interphase formed by interdiffusion between an epoxy amine and PEI, in order (left) and magnified (right). Adapted from [26].

Epoxy resins are the dominant thermoset used in the related literature. The thermoplastics are typically those used in toughened epoxy systems, due to proven compatibility [47]. These thermoplastics are amorphous with glass transition temperatures that exceed the 180 °C curing temperature common among aerospace grade epoxies [57]. Polyethersulfone (PES), polysulfone (PSU) and polyetherimide (PEI) are common examples [92]. PEI is the most common choice for co-curing, not to be confused with epoxy toughening through phase separation, where PES is a popular choice [47]. PEI stands out for co-curing due to excellent mechanical properties combined with good resistance to solvents and environmental exposure for an amorphous thermoplastic [1].

The feasibility of the adapted co-curing process has been most extensively explored through the adhesion of thermoplastic films to epoxy laminates [48, 57]. Although not the most suitable arrangement for measuring thermoplastic-epoxy adhesion, mechanical testing of epoxy composite adherends joined via fusion bonded thermoplastic films routinely exhibited cohesive failure [56]. Failure occurred in the lap shear epoxy composite adherends at values comparable to conventionally co-cured adherends [56] and high-performance adhesives [48, 56], indicating the merit of the thermoplastic-epoxy bond.

Most examples to date have used uncured epoxy pre-polymer at the beginning of the co-curing process. Findings show the nature of the interdiffusion process changes with increasing initial degree of cure [26]. As initial degree of cure increases, the size of the gel

layer, the source of toughness increasing morphologies, diminishes [26]. This is caused by a reduction in the amount of epoxy monomers, which are required for swelling [26]. The remaining section of the interphase, the liquid layer, is characterised by concentrated thermoplastic particles in a thermoset matrix [26], offering poor resistance to crack propagation [144].

Recent developments in composite manufacturing technologies have started to consider the use of semi-cured elements as a way to reduce tooling complexity [13]. In semi-curing, the degree of cure is advanced to where the semi-cured material is rigid and handleable, i.e., the glass transition temperature exceeds ambient temperature. Semi-curing has been shown to have minimal effect on the co-cured bond strength until gelation [13, 102].

Semi-curing still has inefficiency coming from the low stiffness uncured adherend. Replacing the uncured adherend with a thermoplastic composite could be highly beneficial for manufacturing efficiency. Although the interdiffusion process is often regarded to terminate at gelation [26, 56], there appears to be some uncertainty in this. For example, phase separation was observed at degrees of cure just above 0.3 for PEI and a model epoxy system at 180 °C [62], slightly lower than the 0.43 gel point for the system [61]. It has not been shown whether the adhesion will suddenly drop off at semi-cures when the two materials become immiscible, as with thermoset-thermoset adherends at gelation, or if there will be a more gradual reduction.

The state-of-the-art has demonstrated that epoxy and PEI polymers will adhere through interdiffusion. This study investigates this by co-curing thermoplastic laminates with semi-cured thermoset laminates. Notably, to our knowledge, semi-curing in this context has not been extended beyond resins [26] and little has been done to explore the thermoplastic-thermoset co-curing at the laminate level [57].

Diffusion data from a model epoxy pre-polymer system co-cured with PEI was used to create a model of the diffusion process. The results from the model provided a simplified approach of capturing the effect of initial degree of cure on diffusion, based on gel layer thickness. The model was adapted to a commercial epoxy system and the predictions were compared to measurements made from optical micrographs of the co-cured laminates. The mechanical properties of the co-cured laminates were also assessed using mode I fracture toughness. The overall results highlight the potential routes to join thermoplastic and thermoset laminates without the use of fasteners or adhesives.

6.2 Methodology

6.2.1 Experimental Method

In this section, the experimental methods to estimate the gel layer thickness and fracture toughness of co-cured thermoplastic-thermoset laminates are presented. The initial degree of cure of the thermoset laminate was varied to investigate the limitation of the gel layer formation. Three 150 mm x 150 mm thermoplastic-thermoset laminates were manufactured with each thermoset (TS) panel having a different degree of cure at integration. An overview of the process to produces these laminates, which will be discussed in this section, is presented in Figure 6.2.

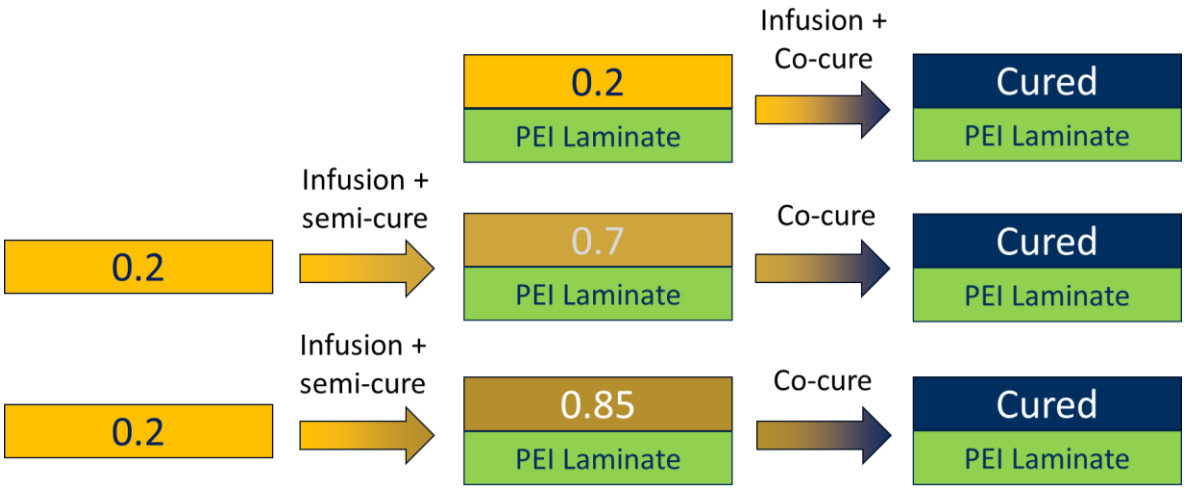

Figure 6.2. An overview of the procedure to produce the three co-cured thermoplastic-thermoset laminates.

6.2.1.1 Materials

An off-the-shelf 2.5 mm thick thermoplastic (TP) laminate TC1000 (Toray-Cetex) was used for this study. The laminate comprised of PEI (Ultem 1000) reinforced with 5-harness satin woven carbon fabric (FT300B) with 280 gm^{-2} fibre areal weight [145]. The TS laminate was manufactured using infusion and comprised of a single part epoxy resin (EP2410, Solvay) reinforced with 8 plies of 5-harness satin woven carbon fabric to match the thickness of the TS laminate. Due to the age of the resin system, the degree of cure had progressed to 0.2.

6.2.1.2 Thermoset Semi-Curing

The following gives details of the infusion and semi-cure step on the bottom two rows of Figure 6.2. Two TS panels were manufactured using the vacuum assisted hot resin infusion and bagging scheme shown in Figure 6.3. The resin was heated to 90 °C and degassed for 45 minutes. The bagged preform was heated to 120 °C at a rate of 2 $°Cmin^{-1}$ and held for 30 minutes. Once the resin degassing was complete the preform was infused. With the cure

schedule, DOC of 0.7 and 0.85 were achieved. The lower DOC of 0.7 was just below the gel point of 0.76 at 180 °C. While the upper DOC of 0.85 exceeded the gel point.

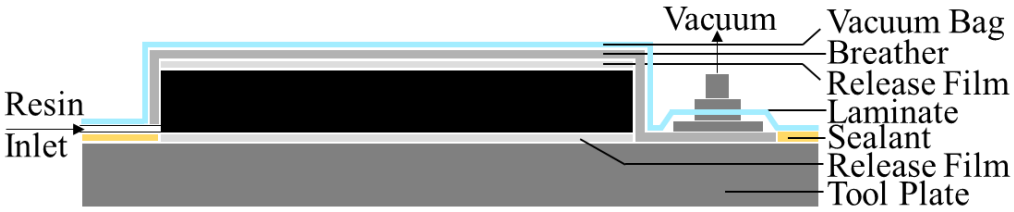

Figure 6.3. Vacuum assisted hot resin infusion and bagging scheme.

The cure schedule was designed using the cure-kinetics model [102] combined with the predicted thermal profile of the preform. The profile consisted of a temperature ramp of 2 °Cmin^{-1} from 120 °C to 160 °C. The dwell time was varied for the two panels to achieve the distinct DOC. A dwell time of 59 minutes and 75 minutes for DOC of 0.7 and 0.85, respectively, was applied. This dwell was followed by an imposed cool-down rate of 2 °Cmin^{-1} to 30 °C.

6.2.1.3 Thermoplastic-Thermoset Co-Curing

For the two co-cure steps in Figure 6.2, the two partially cured panels were placed on tool plates with a PEI plate on top and vacuum bagged. A 12 µm thick TEFLON film was placed at one edge of the panel to provide a pre-crack at the interface. The layups were cured in the oven, the cycle included a 2 °Cmin^{-1} ramp to 180 °C followed by a 2-hour dwell. A vacuum pump was connected to the vacuum bag to ensure a vacuum was maintained throughout the process. The initial cures (IC) of 0.7 and 0.85 DOC shall now be abbreviated to IC70 and IC85 respectively.

As indicated by the top row in Figure 6.2, the third panel was infused with the resin and directly co-cured with a PEI plate on top. Infusion took place at 120 °C before a 2 °Cmin^{-1} ramp to 180 °C. The aim was to minimise the initial degree of cure at the start of co-curing. Again, a TEFLON film was placed at one edge of the panel. The initial 0.2-degree of cure of the resin shall be abbreviated to IC20.

To verify the initial degree of cure of the resin and semi-cure of the two partially cured panels, samples of the resin were taken from the surface of the release films used as part of the layups during the infusions and analysed using a Differential Scanning Calorimeter (DSC). The DSC analysis involved a 5 °Cmin^{-1} modulated temperature ramp from -50 °C to 290 °C. Oscillations with a period of 40 seconds and an amplitude of 1.5 °C were used as the modulation parameters.

6.2.1.4 Double Cantilever Beam Specimen Preparation and Testing

Five Double Cantilever Beam (DCB) specimens were to be cut from each of the three co-cured panels using a water-cooled diamond saw. A diagram of a specimen is shown in Figure 6.4. The ASTM standard test method [146] was followed with a few differences. At 125 mm x 20 mm the specimens were shorter than the 140 mm in the standard. The thicknesses of the IC20 specimens were between 5.7 mm and 6 mm, above the suggested 3 mm – 5 mm range. The layup was not unidirectional.

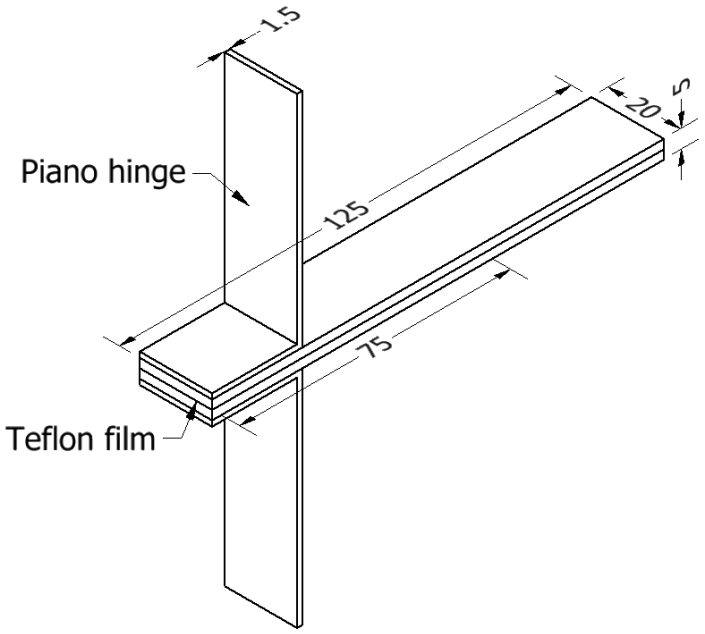

Figure 6.4. Double Cantilever Beam Specimen

When attempting to cut the IC85 plates, the two adherends separated cleanly at the interface, indicating minimal adhesion. As a result, testing was only conducted on the remaining two panels (IC20 and IC70).

The DCB specimens were tested on a Shimadzu testing machine with a 1 kN load cell. The load was applied with a head rate of 2 $mm.min^{-1}$. Five repeats were planned for both sets of specimens (one of the IC70 samples fell apart before testing). In addition to the force measurements from the testing machine, a video gauge was used to monitor the crack displacement.

6.2.1.5 Microscopy Specimen Preparation

Four 30 mm long samples were cut from the IC20 and IC70 plates. The samples were potted in a degassed mixture of Prime 37 resin and Ampreg 3X hardener, prepared in a 3:1 ratio, and

left to cure at room temperature overnight. The potted samples were ground and polished to a 0.05 μm fineness using an EcoMet Grinder-Polisher.

To improve the observable detail, the thermoplastic-thermoset interphases were etched to dissolve the thermoplastic. Droplets of the solvent N-Methyl-2-pyrrolidone (NMP) were applied directly to the surface with a pipette, allowed to stand for 30 seconds and removed by wiping followed by washing with ethanol then distilled water, the surface was dried using compressed air [61].

6.2.1.6 Gel layer Thickness Measurements

For each initial degree of cure, the gel layer of the prepared specimens were measured at 3 mm increments, for a total of 40 measurements. To enable this, optical micrographs were taken across the width of each sample, the measurements were made using ImageJ.

In the case of the IC20 samples, fibres occasionally migrated across the interface. At the 13 locations this occurred, no measurements were taken, it was not clear whether the fibres prevented an interphase from forming or simply obscured it from view.

6.2.1.7 Fractographic Analysis

To investigate the differences in the interphases and failure mechanisms between the three initial degrees of cure the failed interface surfaces were studied. A Zeiss Axio Zoom.V16 microscope was used to capture high resolution images of the surfaces. Failed IC20 and IC70 DCB specimens were analysed. For IC85, the failed surfaces of the thermoplastic and thermoset plates that came apart before cutting were analysed.

6.2.2 Diffusion Model Method

6.2.2.1 Data Cleaning

In-situ interdiffusion measurements of gel layer thickness collected at TU Delft following the procedure outlined by Teuwen et al [62] were analysed. The interdiffusion process was between a model epoxy resin system and Ultem 1000 PEI film. The absence of additives in the model epoxy system produced an accurate representation of the underlying interdiffusion process. The data considered were collected at isothermal temperatures of 150 °C, 160 °C, 170 °C and 180 °C. Five runs were performed at each temperature and the results are the mean of the five runs.

The aim was to produce a diffusion rate model fit, the enhancement of noise through this process can be an issue. To reduce the influence of noise on the characterisation process, the data was cleaned. Classical diffusion models suggest interphase growth must be monotonic,

however, the data contained instances of negative growth. These instances were removed for most of the process. However, the noise in the measurements combined with the slow rate of diffusion towards the end of the process produced a high proportion of negative values. To ensure the late phase of the process was represented, negative growth was not removed beyond a degree of cure of 0.2.

6.2.2.2 Diffusion Model

With the same materials and conditions used here [63], and others [26, 56], the diffusion of PEI into epoxy was shown to be the dominant contributor to the interphase thickness. The diffusion of PEI into epoxy exhibits Fickian behaviour. This result motivated a Fickian approach to modelling interphase formation.

Fickian diffusion in a semi-infinite medium classically results in a penetration depth,

$$h = 2\sqrt{Dt} \tag{6.1}$$

a local form also writes,

$$\frac{dh^2}{dt} = 4D \tag{6.2}$$

which is equivalent to,

$$\frac{dh}{dt} = \frac{2D}{h} \tag{6.3}$$

This instantaneous form is used to account for processes with evolving values of D. This is the case for non-isothermal, reactive processes such as the one considered here.

In accordance with the Stokes-Einstein relation, diffusivity is dependent on viscosity. The viscosity of the system is influenced by the temperature and the degree of cure. For simplicity, we considered a separate form $D = D(T, \alpha) = f(T)g(\alpha)$. f accounts for the thermo-dependence of the diffusivity which can be modelled with an Arrhenius law,

$$f(T) = D_\infty e^{\frac{-E_a}{RT}} \tag{6.4}$$

Where D_∞ was the ultimate diffusivity, E_a the activation energy, R the universal gas constant and T absolute temperature. $g(\alpha)$ was to be determined.

The experimental diffusion data showed that the rate of gel layer growth decreased sharply at the beginning of the process before quickly plateauing, attributed to the dependency of diffusivity on degree of cure. Noting the noise, Figure 6.5 indicated that an exponential

(6.5)

function of degree of cure captured the trend in the growth rate data. g was made $e^{b\alpha}$, where b is a constant. This produced the model of diffusion rate,

$$\frac{dh}{dt} = \frac{f(T)e^{b\alpha}}{h}$$

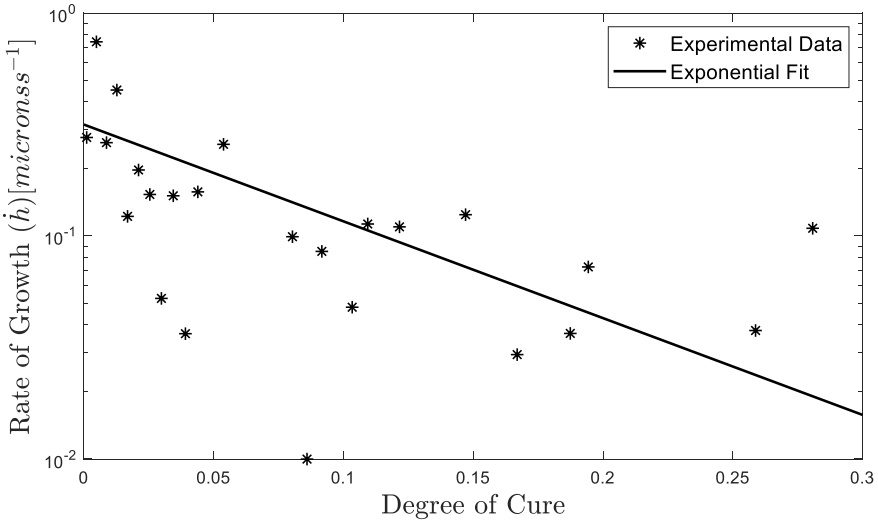

Figure 6.5. Rate of gel layer growth with degree of cure at 150°C

The degree of cure during diffusion was calculated using a cure kinetics model developed for the epoxy system by Teuwen et al [62]. Solving it using an Euler explicit time integration scheme, convergence analyses showed that results were consistent when time steps were below 0.1 seconds. An initial degree of cure of 0 was used. The data analysis also showed that there was a time offset due to the experimental acquisition method. The shift correction t_0 was the time difference between the start of the process and the first measurement.

6.2.2.3 Initial Data Characterisation

The interdiffusion thickness measurements were taken at 15-second intervals [62], resulting in an offset between the times of the first measurement and the start of the process. Before numerical methods were implemented, the values of the offsets (t_0) were found to correct the measurement timings. Equation (6.5) was rearranged,

$$ln\left(h\frac{dh}{dt}\right) = \ln(f(T)) + b\alpha \tag{6.6}$$

the result was plotted against degree of cure (Figure 6.6). A linear fit, motived by the nature of rate of cure decay observed in the data, was performed using MATLAB. Given the noise in the measurements, the non-insignificant R^2 values suggested a linear representation was

plausible. The gradient of the produced line was b and the intercept was the natural logarithm of f(T).

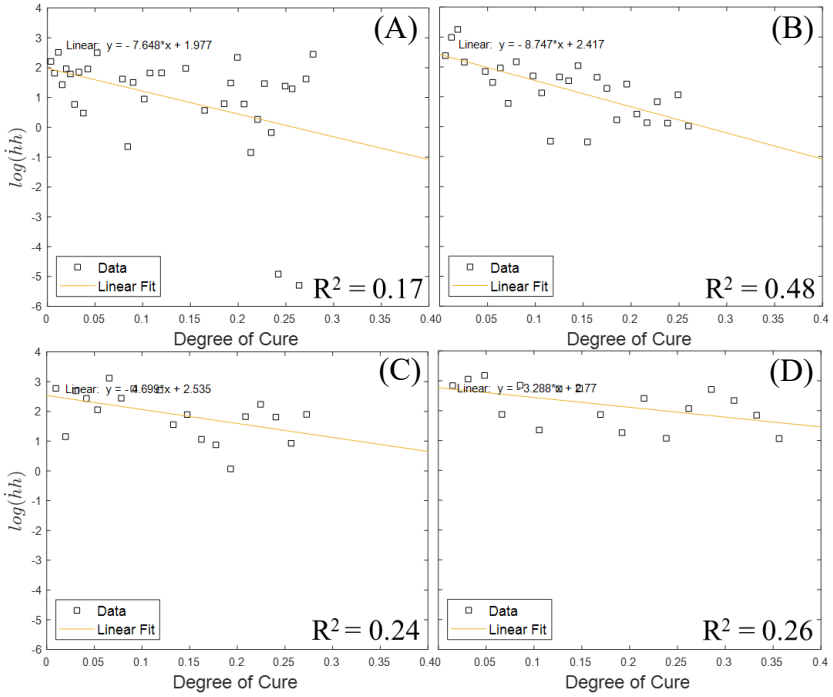

Figure 6.6. Natural logarithm of the product of diffusion depth and diffusion rate against degree of cure at 150 °C (A), 160 °C (B), 170 °C (C) and 180 °C (D)

To find t_0, Equation (6.6) was integrated and rearranged in terms of time,

$$t + t_0 = \frac{h^2}{2f(T)} \tag{6.7}$$

The value of t_0 at each temperature was found by setting $t = 0$ and using the initial gel layer thickness measurement. The obtained values of t_0 are shown in Table 6.1. There was clear uncertainty in the values for t_0, the value at 160 °C exceeded the 15-second interval between measurements. Given the dependence of t_0 on f, which has been derived from the data, and the scatter in the data visible in Figure 6.6, noise likely contributed to this uncertainty. To illustrate the range of potential influence noise had on t_0, when the data at each data point for each temperature was increased by 1 standard deviation, the increase in t_0 ranged from 2% at 170 °C to 67% at 160 °C.

Table 6.1. Times between the start of the process and the first measurements

Temperature [°C]	t_0 [s]
150	4.536
160	16.896
170	9.554
180	3.817

6.2.2.4 Numerical Solution

The time of the last measurement in each case corresponded with the onset of phase separation. The exponential decay of growth rate assumed by the model did not capture the stop in gel layer growth at the onset of phase separation suggested for isothermal conditions [62]. To avoid overpredicting the thickness for a given initial degree of cure, it was necessary for diffusion to stop at an appropriate degree of cure. A step function was added to the model such that at a given temperature, diffusion stopped at the degree of cure predicted for the onset of phase separation using the cure kinetics model. The model with the step function applied took the form,

$$\frac{dh}{dt} = \frac{f(T)e^{b\alpha}}{h} \frac{-\Delta}{\max\left(\varepsilon, \alpha - \alpha_{ops}(T)\right)} \tag{6.8}$$

Where α_{ops} is the degree of cure at the onset of phase separation, ε is arbitrarily small (set to 1e-16) and Δ is a constant giving the sharpness of the step. When fitting, parameters values were consistent at values of Δ less than 1e-3, to be conservative a value of 1e-4 was used.

The optimal value for b and values of *f*(T) were found using the fminsearch solver in MATLAB. The t_0 shifted data was the input. The *f*(T) values obtained when finding t_0 were used as the initial values. The initial b value was obtained by combining the plots in Figure 6.6 and forcing a fitting line through the origin, giving a value of -5.446.

By solving Equation (6.7) coupled with the cure kinetics model [62], values of *f*(T) and b that minimised the mean squared error to the experimental data were found. The coupled ordinary differential equations (ODE) for α and h were solved using ode45 in MATLAB, the initial value of h was 1e-16 Table 6.2 shows the optimal parameter values and the α_{ops} values predicted from the diffusion data using the cure kinetics model [62]. Ode45 uses variable time steps sizes, selecting the size based on which of the coupled equations requires the smallest step. The step size correlated with the rate of reaction. Time steps were small during the initial stages of reaction when rate reaction was slow, before sharply increasing to the max step size when reaction rate increased, this relationship is illustrated in Figure 6.7.

The solver selected a maximum step size of 150 seconds, this was justified as no material difference was observed in the results at orders of magnitude below 1000 seconds. Comparisons of the model with experimental data in Figure 6.8 indicated the validity of the model.

Table 6.2. Diffusion model constants using the fminsearch MATLAB solver and the predicted α_{ops} values.

Temperature[°C]	f [μms^{-2}]	b	α_{ops}
150	5.2861	-4.5920	0.2881
160	10.2109		0.2830
170	15.5584		0.2991
180	21.9956		0.3853

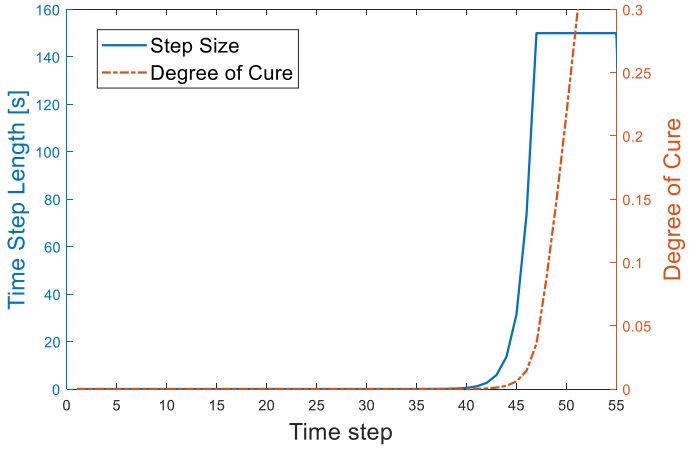

Figure 6.7. The time step size used by the ode45 solver and the simulated degree of cure against time step number.

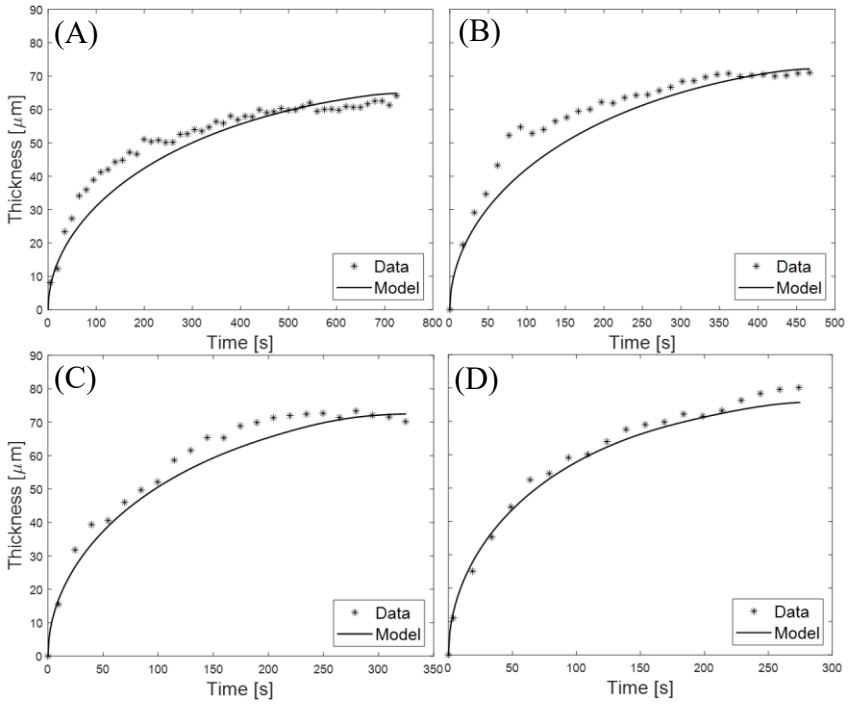

Figure 6.8. Experimental and modelled gel layer thickness data at 150 °C (A), 160 °C (B), 170 °C (C) and 180 °C (D).

Using the assumed Arrhenius temperature dependence, the diffusivity could be decomposed, to give D_∞ and E_a. The natural logarithm of the *f* values in Table 6.2 were plotted against the reciprocal of absolute temperature, Figure 6.9 shows the result. The fit gave a D_∞ of 1.0663e+10 $\mu m^2 s^{-1}$ and an E_a of 75113 $Jmol^{-1}$.

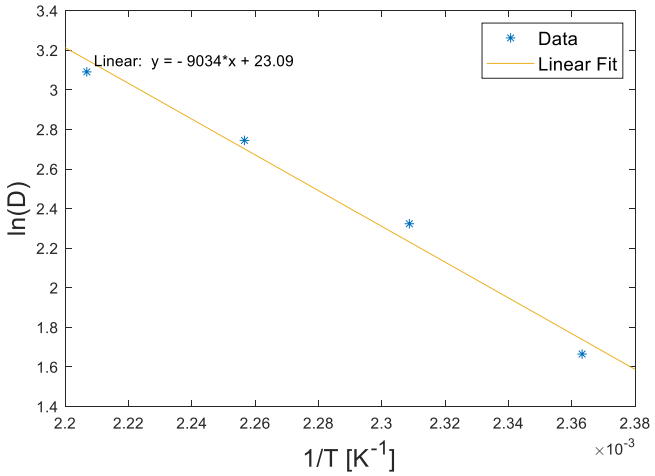

Figure 6.9. Arrhenius temperature fit of diffusivity.

6.2.2.5 Adapting the Model for EP2410

Unlike the model system used for the diffusion measurements [62], EP2410 contains undisclosed additives which may affect PEI diffusivity [56]. To apply the model to diffusion with EP2410, the epoxy systems were assumed to have similar E_a. f was only altered according to D_∞. The onset of phase separation was set to occur at a degree of cure of 0.76, the gel point of EP2410 at 180 °C [102].

6.3 Results and Discussion

6.3.1 Microscopy

Micrographs shown in Figure 6.10 of the failed interfaces indicated a decline in the level of interaction between the two adherends as initial degree of cure increased. Figure 6.11 shows that with IC20 specimens, fibre damage and what appears to be polymer deposition from the opposing adherend were present on both sides. With IC70 specimens no fibre damage was visible, evidence of adhesion was limited to damage to the surface layer of polymer on each surface. With the IC85 plates, the surfaces appeared smooth, with little evidence of interaction with the opposing plate. The lack of evidence of interphase formation on the IC85 plates agrees with previous work showing interdiffusion does not occur post gelation [26] and is consistent with the plates coming apart when trying to cut them into DCB specimens. As a result, the remaining analysis could only be performed with the IC20 and IC70 specimens.

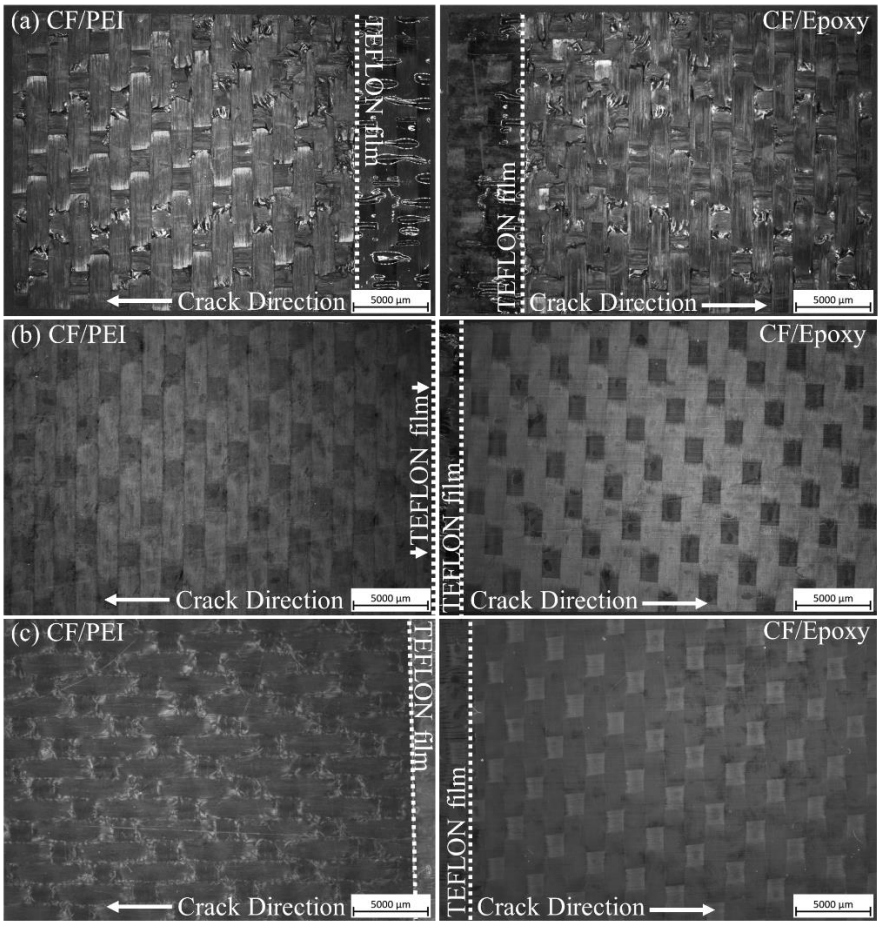

Figure 6.10. Optical micrographs of fractured surfaces between adherends of IC20 (a), IC70 (b) and IC85 (c).

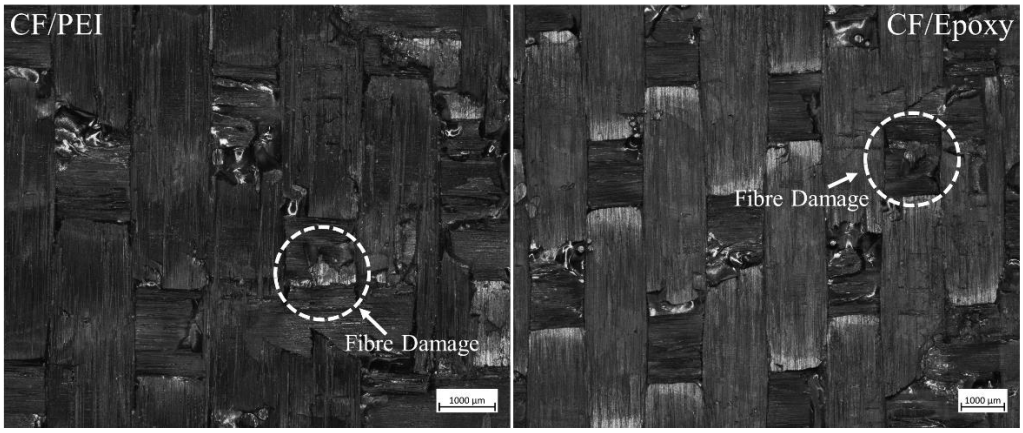

Figure 6.11. Close up of the fracture surface on an IC20 specimen with visible fibre damage (not aligned).

The gel layer thickness measurements were aggregated for each initial degree of cure and displayed in Figure 6.12, the bars represent the mean, and the error bars represent the standard deviation. The mean gel layer thickness for IC20 was almost double that of IC70. The variability was also greater. The negligible resistance to failure of the IC85 plates and the smooth failure surface suggested no gel layer was formed.

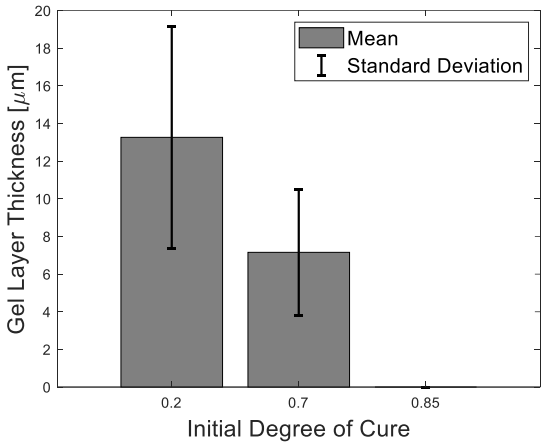

Figure 6.12. Gel layer thicknesses of IC20, IC70 and IC85 samples.

Micrographs of IC20 and IC70 specimens in Figures 6.13 and 6.14 respectively highlight differences between the gel layers. There was a difference in the way fibres interact with the gel layer. With the IC20 specimens, it was common to see fibre bundles from the thermoplastic laminate migrate into the thermoset laminate, crossing the interface as in Figure 6.13B. The gel layer formation appeared to be disrupted in these locations. In contrast, in the IC70 specimens the fibres appeared unable to migrate across the interface, preventing this disruption. There was an apparent trend in the IC70 specimens where the gel layer thickness increased in regions away from the fibres, Figure 6.14B demonstrates this transition.

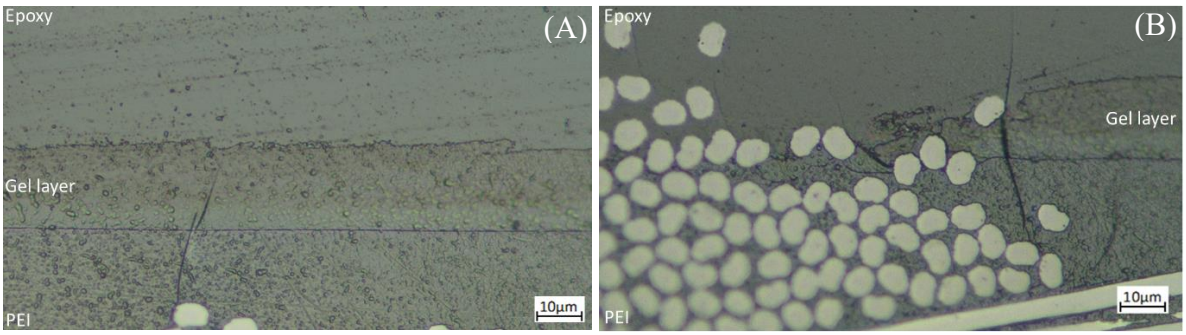

Figure 6.13. Optical micrographs of the epoxy-PEI interphase of an IC20 specimen. Clean gel layer (A), gel layer with fibre interaction (B).

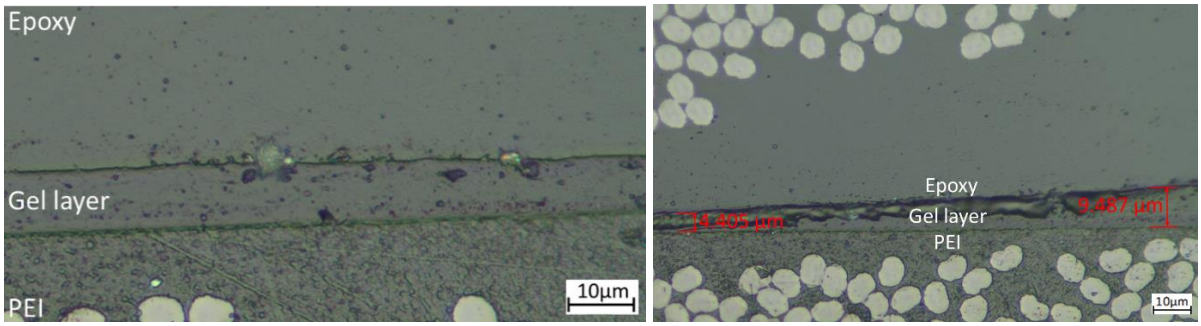

Figure 6.14. Optical micrographs of the epoxy-PEI interphase of an IC70 specimen. Clean gel layer (A), gel layer thickness changing with fibre proximity (B).

Figures 6.13A and 6.14A show a clear difference in the appearance of the two interphases. For the IC20 specimen, the gel layer was delimited by the sharp epoxy penetration front on one side and a more jagged, less well defined boundary on the other. With the IC70 specimen both boundaries were clearly defined. In the IC20 sample there was a gradient in colour between the two fronts. The darker region in the gel layer towards the epoxy side has been attributed to spinodal decomposition in previous papers [61-63], as the dissolved PEI phase separates. This region was less apparent in IC70, which was consistent with the level of swelling decreasing with greater initial degree of cure [26].

6.3.2 Double Cantilever Beam Test Results

The mean and standard deviation of the G_{IC} values for the two initial degrees of cure are shown in Figure 6.15, note a logscale was used on the y-axis to aid visualisation. According to a standard definition of outliers, values further than 1.5 times the interquartile range outside the upper and lower quartiles, a measurement was removed from each set of measurements. In both sets this was the greatest value, a value of 1793 Jm^{-2} from the IC20 measurements and a value of 11 Jm^{-2} from the IC70 measurements.

Thermoset-thermoset co-curing using the same epoxy system as in this study produced G_{IC} values of around 200 Jm^{-2} [102] (Figure 6.15), considerably lower than demonstrated by the IC20 specimens. This result clearly indicated the benefit of the gel layer morphology formed with the IC20 specimens compared to a purely thermoset interface.

The difference in the mean G_{IC} values was approaching three orders of magnitude between IC20 and IC70, compared to a factor of two between the mean gel layer thicknesses. This result suggested that the level of adhesion is not solely dependent on gel layer thickness. The difference in the level of surface contact was clearly influential. Additional factors such

morphology changes as observed in the literature [26] and fibre bridging across the interphase could also have had an effect [65].

The significant drop in G_{IC} between the two initial degrees of cure was consistent with a diminishing gel layer with increasing initial degree of cure [26]. Whereas the gel layer produces toughness enhancing morphologies, the liquid layer that remains offers limited resistance to crack propagation [26]. The differences in the interphase micrographs supported this theory. The adhesion in the IC85 sample was sufficient to hold the two plates together, so the level of adhesion was minimal but non-zero, signified by the bar in Figure 6.15.

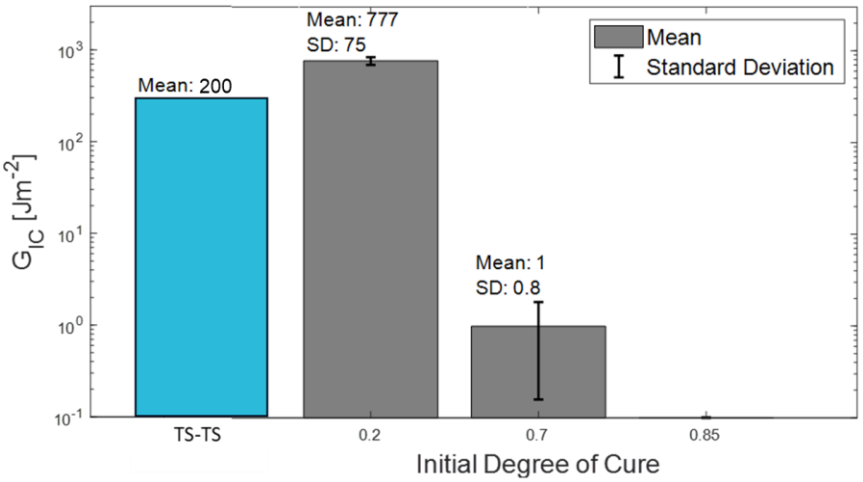

Figure 6.15. Mode 1 interlaminar fracture toughness (G_{IC}) of IC20, IC70 and IC85 specimens. The G_{IC} between uncured EP2410 laminates (TS-TP) [102] is also included.

Figure 6.16 shows the mean values of the load-displacement results for the two initial degrees of cure tested. The error bars represent one standard deviation. To reflect that repeats failed after different displacements, the plots are divided, with means and standard deviation at a given displacement only applicable to the repeats that reached that displacement. The plots illustrate the difference in the nature of the interfacial failure. While IC20 specimens withstood peak loads exceeding 130 N, IC70 specimens had peak loads just above 9 N. The error bars clearly show the greater variability of the results for the IC70 specimens, indicating the reduced reliability of the bond as initial degree of cure was increased.

In the case of IC70 specimens, an apparent inability to form an interphase near the crack initiator, evidenced by the gradual climb to peak load, resulted in no more than 2.5 mm of crack propagation before catastrophic failure. This contrasted with IC20 specimens where the peak load occurred at the onset of crack propagation and at least 15 mm of stable propagation was possible in each case. Although not subjected to DCB testing, the ability of

the IC85 sample to hold together meant the adhesion was at least equal to the weight of one plate, roughly 0.8 N.

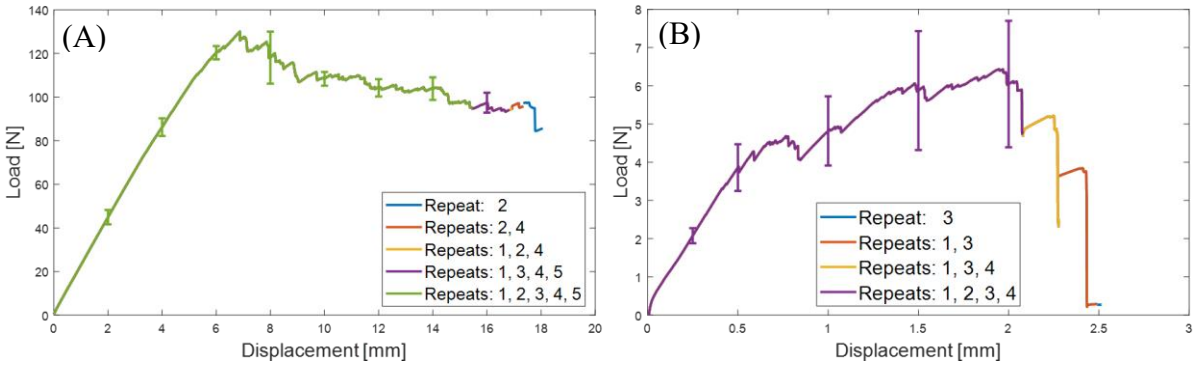

Figure 6.16. Mean load-displacement results and standard deviations from double cantilever beam tests of IC20 (A) and IC70 (B) specimens.

A factor that could have had a serious effect on G_{IC} in the precured samples was the apparent intermittency of the interphase. This took two forms. There were regions of no surface contact (Figure 6.17A) and there were regions where despite surface contact, no interphase was observed (Figure 6.17B). As shown of Figure 6.17A, the precured interphase contained a significant amount of what appeared to be voids, measured as being 20% of the combined interphase lengths.

The significant absence of bonding was only present in IC70 specimens, making it a probable cause for the low resistance to crack propagation and short propagation distances measured during the DCB tests. This intermittency of the interphase was likely a consequence of the different manufacturing processes, the greater viscosity of the near gel resin being unable to produce the intimate contact possible during the direct infusion.

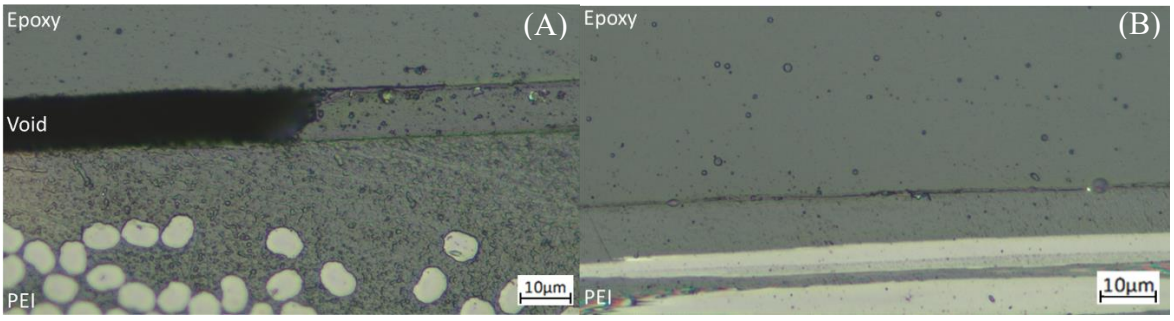

Figure 6.17. IC70 interface with a void (A) and no visible interphase formation (B).

6.3.3 Model Predictions

Using the measurements from section 6.3.1, the diffusion model was adapted for EP2410. To approximate D_∞ for EP2410 a value was selected such that the predicted gel layer thickness at 180 °C, starting from a degree of cure of 0.2, matched the mean of the IC20 experimental

measurements. This value was 5.1e+8 $\mu m^2 s^{-1}$. Using this value, the model was used to predict the change in gel layer thickness as the initial degree of cure was increased. It was assumed that the onset of phase separation was unaffected by the initial degree of cure. Figure 6.18 shows the results alongside the measured thickness and G_{IC} values.

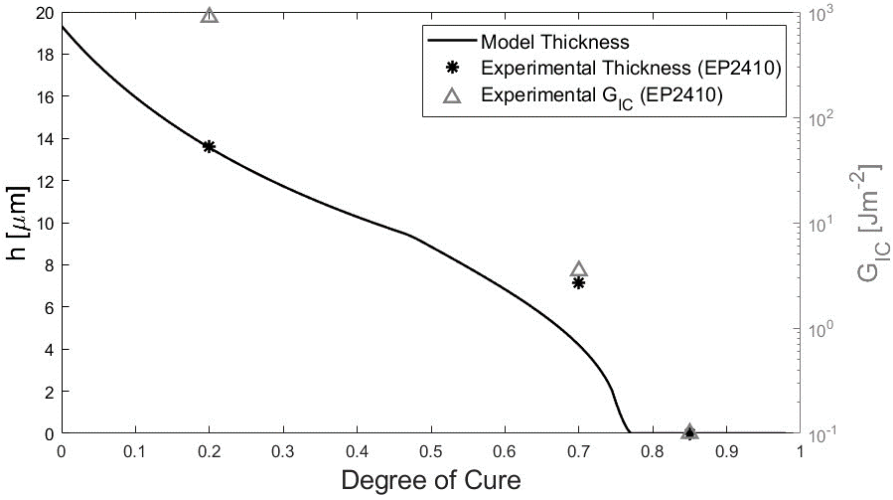

Figure 6.18. Gel layer thickness with initial degree of cure at 180 °C, predicted and measured, and corresponding measured Mode 1 fracture toughness.

Until initial degrees of cure approaching gelation, the model predicted a near linear decline in gel layer thickness, reaching zero at the predicted onset of gelation. Under the assumption interphase formation stopped at gelation, the model underpredicted the gel layer thickness for IC70 specimens. The model predicted a thickness of 4.19 μm, compared to the mean measurement of 7.16 μm. Given the model assumed the temperature history was perfectly followed, when making such comparisons it is important to note the contribution of the offset between the imposed temperature history and that seen by the material, explored in Chapter 4.

The underpredictions of the model shown in Figure 6.18 could be explained by the literature. The assumption of the model is consistent with the observation from Lestriez et al [26] that no interdiffusion occurred between thermoplastics and thermosets joined beyond the onset of phase separation. However, Farooq et al observed interdiffusion beyond phase separation when the process was started from an uncured state, due to fractionation effects [61]. This suggests that although interdiffusion will not occur when initiated at degrees of cure beyond phase separation, when started from a lower degree of cure, diffusion will proceed beyond the onset of phase separation predicted for the bulk resin. This is enabled by the lower rate of cure of epoxy monomers that have diffused into regions of high thermoplastic content [61]. Consequently, the hard cutoff imposed by the model led to an underprediction of diffusion

depth. It is noted that Farooq et al [61] did not test for this effect under isothermal conditions.

This interpretation of the data suggests that like with classical co-curing, there is an initial degree of cure, believed to be the gel point, beyond which no interaction occurs between the adherends. However, in contrast, the extent of the interaction appears to decrease from an uncured state to this point. These findings suggest that with thermoplastic-thermosets, semi-curing is less beneficial than in the classical case of thermoset-thermoset bonding explored by Motsch-Eichmann et al [13]. The DCB results indicated that unlike in the classical case, the level of adhesion diminishes significantly with increasing initial degree of cure before gelation. Furthermore, performing the infusion of the thermoset laminate with the thermoplastic laminate in contact produced better surface contact. Given most aerospace structural applications prioritise specific mechanical performance, the improvement in handleability cannot be justified in this context.

6.4 Conclusion

In this work, specimens were produced by co-curing epoxy laminates with PEI laminates at 0.2 (IC20), 0.7 (IC70) and 0.85 (IC85) degrees of cure. The failure of the IC85 sample during manufacturing demonstrated the limited adhesion possible post gelation. This was confirmed by fractographic analysis.

The remaining two sets of samples were analysed using optical microscopy and DCB testing. Clear boundaries either side of the gel layer indicated phase separation had occurred at both initial degrees of cure. Measurements from optical micrographs showed that the increased initial degree of cure resulted in the mean gel layer thickness being halved. The micrographs revealed significant porosity across the interface of the IC70 samples exclusively, indicating the superiority of joining the laminates before infusion and a less cured resin for establishing surface contact.

The difference between the mean G_{IC} values for the two initial degrees of cure were much more pronounced than the mean thicknesses of the gel layer. The difference approached three orders of magnitude, compared to the factor of two separating the thickness measurements. This result indicated thickness alone is not a linear indicator of adhesion quality at the interface. It confirms factors such as morphology and surface contact have a significant influence on adhesion, as indicated by the literature. The G_{IC} values of the IC20 specimens were significantly greater than co-cured laminates with the same epoxy system from previous

work, providing evidence of the benefit of a thermoplastic-thermoset interphase with a low initial degree of cure.

A simplified model for gel layer thickness was derived from diffusion data with a model epoxy system. Using the thickness measurements from the laminates as guides, the influence of initial degree of cure on gel layer thickness was predicted. The model suggested that unlike thermoset-thermoset co-curing, adhesion is influenced by any increase in initial degree of cure in thermoplastic-thermoset co-curing. Based on this result, semi-curing the thermoset adherend did not seem viable. Given the significant drop in adhesion between IC20 and IC70, and the importance of specific mechanical performance in aerospace structurers, the efficiency gains cannot justify the drop in performance.

Further topics include extending the work of Farooq et al [61] to explore the effect of temperature history on the onset of phase separation. Crucially, this would involve testing if diffusion occurs post phase separation without an increase in temperature, as suggested by this study.

It would be beneficial to validate the assumption made in this work that the initial degree of cure did not affect the degree of cure at the onset of phase separation. This would give insight into the early stages of the process and the influence of resin storage history.

Phase separation is typically stated to occur around the onset of gelation. Given miscibility influences the degree of cure phase separation actually occurs, an understanding of how epoxy functionality and additives effect it would indicate the relevance of past work with model systems, to future studies with systems more representative of aerospace materials.

Disclosure statement

The authors report there are no competing interests to declare.

Data access statement

All presented data will be made available upon request.

Funding

This work was supported by the EPSRC Future Composites Manufacturing Research Hub under Grant EP/P006701/1.

Acknowledgements

The authors wish to thank Dr Robin Hartley of the University of Bristol for assistance with experimental work and access to data analysis software, Charlie Brewster of the University of Bristol for chemistry expertise and assistance with experimental work, and many colleagues at the University of Bristol for insight and use of data regarding Solvay EP2410.

Chapter 6 Closing Remarks

This chapter fulfilled Objective 4, indicating semi-curing has a strong influence on the adhesion between co-cured thermoplastic-thermoset adherends. This was shown not only to be due to changes in interdiffusion, but also from practical issues, the more viscous resin limiting the level of intermate contact between the adherends.

The decreased gel layer thickness with the 0.7 semi-cured samples showed initial degree of cure affected the interdiffusion process before gelation. The lack of adhesion with the 0.85 semi-cured sample, suggested gelation is the cut off for the initiation of interphase formation.

In contrast to thermoset-thermoset co-curing where adhesion appears unaffected until gelation [13], the results indicated semi-curing is far less suitable in the thermoplastic-thermoset context. In aerospace structures where specific mechanical performance is critical, efficiency gains from the stiffer thermoset adherend cannot justify the reduction in structural performance.

In terms of process uncertainty, given the sensitivity of adhesion to initial degree of cure, it is important the degree of cure of a sample is well understood to achieve reliable joints. This would be particularly important if semi-curing were employed, requiring an understanding of process variability and the resulting effects, as considered in Chapter 4.

7 Conclusions and Future Work

7.1 Conclusions

This thesis has discussed four work packages that were performed to better understand variability in composite manufacturing, and thermoplastic-thermoset laminate co-curing.

7.1.1 The Influence of Key Processing Parameters on Thermoset Laminate Curing

The first work package looked at determining the most influential parameters in composite processing, accounting for real world variability. The purpose being to enable a more targeted approach for increasing the robustness of the process. It was found that cure temperature was the dominant influence and diffusion limiting cure kinetic effects became highly influential post vitrification. The indication being that the most effective way to increase robustness is to invest in process equipment with temperature uniformity and repeatability.

Although the influence hierarchy was established through the analysis of a single epoxy system, the similar processing conditions and performance requirements among aerospace grade epoxies suggests a generality of the results. Furthermore, the dominance of the most influential parameters suggests variability between systems was unlikely to significantly affect the top of the hierarchy. Therefore, the objective of identifying the most influential parameters on the curing of aerospace grade epoxy was addressed.

7.1.2 Effects of Heat Transfer Coefficient Variations on Composite Curing

The second work package explored how process variability translates to variability in the output of the curing process. The source of variability considered was heat transfer coefficient (HTC), using measurements from industrial scale ovens and autoclaves. A coupled finite element model was used to simulate the effect of the measured conditions on composite curing. It was found that the higher HTCs in the autoclaves gave greater robustness to variability. Hence, despite greater variability in the autoclave measurements, the two types of vessels were predicted to produce outputs with comparable variability.

Metrics related to the transverse temperature distribution and cure kinetics, enabled the effects of the measured HTC variability on the process to be quantified. Given the significant influence of the thermal environment on the curing reaction shown in Chapter 3, these results provide a good indicator of the influence of process variability on the output. Hence, taking Hexply M21 to be broadly representative of aerospace grade epoxy systems, this chapter

addressed the objective of quantifying the effect of measured process variability on the curing of aerospace grade epoxy.

7.1.3 Controlling the Cure Gradient Through Tool Design

The third work package looked at curing environments to produce stiff semi-cured parts with sufficient reactivity at the bonding surface for co-curing. Using a coupled model, combinations of tool material, tool geometry and HTC were considered to achieve the required cure gradient. In the omega stringer case study, the cure gradient was maximised with a thin composite tool at the web and a thick aluminium tool at the flange (where the bonding surface was). The size of the cure gradient could be increased using a lower value of HTC, suggesting the suitability of an out-of-autoclave approach. Much greater cure gradients were possible using heat mats to directly apply heat at locations away from the bonding surface.

This chapter addressed the objective of proposing manufacturing concepts to achieve the desired degree of semi-cure for co-curing. Although the analysis was limited to a single geometry, the methodology behind the two proposals was based on the underlying physics, hence the solutions are transferable.

7.1.4 The Effect of Initial Degree of Cure on Thermoplastic-Thermoset Laminate Interphases

The fourth work package investigated the effect of initial degree of cure on thermoplastic-thermoset co-curing. Specimens were fabricated by co-curing PEI composite laminates with epoxy laminates at three initial degrees of cure, 0.2, 0.7 and 0.85. Double cantilever beam tests indicated that adhesion does not form post gelation and in contrast to classical co-curing adhesion reduced with degrees of cure up to gelation. Microscopy showed average interphase thickness to half from an initial degree of cure of 0.2 to 0.7.

A numerical model derived from co-cured thermoplastic-thermoset interphase thickness data predicted a near linear decrease in interphase thickness with increasing initial degree of cure, with the rate of decay increasing sharply approaching gelation. Compared to the thickness measurements from the laminates, the model appeared to under-predict the interphase thickness for a given degree of cure. This was believed to be due to the common assumption that interphase growth stopped at gelation being too strong. The results were supported by a finding in the literature, that due to fractionation effects, interdiffusion occurs beyond gelation predicted for the bulk. The reduction in adhesion with increasing degree of cure

meant that the semi-curing of thermoset adherends to increase handleability and reduce tooling complexity is unlikely to be viable for primary aerospace structures.

Through showing the detrimental effect increasing initial degree of cure has on interphase formation and predicting the nature of this effect, this chapter addressed Objective 4, to investigate the influence of the degree of semi-curing on thermoplastic-thermoset interphase formation.

7.2 Summary of Contributions

The dominant influence of the thermal environment was a key finding when ranking the influence of process parameters on thermoset curing. Considering this, the analysis of the variability in a range of industrial vessels was a useful contribution for understanding the uncertainty in the degree of cure/semi-cure. These preliminary findings were applied to thermoplastic-thermoset co-curing by characterising the influence of initial degree of cure on interphase formation.

In light of the measured variability in the curing environment, the result that any amount of semi-curing negatively effects interphase formation was important. The finding indicated the semi-curing of thermoset adherends before co-curing with thermoplastics, for assembling efficiency, is not suitable given the importance of specific mechanical properties in aerospace structures. This result does not follow from classical co-curing of thermosets and was the first to consider initial degree of cure with thermoplastic-thermoset laminate co-curing.

To mitigate the effect of semi-curing prior to co-curing, tooling and heating concepts for semi-cured parts with cure gradients favourable for co-curing were demonstrated using simulations.

7.3 Future Work

Thermoplastic-thermoset interphase formation has mostly been studied using model epoxy systems in the literature. In a few cases, including this work, commercially formulated aerospace grade epoxies have been shown to produce smaller interphases, which may be due to unknown and proprietary additives. In all these cases, numerous factors such as fibres, curing agents, epoxy functionality and initial degree of cure have been present simultaneously, preventing definite conclusions about individual influences. A more systematic approach to understanding how additives and epoxies influence the interdiffusion process would provide clear insights for more optimal material selection.

Chapter 6 of this work focused on key values of initial degree of cure to assess the nature of the process at these points. Performing tests with initial degrees of cure between 0 and gelation would allow the nature of the influence of initial degree of cure on the interdiffusion process to be more precisely characterised. The same combination of interphase thickness and adhesion measurements used in this work would provide clear indicators of the overall change in the process. Detailed mechanical characterisation would provide useful insight into how the changes in the interdiffusion process influence the structural performance of the interphase, an important design consideration.

The ability of thermoplastic-thermoset co-curing to create strong bonds has been demonstrated in this and previous work. However, to determine the merits and potential applications for the bonds produced, testing must go beyond the level of adhesion, to give a more complete characterisation. For example, given the resistance of the interphase to crack propagation, the ability of the joints to tolerate fatigue, e.g., through cyclic loading, would be an interesting result. A more complete understanding of the mechanical performance of the interphase is necessary to understand the full effect of the factors mentioned above.

In-depth characterisation will be central to the extension of this process to industrial applications, such as those outlined in Section 1.2.3. For example, the impact resistance of a thermoplastic-thermoset interphase would be significant for a co-cured thermoplastic wind turbine blade leading edge protector. The longevity benefits of the thermoplastic would only be realised providing impacts from particles did not cause the interphase to delaminate prematurely.

Given the nascence of this process it would be prudent to continue the consideration of variability into future work. For this process to be performed safely at industrial scale, it would critical that the variability of interfacial properties under the prevailing manufacturing conditions is understood.

8 References

1. Dutton, S., D. Kelly, and A. Baker, *Composite materials for aircraft structures*. 2004: American Institute of Aeronautics and Astronautics.
2. Guo, Q., *Thermosets: structure, properties, and applications*. 2018, Amsterdam: Woodhead Publishing.
3. Advani, S.G. and K.-T. Hsiao, *Manufacturing techniques for polymer matrix composites (PMCs)*. Woodhead Publishing Series in Composites Science and Engineering. 2012, Cambridge: Woodhead Publishing Limited.
4. Agius, S., K. Magniez, and B. Fox, *Cure behaviour and void development within rapidly cured out-of-autoclave composites.* Composites Part B: Engineering, 2013. **47**: p. 230-237.
5. Dodiuk, H., *Handbook of thermoset plastics*. 2022, Norwich, NY: William Andrew.
6. Ma, H., M.A. Aravand, and B.G. Falzon, *Phase morphology and mechanical properties of polyetherimide modified epoxy resins: A comparative study.* Polymer, 2019. **179**: p. 121640.
7. August, Z., et al., *Recent developments in automated fiber placement of thermoplastic composites.* SAMPE J, 2014. **50**(2): p. 30-37.
8. Kinvi-Dossou, G., et al., *Innovative acrylic thermoplastic composites versus conventional composites: Improving the impact performances.* Composite Structures, 2019. **217**: p. 1-13.
9. Bhudolia, S.K., P. Perrotey, and S.C. Joshi, *Enhanced vibration damping and dynamic mechanical characteristics of composites with novel pseudo-thermoset matrix system.* Composite Structures, 2017. **179**: p. 502-513.
10. Van Ingen, J.W., et al. *Development of the Gulfstream G650 induction welded thermoplastic elevators and rudder*. in *Proceedings of the international SAMPE symposium and exhibition, Seattle, WA, USA*. 2010.
11. Pearson, A., *Stratasys additive manufacturing chosen by Airbus to produce 3D printed flight parts*. 2020, Stratasys: stratasys.com.
12. Soutis, C., *Aerospace engineering requirements in building with composites*, in *Polymer composites in the aerospace industry*. 2020, Elsevier. p. 3-22.
13. Motsch-Eichmann, N., et al., *Experimental investigation of modified co-curing process for carbon fiber/epoxy-laminates.* Journal of Micromechanics and Molecular Physics, 2021. **6**(03): p. 1-12.
14. Villegas, I.F. and P.V. Rubio, *On avoiding thermal degradation during welding of high-performance thermoplastic composites to thermoset composites.* Composites Part A: Applied Science Manufacturing, 2015. **77**: p. 172-180.
15. Cortés, E., et al., *On the material characterisation of wind turbine blade coatings: the effect of interphase coating–laminate adhesion on rain erosion performance.* Materials, 2017. **10**(10): p. 1146.
16. Bartolomé, L. and J. Teuwen, *Prospective challenges in the experimentation of the rain erosion on the leading edge of wind turbine blades.* Wind Energy, 2019. **22**(1): p. 140-151.
17. Ren, Z., et al., *Offshore wind turbine operations and maintenance: A state-of-the-art review.* Renewable and Sustainable Energy Reviews, 2021. **144**: p. 110886.
18. Liu, P. and C.Y. Barlow, *Wind turbine blade waste in 2050.* Waste Management, 2017. **62**: p. 229-240.
19. Herring, R., et al., *The increasing importance of leading edge erosion and a review of existing protection solutions.* Renewable and Sustainable Energy Reviews, 2019. **115**: p. 109382.

20. Erartsin, O., J.S.M. Zanjani, and I. Baran, *Unravelling the interphase-bond strength relationship in novel co-bonded thermoplastic-thermoset hybrid composites for leading edge protection of wind turbine blades.* Polymer Testing, 2023. **117**: p. 107856.
21. Gardiner, G. *Developing repairs for thermoplastic composite aerostructures*. 2023 [cited 2023 09/03/2023]; Available from: https://www.compositesworld.com/articles/developing-repairs-for-thermoplastic-composite-aerostructures.
22. Law, H. and V. Koutsos, *Leading edge erosion of wind turbines: Effect of solid airborne particles and rain on operational wind farms.* Wind Energy, 2020. **23**(10): p. 1955-1965.
23. Mason, H. *Novel processes for hybrid thermoset-thermoplastic pultruded parts*. 2023 [cited 2023 09/03/2023]; Available from: https://www.compositesworld.com/articles/demonstrating-novel-processes-for-hybrid-thermoset-thermoplastic-pultruded-parts-.
24. McIlhagger, A., E. Archer, and R. McIlhagger, *Manufacturing processes for composite materials and components for aerospace applications*, in *Polymer composites in the aerospace industry*. 2020, Elsevier. p. 59-81.
25. Inoue, T., *Reaction-induced phase decomposition in polymer blends.* Progress in Polymer Science, 1995. **20**(1): p. 119-153.
26. Lestriez, B., J.-P. Chapel, and J.-F. Gérard, *Gradient interphase between reactive epoxy and glassy thermoplastic from dissolution process, reaction kinetics, and phase separation thermodynamics.* Macromolecules, 2001. **34**(5): p. 1204-1213.
27. Mesogitis, T., A.A. Skordos, and A. Long, *Uncertainty in the manufacturing of fibrous thermosetting composites: A review.* Composites Part A: Applied Science and Manufacturing, 2014. **57**: p. 67-75.
28. Potter, K. *Understanding the origins of defects and variability in composites manufacture*. in *International conference on composite materials (ICCM)-17, Edinburgh, UK*. 2009.
29. Witik, R.A., et al., *Economic and environmental assessment of alternative production methods for composite aircraft components.* Journal of Cleaner Production, 2012. **29**: p. 91-102.
30. Mesogitis, T., A.A. Skordos, and A. Long, *Stochastic simulation of the influence of cure kinetics uncertainty on composites cure.* Composites Science Technology, 2015. **110**: p. 145-151.
31. Collinson, M., et al., *Novel composite curing methods for sustainable manufacture: A review.* Composites Part C: Open Access, 2022. **9**: p. 100293.
32. Rana, S. and R. Fangueiro, *Advanced composite materials for aerospace engineering: processing, properties and applications*. 2016: Woodhead Publishing.
33. Sinmazçelik, T., et al., *A review: Fibre metal laminates, background, bonding types and applied test methods.* Materials Design, 2011. **32**(7): p. 3671-3685.
34. Stokes-Griffin, C.M. and P. Compston, *Investigation of sub-melt temperature bonding of carbon-fibre/PEEK in an automated laser tape placement process.* Composites Part A: Applied Science Manufacturing, 2016. **84**: p. 17-25.
35. Park, J. and S.C. Kim, *Phase separation during synthesis of polyetherimide/epoxy semi-IPNs.* Polymers for Advanced Technologies, 1996. **7**(4): p. 209-220.
36. Cui, J., et al., *Studies on the phase separation of polyetherimide-modified epoxy resin, 2. Effect of molecular weight of PEI on the structure formation.* 1997. **198**(10): p. 3267-3276.

37. Sela, N. and O. Ishai, *Interlaminar fracture toughness and toughening of laminated composite materials: a review.* Composites, 1989. **20**(5): p. 423-435.
38. Cho, J., et al., *Effects of morphology on toughening of tetrafunctional epoxy resins with poly (ether imide).* Polymer, 1993. **34**(23): p. 4832-4836.
39. Hwang, J., et al., *Phase separation behavior of cyanate ester resin/polysulfone blends.* 1999. **74**(1): p. 33-45.
40. Bucknall, C.B. and A.H. Gilbert, *Toughening tetrafunctional epoxy resins using polyetherimide.* Polymer, 1989. **30**(2): p. 213-217.
41. Yasaee, M., et al., *Control of compressive fatigue delamination propagation of impact damaged composites using discrete thermoplastic interleaves.* Applied Composite Materials, 2015. **22**: p. 559-572.
42. Byers, B.A., *Behavior of Damaged Graphite/Epoxy Laminates Under Compression Loading*. 1980, Boeing Commercial Airplane Co Seattle Wa.
43. Yasaee, M., et al., *Mode I interfacial toughening through discontinuous interleaves for damage suppression and control.* Composites Part A: Applied Science and Manufacturing, 2012. **43**(1): p. 198-207.
44. Yasaee, M., et al., *Damage control using discrete thermoplastic film inserts.* Composites Part A: Applied Science and Manufacturing, 2012. **43**(6): p. 978-989.
45. Prichard, J.C. and P. Hogg, *The role of impact damage in post-impact compression testing.* Composites, 1990. **21**(6): p. 503-511.
46. Banea, M. and L.F. da Silva, *Adhesively bonded joints in composite materials: an overview*. Proceedings of the Institution of Mechanical Engineers, Part L: Journal of Materials: Design Applications, 2009. **223**(1): p. 1-18.
47. Deng, S., et al., *Thermoplastic–epoxy interactions and their potential applications in joining composite structures–A review*. Composites Part A: Applied Science Manufacturing, 2015. **68**: p. 121-132.
48. Paton, R., et al. *A breakthrough in the assembly of aircraft composite structures*. in *25th International Congress of the Aeronautical Sciences, Hamburg, Germany*. 2006.
49. Shi, H., J. Sinke, and R. Benedictus, *Surface modification of PEEK by UV irradiation for direct co-curing with carbon fibre reinforced epoxy prepregs.* International Journal of Adhesion, 2017. **73**: p. 51-57.
50. Villegas, I.F., et al., *Process and performance evaluation of ultrasonic, induction and resistance welding of advanced thermoplastic composites.* Journal of Thermoplastic Composite Materials, 2013. **26**(8): p. 1007-1024.
51. Yousefpour, A., M. Hojjati, and J.-P. Immarigeon, *Fusion bonding/welding of thermoplastic composites.* Journal of Thermoplastic composite materials, 2004. **17**(4): p. 303-341.
52. Schmid Fuertes, T.A., et al., *Bonding of CFRP primary aerospace structures–discussion of the certification boundary conditions and related technology fields addressing the needs for development.* 2015. **22**(8): p. 795-808.
53. Moosburger-Will, J., et al., *Joining of carbon fiber reinforced polymer laminates by a novel partial cross-linking process.* Journal of Applied Polymer Science, 2015. **132**(27).
54. Oyama, H.T., J. Lesko, and J. Wightman, *Interdiffusion at the interface between poly (vinylpyrrolidone) and epoxy.* Journal of Polymer Science Part B: Polymer Physics, 1997. **35**(2): p. 331-346.
55. Gibbs, J.W., *On the equilibrium of heterogeneous substances.* American Journal of Science, 1878. **3**(96): p. 441-458.

56. Villegas, I.F. and R. van Moorleghem, *Ultrasonic welding of carbon/epoxy and carbon/PEEK composites through a PEI thermoplastic coupling layer.* Composites Part A: Applied Science Manufacturing, 2018. **109**: p. 75-83.
57. Tsiangou, E., et al., *Investigation on energy director-less ultrasonic welding of polyetherimide (PEI)-to epoxy-based composites.* Composites Part B: Engineering, 2019. **173**: p. 107014.
58. Brauner, C., et al., *Co-curing behaviour of thermoset composites with a thermoplastic boundary layer for welding purposes.* Advanced Composites Letters, 2020. **29**.
59. Hou, M. *Thermoplastic adhesive for thermosetting composites*. in *Materials Science Forum*. 2012. Trans Tech Publ.
60. Voleppe, Q., et al., *Enhanced fracture resistance of thermoset/thermoplastic interfaces through crack trapping in a morphology gradient.* Polymer, 2021. **218**: p. 123497.
61. Farooq, U., et al., *Effect of a Dwell Stage in the Cure Cycle on the Interphase Formation in a Poly (ether imide)/High T g Epoxy System.* ACS Applied Polymer Materials, 2021. **3**(12): p. 6111-6119.
62. Teuwen, J., et al. *Gradient interphases between high T g epoxy and polyetherimide for advanced joining processes*. in *ECCM18–18th European conference on composite materials, Athens, Greece*. 2018.
63. Zweifel, L., et al., *In Situ Characterization of the Reaction-Diffusion Behavior during the Gradient Interphase Formation of Polyetherimide with a High-Temperature Epoxy System.* Polymers, 2022. **14**(3): p. 435.
64. Bonnaud, L., et al., *Different parameters controlling the initial solubility of two thermoplastics in epoxy reactive solvents.* Journal of applied polymer science, 2002. **83**(6): p. 1385-1396.
65. Surendran, A., et al., *An overview of viscoelastic phase separation in epoxy based blends.* Soft Matter, 2020. **16**(14): p. 3363-3377.
66. Varley, R.J., J. Hodgkin, and G.P. Simon, *Toughening of a trifunctional epoxy system: Part VI. Structure property relationships of the thermoplastic toughened system.* Polymer, 2001. **42**(8): p. 3847-3858.
67. Alfrey Jr, T., E. Gurnee, and W. Lloyd. *Diffusion in glassy polymers*. in *Journal of Polymer Science Part C: Polymer Symposia*. 1966. Wiley Online Library.
68. Wilmers, J. and S. Bargmann, *Simulation of non-classical diffusion in polymers.* Heat and Mass Transfer, 2014. **50**(11): p. 1543-1552.
69. Sanopoulou, M., D. Stamatialis, and J. Petropoulos, *Investigation of case II diffusion behavior. 1. Theoretical studies based on the relaxation dependent solubility model.* Macromolecules, 2002. **35**(3): p. 1012-1020.
70. Thomas, N.L. and A.J.P. Windle, *A theory of case II diffusion.* 1982. **23**(4): p. 529-542.
71. Vrentas, J., C. Jarzebski, and J. Duda, *A Deborah number for diffusion in polymer-solvent systems.* AIChE Journal, 1975. **21**(5): p. 894-901.
72. Durning, C., et al., *A study of case II transport by laser interferometry.* Macromolecules, 1995. **28**(12): p. 4234-4248.
73. Sauer, B.B. and D.J. Walsh, *Use of neutron reflection and spectroscopic ellipsometry for the study of the interface between miscible polymer films.* Macromolecules, 1991. **24**(22): p. 5948-5955.
74. Peterlin, A., *Diffusion in a network with discontinuous swelling.* Journal of Polymer Science Part B: Polymer Letters, 1965. **3**(12): p. 1083-1087.

75. Voleppe, Q., T. Pardoen, and C. Bailly, *Interdiffusion and phase separation upon curing in thermoset-thermoplastic interphases unravelled by the characterization of partially cured systems.* Polymer, 2016. **106**: p. 120-127.
76. Robeson, L., *Historical perspective of advances in the science and technology of polymer blends.* Polymers, 2014. **6**(5): p. 1251-1265.
77. Riccardi, C., et al., *Thermodynamic analysis of the phase separation in polyetherimide-modified epoxies.* Journal of Polymer Science Part B: Polymer Physics, 1996. **34**(2): p. 349-356.
78. Flory, P.J., *Principles of polymer chemistry*. 1953: Cornell University Press.
79. Gan, W., et al., *Effects of the molecular weight of poly (ether imide) on the viscoelastic phase separation of poly (ether imide)/epoxy blends.* Journal of applied polymer science, 2009. **114**(5): p. 3158-3167.
80. Mathew, V.S., et al., *Epoxy resin/liquid natural rubber system: secondary phase separation and its impact on mechanical properties.* Journal of materials science, 2010. **45**(7): p. 1769-1781.
81. Tao, Q., et al., *Viscoelastic effects on the phase separation in thermoplastics modified cyanate ester resin.* 2004. **45**(10): p. 3505-3510.
82. Tanaka, H., *Viscoelastic phase separation.* J Journal of Physics: Condensed Matter, 2000. **12**(15): p. R207.
83. Mai, K., J. Huang, and H. Zeng, *Studies of the stability of thermoplastic-modified bismaleimide resin.* Journal of applied polymer science, 1997. **66**(10): p. 1965-1970.
84. Kim, S.C. and H.R. Brown, *Impact-modified epoxy resin with glassy second component.* Journal of materials science, 1987. **22**: p. 2589-2594.
85. Pearson, R. and A. Yee, *Toughening mechanisms in elastomer-modified epoxies: Part 3 The effect of cross-link density.* Journal of materials science, 1989. **24**: p. 2571-2580.
86. Cui, J., et al., *Studies on the phase separation of polyetherimide-modified epoxy resin, 3. Morphology development of the blend during curing.* 1998. **199**(8): p. 1645-1649.
87. Dumont, D., *Thermoplastic as carrier for delivering carbon nanotubes and layered clay in epoxy resin for composite applications*. 2013, Phd Thesis, Université catholique de Louvain.
88. Kim, B.S., T. Chiba, and T. Inoue, *Phase separation and apparent phase dissolution during cure process of thermoset/thermoplastic blend.* Polymer, 1995. **36**(1): p. 67-71.
89. Ueberreiter, K. and F. Asmussen, *Velocity of dissolution of polymers. Part I.* Journal of Polymer Science, 1962. **57**(165): p. 187-198.
90. Heitzmann, M.T., et al. *Morphology of an interface between polyetherimide and epoxy prepreg*. in *Advanced Materials Research*. 2012. Trans Tech Publ.
91. Girard-Reydet, E., et al., *Epoxy-aromatic diamine kinetics. 2. Influence on epoxy-amine network formation.* Macromolecules, 1995. **28**(23): p. 7608-7611.
92. Vandi, L.-J., et al. *Interface diffusion and morphology of aerospace grade epoxy co-cured with thermoplastic polymers*. in *28th International Congress of the Aeronautical Sciences (ICAS), Brisbane, Australia, Sept*. 2012.
93. Ibeh, C.C., *Thermoplastic materials: properties, manufacturing methods, and applications*. 2011: CRC Press.
94. Siddhamalli, S.K., *Phase-separation behavior in poly (ether imide)-modified epoxy blends.* Polymer-Plastics Technology Engineering, 2000. **39**(4): p. 699-710.
95. Solvay, *TECHNICAL DATA SHEET PRISM™ EP2410 RESIN FOR INFUSION* 2018.

96. Karkanas, P.I. and I.K. Partridge, *Cure modeling and monitoring of epoxy/amine resin systems. I. Cure kinetics modeling.* Journal of applied polymer science, 2000. **77**(7): p. 1419-1431.
97. Karkanas, P.I., I.K. Partridge, and D. Attwood, *Modelling the cure of a commercial epoxy resin for applications in resin transfer moulding.* Polymer International, 1996. **41**(2): p. 183-191.
98. Kamal, M. and S. Sourour, *Kinetics and thermal characterization of thermoset cure.* J Polymer Engineering Science, 1973. **13**(1): p. 59-64.
99. Garschke, C., et al., *Cure kinetics and viscosity modelling of a high-performance epoxy resin film.* Polymer Testing, 2013. **32**(1): p. 150-157.
100. Cole, K., J. Hechler, and D. Noel, *A new approach to modeling the cure kinetics of epoxy/amine thermosetting resins. 2. Application to a typical system based on bis [4-(diglycidylamino) phenyl] methane and bis (4-aminophenyl) sulfone.* J Macromolecules, 1991. **24**(11): p. 3098-3110.
101. Hubert, P., et al. *Cure kinetics and viscosity models for Hexcel 8552 epoxy resin*. in *International SAMPE symposium and exhibition*. 2001. SAMPE; 1999.
102. O'Leary, M., et al. *The Effect of Semi-Curing on Infused Laminate Interfacial Properties*. in *The 20th European Conference on Composite Materials (ECCM20)*. 2022.
103. Mesogitis, T., J. Kratz, and A.A. Skordos, *Heat transfer simulation of the cure of thermoplastic particle interleaf carbon fibre epoxy prepregs.* Journal of Composite Materials, 2019. **53**(15): p. 2053-2064.
104. Loos, A.C. and G.S. Springer, *Curing of epoxy matrix composites.* Journal of composite materials, 1983. **17**(2): p. 135-169.
105. Li, C., et al., *In-situ measurement of chemical shrinkage of MY750 epoxy resin by a novel gravimetric method.* Composites Science and Technology, 2004. **64**(1): p. 55-64.
106. Skordos, A.A. and I.K. Partridge, *Inverse heat transfer for optimization and on-line thermal properties estimation in composites curing.* Inverse Problems in Science and Engineering, 2004. **12**(2): p. 157-172.
107. Fernlund, G., et al., *Process modeling for dimensional control--sensitivity analysis of a composite spar process.* Society for the Advancement of Material and Process Engineering, Evolving and Revolutionary Technologies for the New Millenium, 1999. **44**: p. 1744-1755.
108. Kluge, N., et al., *An experimental study of temperature distribution in an autoclave.* Journal of Reinforced Plastics, 2016. **35**(7): p. 566-578.
109. Slesinger, N., et al. *Heat transfer coefficient distribution inside an autoclave*. in *17th international conference on composite material ICCM*. 2009. Edinburgh, UK: IOM Communications.
110. Johnston, A.A., *An integrated model of the development of process-induced deformation in autoclave processing of composite structures*. 1997, University of British Columbia.
111. Tsiangou, E., et al. *Ultrasonic welding of CF/Epoxy to CF/PEEK composites: Effect of the energy director material on the welding process*. in *Proceedings of the 18th European Conference on Composite Materials (ECCM18), Athens, Greece*. 2018.
112. Fisher, A., et al., *The influence of key processing parameters on thermoset laminate curing.* Composites Communications, 2023.
113. Fisher, A., A. Levy, and J. Kratz, *Effects of heat transfer coefficient variations on composite curing.* Journal of Composite Materials, 2022.

114. Matveev, M., et al., *A numerical study of variability in the manufacturing process of thick composite parts.* Composite Structures, 2019. **208**: p. 23-32.
115. METALEX, *Aluminium plate thickness tolerences*. Poole, UK.
116. Corporation, H., *HexPly® M21 180°C (350°F) curing epoxy matrix Product Data Sheet*. 2020.
117. Peters, S.T., *Handbook of composites*. 2013: Springer Science & Business Media.
118. Diatex. *Vacuum Bagging Materials*. [cited 2023 21/07/2023]; Available from: https://composite-integration.co.uk/products/vacuum-bagging-materials-2/.
119. Ghamlouch, T., *Analysis of convective transfer around simple molds inside a model autoclave*. 2018, Université de Nantes.
120. Wang, X., et al., *Correlated rules between complex structure of composite components and manufacturing defects in autoclave molding technology.* Journal of reinforced plastics and composites, 2009. **28**(22): p. 2791-2803.
121. Bohne, T., et al., *Simulation and validation of air flow and heat transfer in an autoclave process for definition of thermal boundary conditions during curing of composite parts.* Journal of Composite Materials, 2018. **52**(12): p. 1677-1687.
122. Kakac, S., Y. Yener, and A. Pramuanjaroenkij, *Convective heat transfer*. Vol. 2. 1995: CRC press Boca Raton.
123. Zhu, J., T. Frerich, and A.S. Herrmann, *CFD modeling and validation of heat transfer inside an autoclave based on a mesh independency study.* Journal of Composite Materials, 2021. **55**(18): p. 2469-2487.
124. Zobeiry, N., et al., *Multiscale characterization and representation of composite materials during processing.* Philosophical Transactions of the Royal Society A: Mathematical, Physical Engineering Sciences, 2016. **374**(2071): p. 20150278.
125. Weber, T.A., et al., *A fast method for the generation of boundary conditions for thermal autoclave simulation.* Composites Part A: Applied Science, 2016. **88**: p. 216-225.
126. Campbell Jr, F.C., *Manufacturing processes for advanced composites*. 2004, Oxford: elsevier.
127. Hu, H., et al., *Monitoring the gelation and effective chemical shrinkage of composite curing process with a novel FBG approach.* Composite structures, 2017. **176**: p. 187-194.
128. Pusatcioglu, S., et al., *Effect of temperature gradients on cure and stress gradients in thick thermoset castings.* Journal of Applied Polymer Science, 1980. **25**(3): p. 381-393.
129. Yi, S. and H.H. Hilton, *Effects of thermo-mechanical properties of composites on viscosity, temperature and degree of cure in thick thermosetting composite laminates during curing process.* Journal of Composite Materials, 1998. **32**(7): p. 600-622.
130. Ostrogorsky, A., *Simple explicit equations for transient heat conduction in finite solids.* 2009.
131. Lienhard, I. and H. John, *A Heat Transfer Textbook*. 2020, Cambridge, MA: Phlogiston Press.
132. Nam, H., et al., *Experimental study on the emissivity of stainless steel.* 2001.
133. Omega Engineering, I., *The Infrared Temperature Handbook*. Vol. 29. 1994: Omega Engineering, Incorporated.
134. Slesinger, N.A., *Thermal modeling validation techniques for thermoset polymer matrix composites*. 2010, University of British Columbia.
135. Guo, Z.-S., S. Du, and B. Zhang, *Temperature field of thick thermoset composite laminates during cure process.* Composites science technology, 2005. **65**(3-4): p. 517-523.

136. *HexPly M21 Product Data Sheet*, HEXCEL, Editor. 2020.
137. *Invar - Nickel Iron Alloy*. Available from: https://www.azom.com/properties.aspx?ArticleID=515.
138. Fourier, J.B.J. and G. Darboux, *Théorie analytique de la chaleur*. Vol. 504. 1822: Didot Paris.
139. Li, Y., et al., *A review on the tooling technologies for composites manufacturing of aerospace structures: materials, structures and processes.* Composites Part A: Applied Science and Manufacturing, 2022. **154**: p. 106762.
140. Ó Brádaigh, C.M., et al. *Electrically-heated ceramic composite tooling for out-of-autoclave manufacturing of large composite structures*. in *Proceedings of SAMPE 2011 Conference*. 2011.
141. Khairul Alam, M. and M.S. Anghelescu, *Analysis of deformation and residual stresses in composites processed on a carbon foam tooling.* Journal of composite materials, 2009. **43**(19): p. 2057-2070.
142. Hasan, Z., *Tooling for composite aerospace structures: manufacturing and applications*. 2020: Butterworth-Heinemann.
143. Bard, S., et al., *Influence of fiber volume content on thermal conductivity in transverse and fiber direction of carbon fiber-reinforced epoxy laminates.* Materials, 2019. **12**(7): p. 1084.
144. Girard-Reydet, E., et al., *Polyetherimide-modified epoxy networks: Influence of cure conditions on morphology and mechanical properties.* Journal of Applied Polymer Science, 1997. **65**(12): p. 2433-2445.
145. Toray, *Toray Cetex® TC1000 Design PEI*, in *Product Data Sheet*. 2019.
146. ASTM, *D5528-01(2013) Standard test method for mode I interlaminar fracture toughness of unidirectional fiber-reinforced polymer matrix composites*. 2013, ASTM International West Conshohocken, PA.
147. ASTM, *ASTM D4541-17 Standard Test Method for Pull-Off Strength of Coatings Using Portable Adhesion Testers*. 2017, ASTM International: West Conshohocken, PA.
148. Lewis, F., *Mechanical Engineering Handbook Ed. Frank Kreith Boca Raton: CRC Press LLC, 1999.* 1999.
149. Hilpert, R., *Heat transfer from cylinders.* Forsch. Geb. Ingenieurwes, 1933. **4**(5): p. 215.
150. Raznjevic, K., *Handbook of thermodynamic tables and charts*. 1976, Washington DC: Hemisphere Publication Corporation.
151. Kothandaraman, C., *Fundamentals of heat and mass transfer*. 3rd ed. 2006, New Delhi: New Age International.
152. Dixon, J.C., *The shock absorber handbook*. 2nd ed. 2007, Chichester, England: John Wiley.
153. Ziegler, F., *The multiple meanings of the Stefan-number (and relatives) in refrigeration.* International journal of Refrigeration, 2010. **33**(7): p. 1343-1349.

Appendices

Appendix A. Epoxy-PEI Stud Pull Tests

To select an epoxy system that would reliably adhere when co-cured with polyetherimide (PEI) a set of qualitive tests was performed. A PEI composite laminate was co-cured with epoxy systems with three different functionalities, and a commercial aerospace grade system. Stud pull tests were performed to indicate the level of adhesion in each case.

A.1 Materials and Methods

Di-, tri- and tetra functional epoxies were considered. The epoxies were diglycidyl ether of bisphenol F (DGEBF), triglycidyl-p-aminophenol (TGPAP) and tetraglycidyl methylene dianiline (TGMDA). The epoxy systems were prepared by mixing each resin with diaminodiphenyl sulfone (DDS) hardener in a 1:1 molar ratio. The commercial epoxy system was Solvay EP2410.

The thermoplastic laminate was Toray-Cetex 1000, consisting of Ultem 1000 PEI reinforced with 5-harness satin woven carbon fabric with 280 gm^{-2} fibre areal weight. The thermoplastic laminate adherends measured 50 mm x 50 mm x 2.5 mm.

To produce the stud pull test specimens (Figure A1) the 20 mm diameter bonding surface of the aluminium studs were prepared through abrasion with 10 grit sandpaper, followed by degreasing with acetone. A small quantity of epoxy was applied to the bottom surface of each stud. Each stud was pressed onto the centre of a thermoplastic composite adherend, any seepage was removed using a cotton swab.

Two temperature histories were considered. Specimens for all systems were cured at 160 °C for 6.5 hours. To test the effect of a pre-dwell, EP2410 and DGEBF/DDS specimens were cured with a temperature history consisting of a 120 °C pre-dwell for 0.5 hours followed by a 180 °C dwell for 2 hours. Five specimens were made for the epoxy systems in each test.

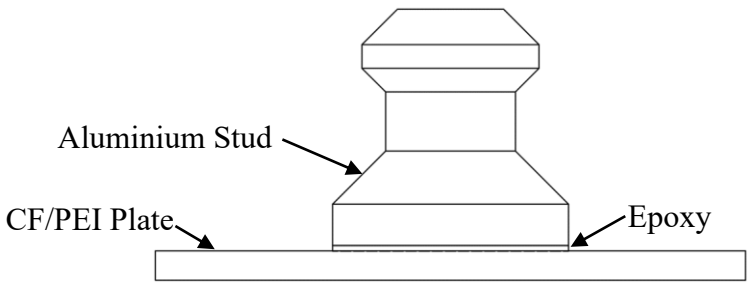

Figure A1. Stud Pull Off Test Specimen Arrangement.

The adhesion between the cured epoxy systems and the thermoplastic laminate was determined by performing the pull-off test specified by ASTM D4541 [147]. The testing arrangement is displayed in Figure. A2. The thermoplastic adherends were secured to a work bench using clamps. The studs were pulled-off the surface using an automatic pull-off adhesion gauge (Elcometer 510). The gauge applied a uniform pull-off rate of 1 $MPa.s^{-1}$ and measured the required tensile load to cause a fracture between the epoxy and the laminate. The load was calculated by multiplying the applied pressure at failure by the area of the bonding surface of the stud.

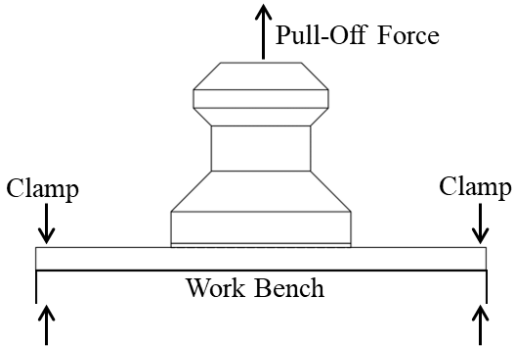

Figure A2. Stud Pull Off Testing Arrangement.

A.2 Results

Figure A3 presents the mean failure force with each epoxy system. The results indicated adhesion was greatest with the co-cured EP2410. There was also an apparent trend with adhesion decreasing with increasing epoxy functionality. Given the importance of viscosity for interdiffusion, this result was attributed to the lower viscosity of the lower functionality systems.

Due to a drop in viscosity at the start of the curing process, epoxy was liable to be displaced from under the studs and the studs were prone to sliding. This effect resulted in several specimens being compromised. This was most significant with TGMDA/DDS where only one specimen could be tested. Three were tested with EP2410, four with DGEBF/DDS and five with TGPAP/DDS. Although there was greater uncertainty for epoxy systems with fewer repeats, there were no apparent anomalies in the data.

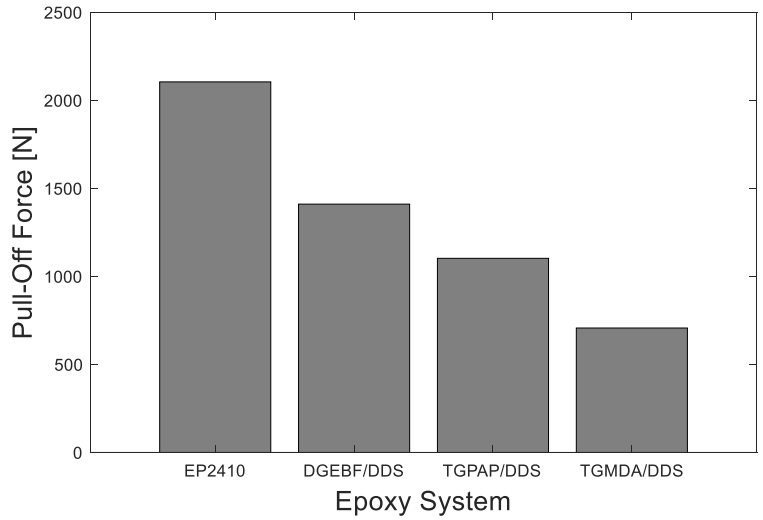

Figure A3. Stud pull test results for the specimens cured at 160 °C.

The use of EP2410 and DGEBF/DDS in the second set of tests was motivated by the greater level of adhesion shown in the first set of tests. The results are presented in Figure A4.

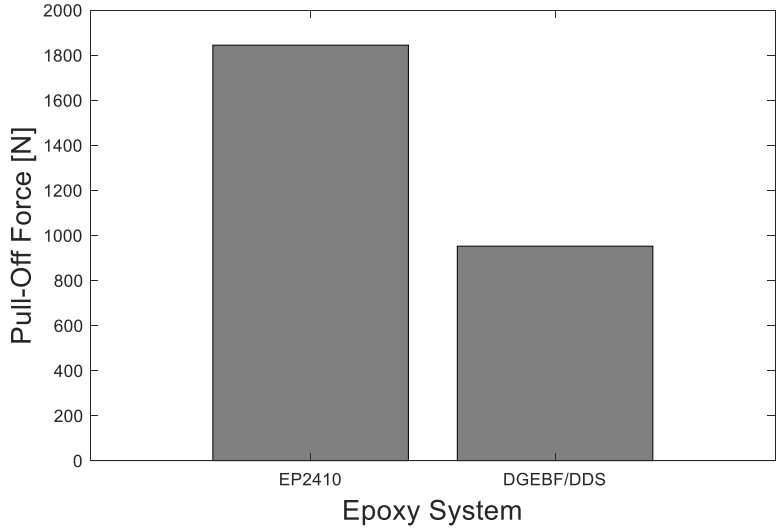

Figure A4. Stud pull test results for EP2410 and DGEBF/DDS specimens cured at 180 °C with a 120 °C pre-dwell.

As with the previous temperature history, the specimens with EP2410 withstood a greater pull-off force. However, with both epoxy systems, the presence of the pre-dwell appeared to reduce the level of adhesion. This result is consistent with the literature which has shown decreasing temperature to reduce the rate of diffusion more than the rate of cure [58, 62], hence the low temperature pre-dwell was detrimental to adhesion.

A.3 Conclusion

The results from the stud pull tests indicated that of the epoxy systems considered, EP2410 would be the most suitable choice for reliable interphase formation. In addition to the in-

house expertise with EP2410, this result motivated the use of this system in the later experimental campaign.

The result with the three model epoxy systems has more generality, indicating that a lower functionality is more conducive to interphase formation during co-curing. However, higher functionality epoxies are often better suited to engineering applications. Hence, to maximise the quality of the laminate as a whole it is likely that a suitable balance will need to be found between adhesion and the properties of the individual constituents, particularly in the case of stiffness as thermoplastics are generally inferior compared to thermosets.

Appendix B. Acid Digestion Data

Table B1. Acid digestion data for the fibre volume fraction of 3 specimens from 3 IMA/M21 panels.

Panel	Specimen		Fibre Volume Fraction %
1	1		60.1
	2		61.8
	3		60.3
		Average	60.7
		Standard Deviation	0.7
2	1		62.0
	2		64.2
	3		60.9
		Average	62.4
		Standard Deviation	1.4
3	1		58.1
	2		58.4
	3		57.4
		Average	58.0
		Standard Deviation	0.4
Overall Average			**60.4**
SD of Averages			**1.8**
Average of SDs			**0.8**

Appendix C. Velocity Field Estimation

Numerous empirical correlations have been derived to capture the relationship between convective heat transfer (HTC) and fluid flow [148]. These equations usually include Nusselt number (*Nu)*, Reynolds number (*Re*) and Prandtl number (*Pr*). *Nu* quantifies the ratio of convective to conductive heat transfer in the fluid. It writes:

$$Nu = \frac{h_{con} l}{k_{gas}} \tag{C1}$$

where h_{con} is HTC, l is the characteristic length and k_{gas} is the thermal conductivity of the gas. *Re* is the ratio of inertial force to viscous forces in the fluid and is defined as

$$Re = \frac{\rho_{gas} v l}{\mu_{gas}} \tag{C2}$$

where v is the flow velocity, μ_{gas} and ρ_{gas} are the dynamic viscosity and density of the gas respectively. *Pr* is the ratio of momentum diffusivity to thermal diffusivity, written

$$Pr = \frac{C_p \mu_{gas}}{k_{gas}} \tag{C3}$$

The average velocity at each calorimeter during the temperature ramp to 180 ºC was computed using the Hilpert correlation for cylinders in cross flow [149], defined as

$$Nu_D = C Re_D^n Pr^{\frac{1}{3}} \tag{C4}$$

where C and n depend on *Re*. The subscript D signifies that the characteristic length is the cylinder diameter. This correlation equation is applicable for $Pr \geq 0.7$ making it suitable for use with gases (*Pr* of air ~ 0.7 [150]). Flow inside autoclaves is generally turbulent [119], given the orders of ρ_{gas}, μ_{gas} (Table C1) and the diameter (D) it was assumed *Re* was in the interval 4000-40000, which corresponded to C and n values of 0.193 and 0.618 respectively [151].

Equation (C4) was rearranged, and the dimensionless numbers expanded to obtain the velocity as,

$$v = \frac{\mu_{gas}}{\rho_{gas} D} \left[\frac{hD}{C} \left(\frac{1}{C_p \mu_{gas} k_{gas}^2} \right)^{\frac{1}{3}} \right]^{\frac{1}{n}} \tag{C5}$$

The properties of air were assumed constant during the ramp, the values used were obtained from standard properties and empirical relations [152] and are shown in Table C1.

Table C1. The air properties at 180 ºC used during the velocity field approximations given in Equation (C5) (adapted from [152]).

Air property	**P = 1 bar**	**P = 3 bars**	**P = 7 bars**
Dynamic Viscosity (Nsm^{-2})	2.504e-5	2.504e-5	2.504e-5
Density (kgm^{-3})	0.769	2.307	5.383
Specific heat capacity ($Jkg^{-1}K^{-1}$)	1019	1019	1019
Thermal conductivity ($Wm^{-1}K^{-1}$)	0.036	0.036	0.036

Appendix D. Approximate Velocity Fields

From Equation (C5) and Table C1 it can be seen that of the variables the velocity is dependent on, only HTC and density changed significantly between the tests. Equation (C5) also shows an inverse linear relationship between velocity and density, while velocity is proportional to HTC to the power of 1/n, which is greater than unity. The effect of these variations is depicted in Figure D1, a box plot of the velocities in the vessels.

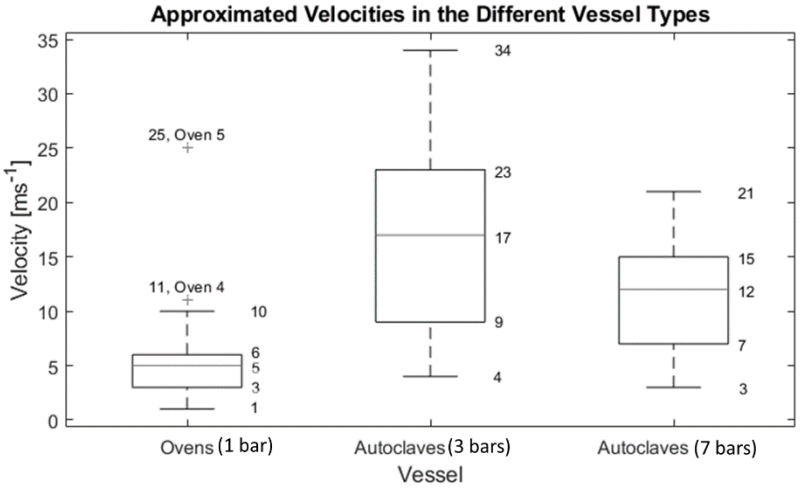

Figure D1. Approximated velocity values in the ovens, and the autoclaves at 3 and 7 bars.

The low HTCs in the ovens translated into low velocities, again the uniquely high value observed in oven 5 is clearly visible. The velocity distribution changed significantly going to the autoclaves at 3 bars, with both the size of the values and variability increasing. This is due to the significant 176% increase in median HTC being sufficient to more than compensate for the accompanying increase in density. However, when the pressure is increased to 7 bars, the opposite is observed. The much smaller, 40% increase in median HTC is unable to compensate for the density which more than doubles, resulting in a plot that is closer to that of the ovens. Consequently, the approximations suggest that past a certain point, increasing pressure results in a slower, less variable velocity field and hence diverges from the trend seen with the HTC measurements.

Appendix E. Heat Transfer Sub-Model

The heat equation in the composite domain writes

$$\rho_c C_{p_c} \frac{dT}{dt} = \frac{d^2 k_c T}{dx^2} + L \frac{d\alpha}{dt} \quad \text{(E1)}$$

where ρ_c is the effective density, C_{p_c} is the effective specific heat capacity, k_c is the effective through thickness thermal conductivity and L is the volumetric latent heat, defined as the product of the total heat of reaction, the density and volume fraction of the resin, taking values 415000Jkg^{-1},1280kgm^{-3} and 0.4 respectively [103].

In the laminate domain, effective density was the density of the fibres and resin joined through rule of mixtures assuming a fibre volume fraction of 0.6. The effective specific heat capacity and conductivity were functions of degree of cure and temperature. The effective specific heat capacity consisted of the values of the fibres $C_{p,f}$ and resin $C_{p,r}$ defined according to Equations (E2) and (E3) respectively, joined through rule of mixtures according to fibre weight fraction.

$$C_{p,f} = A_{f,c_p} T + B_{f,c_p} \quad \text{(E2)}$$

$$C_{p,r} = A_{r,c_p} T + B_{r,c_p} + \frac{\Delta_{r,c_p}}{1 + \exp\left(C_{r,c_p}\left(T - T_g - s\right)\right)} \quad \text{(E3)}$$

where A_{r,c_p} and B_{r,c_p}, C_{r,c_p}, Δ_{r,c_p} and s are constants, the values of which were obtained by Mesogitis et al [103] from differential scanning calorimetry data. T_g is glass transition temperature. The effective transverse thermal conductivity of the laminate k was defined as follows,

$$k = A_k T + B_k \alpha + C_k T \alpha + D_k \quad \text{(E4)}$$

where A_k, B_k, C_k and D_k are constants describing the linear dependence of conductivity on temperature, degree of cure, coupling effects and an offset, the values were derived by Mesogitis et al [103] using laser flash analysis.

The last term on the right-hand side of Equation (E1) was exclusive to the equation applied to the laminate, it represents the exothermic heat generated during the curing reaction and is responsible for the coupling between the cure kinetics and the heat transfer sub-models.

Convective heat transfer at the boundaries was defined by the Neumann boundary condition:

$$\frac{dkT}{dx} = -h(T - T_\infty) \tag{E5}$$

Appendix F. Cure Kinetics Sub-Model

The cure kinetics sub-model is representative of Hexply M21 [136], a high-performance epoxy system with thermoplastic particle interleaf. Mesogitis et al [103] formulated the model for the cure kinetics of this material based on a suitably modified variant of the Kamal and Sourour [98] model,

$$\frac{d\alpha}{dt} = k_1(1-\alpha)^{n_1} + k_2\alpha^m(1-\alpha)^{n_2} \tag{F1}$$

where α is degree of cure, n_1, n_2 and m are reaction orders, and k_1 and k_2 are reaction constants. The reaction constants are composed of a diffusion term in addition to a chemical term to capture the effect of diffusion rate limitation phenomena post-vitrification, these terms are combined as

$$\frac{1}{k_i} = \frac{1}{k_{iC}} + \frac{1}{k_D} \; i = 1,2 \tag{F2}$$

where k_{iC} and k_D are the chemical and diffusion rate constants respectively. Both were assumed to have an Arrhenius temperature dependence

$$k_{iC} = A_i e^{\left(\frac{-E_i}{RT}\right)} \; i = 1,2 \tag{F3}$$

$$k_D = A_D e^{\left(\frac{-E_D}{RT}\right)} e^{\frac{-b}{f}} \tag{F4}$$

where A_i and A_D are the pre-exponential factors, E_i and E_D are the activation energies, R is the universal gas constant, b is a constant and f is the equilibrium free volume, defined as

$$f = w\left(T - T_g\right) + g \tag{F5}$$

where w is the thermal expansion coefficient of the free volume and g is the fractional free volume at T_g. T_g is degree of cure dependent according to the DiBenedetto equation

$$T_g = T_{g0} + \frac{\lambda\alpha\left(T_{g\infty} - T_{g0}\right)}{1 - (1-\lambda)\alpha} \tag{F6}$$

where T_{g0} is the uncured glass transition temperature, $T_{g\infty}$ is the ultimate glass transition temperature and λ is a fitting parameter.

Appendix G. Dimensional Analysis

To determine the contribution of the terms in the model to the rates of heat transfer and cure, and hence the need to include them, a dimensional analysis was performed. For simplicity, during this analysis C_{pc} and k_c were treated as constants with values for 90% DOC at 180ºC. Although C_{pc} and k_c are cure and temperature dependent, the changes they undergo were sufficiently small (22% and 32% respectively) for meaningful qualitative deductions.

To nondimensionalise the heat equation four dimensionless variables were defined. Dimensionless temperature T^*:

$$T^* = \frac{T(x,t) - T_0}{T_{dwell} - T_0} \tag{G1}$$

where T_0 is initial temperature and T_{dwell} is the dwell temperature. Dimensionless time t^* was time divided by the duration of the initial ramp up t_{ramp}. The dimensionless thickness x^* was defined as x divided by the laminate domain thickness $|x_c|$. The ratio of the laminate domain thickness $|x_c|$ to the tool domain thickness $|x_t|$ was denoted by the parameter A. The degree of cure α is already dimensionless.

First considering the nondimensionalisation of the heat equation in the composite domain (Equation E1)). After substitution of the dimensionless parameters and division by the coefficient of the temporal derivative, the coefficient of the spatial derivative took the form of the Fourier number Fo_c, written,

$$Fo_c = \frac{t_{ramp} k_c}{(\rho C_p)_c {x_c}^2} \tag{G2}$$

$$Fo_t = \frac{t_{ramp} k_t}{(\rho C_p)_t {x_t}^2} \tag{G3}$$

The coefficient of the rate of reaction term was the reciprocal of the Stephan number Ste or phase transition number Ph [153], defined as

$$P_h = Ste^{-1} = \frac{L}{(\rho C_p)_c (T_{dwell} - T_0)} \tag{G4}$$

Appendix H. EP2410 Degree of Cure Verification

To verify the initial degree of cure of the uncured and semi-cured EP2410 epoxy in Chapter 6 Differential Scanning Calorimeter (DSC) tests were performed. The DSC analysis involved a 5 °Cmin^{-1} modulated temperature ramp from -50 °C to 290 °C. Oscillations with a period of 40 seconds and an amplitude of 1.5 °C were used as the modulation parameters.

The heat of reaction for the three cure states of EP2410 obtained through the DSC analysis are shown by the area under the heat of reaction curve (blue) in Figures G1, G2 and G3. The total heat reaction of EP2410 with a 5 °Cmin^{-1} ramp rate has been shown to be around 413 Jg^{-1} [102]. Based on these results, the degree of cure of the resin prior to curing was 0.2, the lower degree of semi-cure was 0.7 and the higher degree of semi-cure was 0.85.

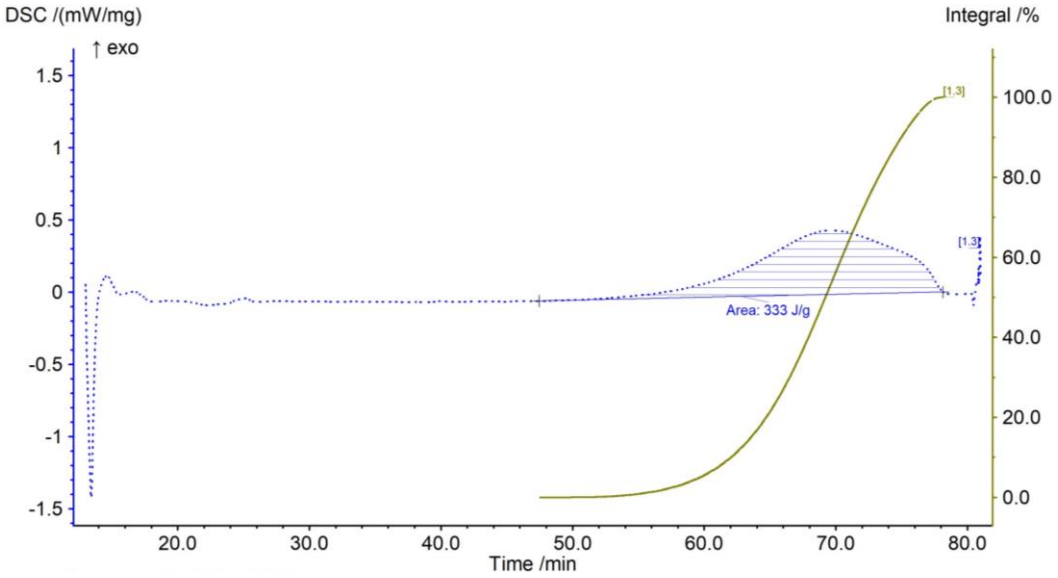

Figure G1. Modulated DSC result with the uncured EP2410 resin.

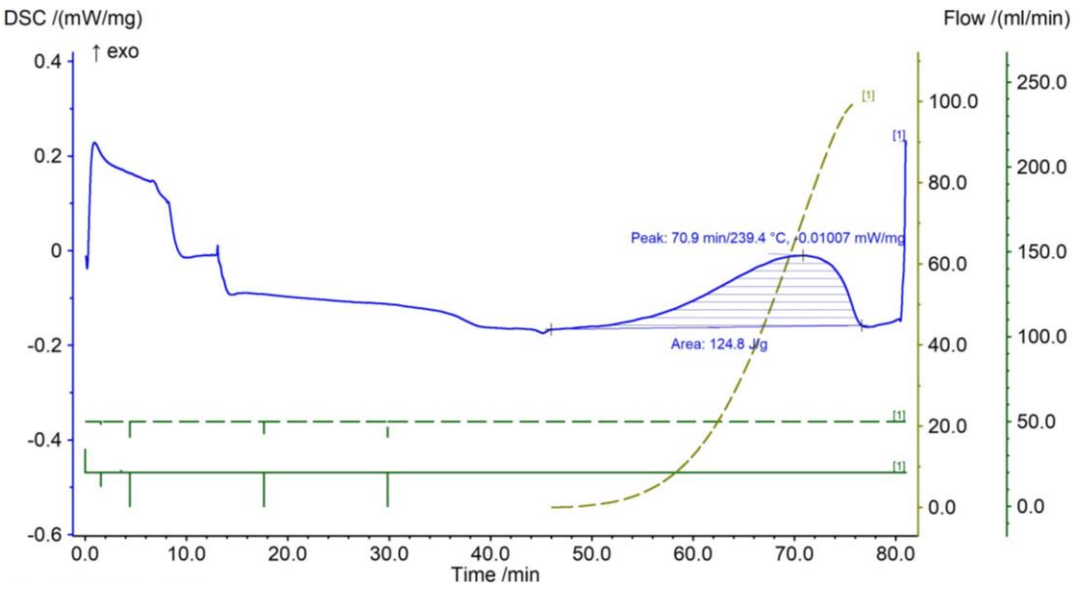

Figure G2. Modulated DSC result with the low degree of semi-cure EP2410 resin.

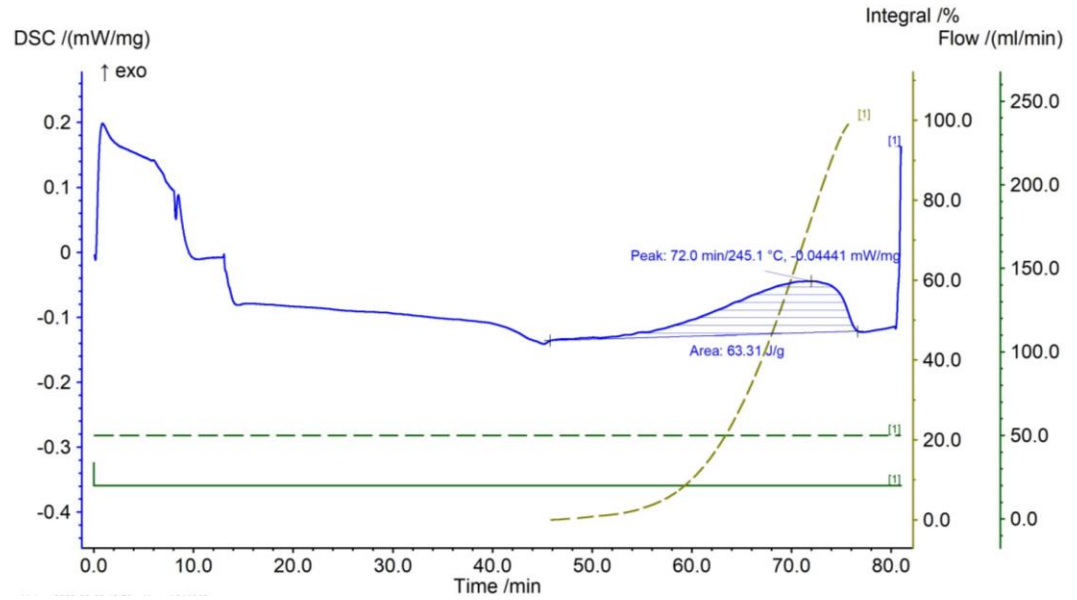

Figure G3. Modulated DSC result with the high degree of semi-cure EP2410 resin.